Loughborough University

This item was submitted to Loughborough University as a PhD thesis by the author and is made available in the Institutional Repository (https://dspace.lboro.ac.uk/) under the following Creative Commons Licence conditions.

creative commons

COMMONS DEED

Attribution-NonCommercial-NoDerivs 2.5

You are free:

- to copy, distribute, display, and perform the work

Under the following conditions:

Attribution. You must attribute the work in the manner specified by the author or licensor.

Noncommercial. You may not use this work for commercial purposes.

No Derivative Works. You may not alter, transform, or build upon this work.

- For any reuse or distribution, you must make clear to others the license terms of this work.
- Any of these conditions can be waived if you get permission from the copyright holder.

Your fair use and other rights are in no way affected by the above.

This is a human-readable summary of the Legal Code (the full license).

Disclaimer

For the full text of this licence, please go to:
http://creativecommons.org/licenses/by-nc-nd/2.5/

BLL No.: D 15297/76

LOUGHBOROUGH
UNIVERSITY OF TECHNOLOGY
LIBRARY

AUTHOR
QUINTANILLA, G E

COPY NO. 021713/02

VOL NO. CLASS MARK

LOAN COPY

25 MAY 1990

6 JUL 1990

- 5 JUL 1991

- 3 JUL 1992

- 2 JUL 1993

18 MAR 1994

29 APR 1994

002 1713 02

NEW MEASURING TECHNIQUES USING HOLOGRAPHIC AND SPECKLE INTERFEROMETRIC RECORDING

by

GUSTAVO EDUARDO QUINTANILLA E.

A Doctoral Thesis

Submitted in partial fulfilment of the requirements

for the award of

Doctor of Philosophy of the Loughborough University of Technology

October 1975

Supervisor: J.N. Butters, BSc, PhD, CEng, FInstP, MIMechE.
Department of Mechanical Engineering

© by Gustavo Eduardo Quintanilla E., 1975

Loughborough University
of Technology Library
Date 8|12|75
Class
Acc. No. 021713|02

To my wife Maria del Carmen

and our daughters

Ana Maria and Beatriz

ACKNOWLEDGEMENTS

I would like to thank Professor John N. Butters for his guidance and encouragement during my present studies, and Dr. Rodolfo Castillo B. for his support.

I also want to thank Dr. David Denby and Mr. Harry Pollard for their friendship, and valuable discussions and help.

I wish to thank also Mr. Kenneth Topley for the photographic work, and Mr. Victor Roulstone for his assistance.

I wish to express my gratitude to Loughborough University of Technology, the British Council, the Consejo Nacional de Ciencia y Tecnologia (Mexico) and the Instituto Tecnologico y de Estudios Superiores de Monterrey (Mexico).

Finally, I would like to thank my parents, Jose and Maria Antonieta.

CONTENTS

ABSTRACT

Electronic and photographic interferometric recording, and their combination, result in several novel optical measuring techniques. The interferometric properties of Holographic and Speckle processes, in these techniques, encompass fields such as Lapse time, Real time and Time average Holographic interferometry, two-wavelength and multiple-index speckle contouring, Figure (moire) interference, photographic bleach processes and electronic processing. Each of these fields is analysed and conclusions are drawn in their interaction with the proposed techniques. A clear and simple approach to optical wave theory is intended with emphasis in scalar wave theory.

One established method, directly comparable with the holographic technique, requires a wavefront shape that matches the nominal shape of the object surface but uses an in-line reference beam to code phases in the (speckled or smooth) image plane. In this manner only surfaces of uniform shape, namely planes, spheres and cylinders, can be contoured using wavefronts generated by conventional optical components. However, surfaces having irregular curvature can be contoured using a novel method incorporating holographic reconstruction of a "master" wavefront such that, effectively, components under test are compared against a master component shape. Alternatively, under certain conditions, two similar object surfaces may be directly compared, one surface acting as a reference for the other. Again the surface shape no longer needs to be regular, and surfaces with deep features can be contoured. For smooth surfaces the methods can be regarded as reduced sensitivity interferometry. The application of

Electronic Speckle Pattern Interferometry to the contouring of transparent objects and analysis of refractive index-change propagation, based on multiple index speckle contouring, is established. By all these methods the optical arrangements are simplified, and real-time operation becomes a practical procedure through the use of video recording plus electronic processing. Photographic processing is eliminated, except in the case of the holographic reconstruction method in which only one hologram is needed for the measurement of many (production line) components. The various principles are explained with reference to results from experiments designed to investigate contouring conditions, fringe interpretation, and accuracy of measurement. Comments are given on the potential applications of these methods in the field of engineering inspection.

INTRODUCTION

During the past decade the recording and retrieval of optical information has become a main subject in the industrial applications of coherent optics. New practical optical measuring techniques have been developed around this subject with the improvement and development of laser sources, light sensitive materials and the introduction of electronic recording systems. It is mainly in the field of non-destructive testing and inspection where those techniques have found the acceptance and sponsorship of industry and research organisations. The research in coherent optics in the non-destructive fields embraces holographic and speckle interferometry and constitute the themes of this work.

Holography was proposed by GABOR (1948) in an intent to improve the power resolution of the electron microscope. His intention was to use the variable magnifying property of the new optical element, the hologram, and in doing so, eliminate the limitations introduced by the microscope objective lens. Unfortunately his invention was an in-line optical system, therefore, superimposed to the signal there was unwanted information.

Paradoxically, with the advent of the laser in 1960, as a reliable source of coherent light, the possibility of overcoming that superposition of information by the holographic off-axis method LEITH et al (1962) led to a vast number of holographic applications other than in electron microscopy. It was said, in the early 60's, that the laser was a tool waiting for the arrival of the problems to be solved.

The holographic process brought about the awareness of researchers to an unparalleled explosion of imaginative non-destructive laboratory techniques and applications in industry during subsequent years. The possibility of exactly superimposing the image of an object under observation on the object itself and thus obtaining usable data from the interference fringes, generated by an infinitesimal change of the object surface, gave rise to divisions in holographic interferometry. These divisions are accounted for by the origin of those interference fringes and the way they are processed. Heat transfer and convection current analysis, stress[1], and strain analysis, vibration analysis and contour generation, are fields in which holographic interferometry has most applications.

Holography, as such, is an art and an impressive means in commercial advertising, superior in many respects to photography, but, with an undesirable graininess appearance. This appearance is due to an inherent property of laser light, coherence, and its interaction with matter. Yet, it is that grainy appearance, speckled appearance, which is the essential part in speckle interferometry, BUTTERS et al (1971).

The speckle offers, in the non-destructive testing (NDT) and non-destructive inspection (NDI) fields, a new line of approach in interferometry; it is considered a sampling function of the object information, thus allowing for the low spatial resolution of present television cameras. The electronic process of the optical information provides an instantaneous presentation of the interference fringes[2] on a television monitor. The overall speckle process, optical and

1. HOVANESIAN, J.D. et al (1968), POST, D. (1972).
2. See Chapter III for interference fringe concept.

electronic, is called electronic speckle pattern interferometry (ESPI), BUTTERS et al (1971). It encompasses the fields in which holography has its merits whilst being unique in other interferometric applications, LEENDERTZ (1970). ESPI is a valuable method in production engineering as a NDT technique where a rapid assessment of strain concentration or a quality shape control in a production line is required, DENBY et al[1].

Holographic and speckle pattern interferometry extend the field of conventional interferometry to non-flat and non-polished object surfaces, in which speckle de-correlation, surface roughness, light amplification, resolution of television cameras and holographic plate processing, present limitations to the systems and are subjects of current research.

1. DENBY, D. et al (1974) and (1975).

CHAPTER I

INTRODUCTION TO OPTICAL WAVE THEORY

VECTOR WAVE THEORY - SCALAR WAVE THEORY

An electromagnetic wave represents the propagation, in free space[1], of a perturbation of the electromagnetic field. Light is the electromagnetic radiation detected by the human eye, visible radiation and its nature is established by Maxwell's equations[2]. According to electromagnetic theory light consists of two mutually orthogonal vectors vibrating transversely in the direction of propagation: the electric vector $\underset{\sim}{E}$ and the magnetic induction vector $\underset{\sim}{B}$. The mathematical model of the nature and propagation of light is simplified, without loss of generality, by considering the electric perturbations since these are responsible for the optical properties. Furthermore, although related by Maxwell's equations, the two field vectors $\underset{\sim}{E}$ and $\underset{\sim}{B}$ satisfy separately the vector wave equation

$$\nabla^2 \underset{\sim}{E}(\underset{\sim}{r},t) = \frac{1}{v_p^2} \frac{\partial^2 \underset{\sim}{E}(\underset{\sim}{r},t)}{\partial t^2} \qquad (1)$$

where $\underset{\sim}{E}(\underset{\sim}{r},t)$ could be either field vector[3].

Let the electric vector be expressed by its Cartesian components, Fig.(1)[4], as

$$\underset{\sim}{E}(\underset{\sim}{r},t) = E_x \hat{i} + E_y \hat{j} + E_z \hat{k} \qquad (2)$$

1. Free space, region in a homogeneous medium free from currents and charges, i.e. $i = 0$ in Maxwell's third equation
$$\oint B.\, dl = \mu_o \left(\varepsilon_o \frac{d\phi_E}{dt} + i\right)$$
2. In the analysis that follows Maxwell's classical electromagnetic theory is used.
3. To allow an easy reading the definition of terms will be at the end of each chapter.
4. On Fig.(1), point s represents a point source for a spherical wavefront or an arbitrary point on the path of a plane wavefront.

in which each harmonic component satisfy the wave equation and is written as

$$E_i(\underset{\sim}{r},t) = A_i(\underset{\sim}{r})\cos\left[\omega t - \underset{\sim}{k}.\underset{\sim}{r} + \phi_i\right] \qquad (3)$$

$$i = x,y,z$$

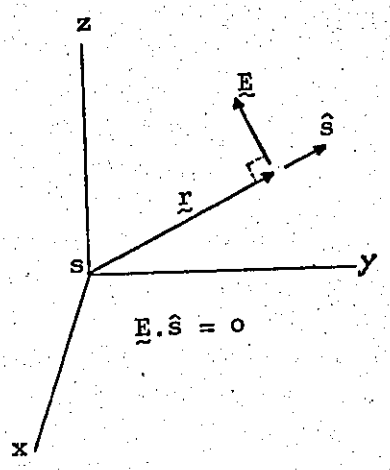

Fig.(1)

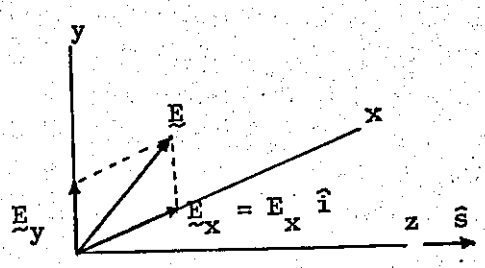

Fig.(2)

For simplicity let us consider the direction of propagation to be along the z axis, Fig. 2. Thus Eq.(1) may be written as

$$\left(\frac{\partial^2 E_x}{\partial x^2} - \frac{1}{v_p^2}\frac{\partial^2 E_x}{\partial t^2}\right)\hat{i} + \left(\frac{\partial^2 E_y}{\partial y^2} - \frac{1}{v_p^2}\frac{\partial^2 E_y}{\partial t^2}\right)\hat{j} = O \qquad (4)$$

Therefore the rectangular components E_x and E_y of $\underset{\sim}{E}$ each satisfy the wave equation and are propagated independently. The transverse nature of $\underset{\sim}{E}$ gives rise to the concept of polarization[1].

Although the interference phenomena are affected by polarization, BORN et al[2], the theory of holography and speckle, themselves an interference phenomenon, are treated from a scalar point of view.

1. See p10.
2. p257

Once the polarization concept is put aside the harmonic solution of the scalar wave equation takes the form

$$E(\underset{\sim}{r},t) = A(\underset{\sim}{r}) \cos (\omega t - \underset{\sim}{k}.\underset{\sim}{r} + \phi) \tag{5}$$

where E represents any component of the electric vector. For convenience Eq.(5) can be written in complex notation form as

$$E(\underset{\sim}{r},t) = R_e \left\{ U e^{j\omega t} \right\} \tag{6}$$

where R_e indicates that only the real part of the expression will be considered[1], and

$$U = A(\underset{\sim}{r}) \exp \left[-j(\underset{\sim}{k}.\underset{\sim}{r} - \phi) \right]$$

$$= A(\underset{\sim}{r}) \exp \left[j\, g(\underset{\sim}{r}) \right] \tag{7}$$

is the complex amplitude of the wave. Its usefulness is established below.

It is the intensity of the wave $E(\underset{\sim}{r},t)$ which excites the photodetector and is defined by[2]

$$I(\underset{\sim}{r}) \triangleq 2 \langle E^2 (\underset{\sim}{r},t) \rangle \tag{8}$$

where

$$\langle E^2 (\underset{\sim}{r},t) \rangle = \lim_{T \to \infty} \frac{1}{2T} \int_{-T}^{T} E^2 (\underset{\sim}{r},t)\, dt \tag{9}$$

1. See BORN et al. p17
2. KLEIN (1970) p122, COLLIER et al (1971), p7. See Appendix A.

then[1]

$$I = 2\langle \left[\frac{1}{2} \left(U e^{j\omega t} + U^* e^{-j\omega t} \right) \right]^2 \rangle$$

$$= UU^* \quad (= |U|^2)$$

$$= A^2(\underset{\sim}{r}) \qquad (10)$$

Therefore the intensity of the wave can be easily found using the complex amplitude U to represent the wave $E(\underset{\sim}{r},t)$.

1. $\langle e^{\pm j2\omega t} \rangle = 0$

INTERFERENCE OF TWO PLANE WAVES

Plane waves

Let us write Eq.(5) in the form[1]

$$E = A \cos(\omega t - \underset{\sim}{k}.\underset{\sim}{r}) \qquad (11)$$

This equation represents a plane wave which propagates with a phase velocity v_p in a direction $\hat{s}$, Fig.3

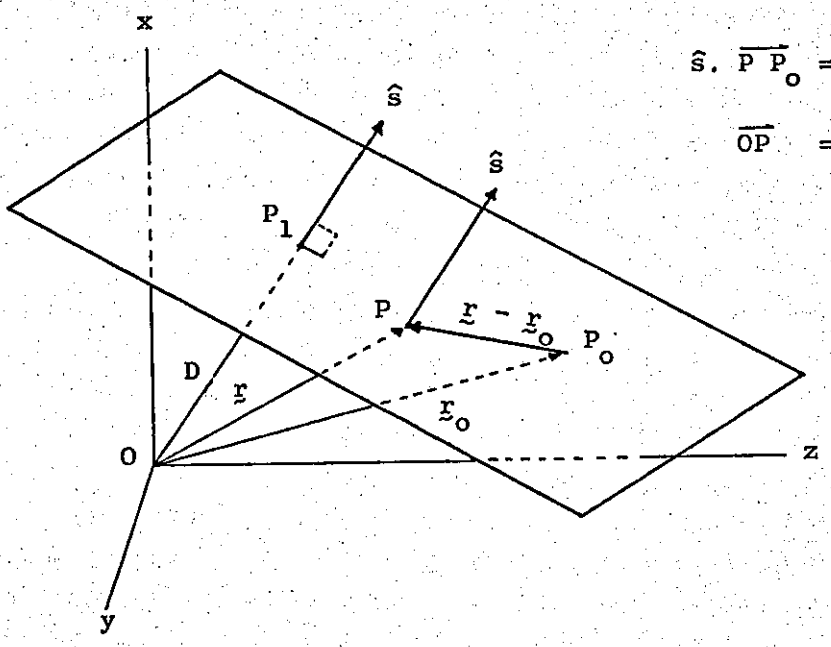

Fig.(3)

The plane contains the points P, P_o, P_1, and the line $\overrightarrow{P\text{-}P_o} = |\underset{\sim}{r}-\underset{\sim}{r}_o|$

1. A is a constant and ϕ is not taken into account in the present analysis.

Then

$$(\underset{\sim}{r} - \underset{\sim}{r}_o).\hat{s} = 0$$

$$\underset{\sim}{r}.\hat{s} = \underset{\sim}{r}_o.\hat{s} = D \qquad (12)$$

represents the equation of a plane with a normal unit vector $\hat{s}$. The argument in Eq.(11) is constant, therefore, at two points in space, for different times, we have

$$\begin{aligned} (\omega t_1 - \underset{\sim}{k}.\underset{\sim}{r}_1) &= C \\ (\omega t_2 - \underset{\sim}{k}.\underset{\sim}{r}_2) &= C \end{aligned} \qquad (13)$$

From the last two expressions and Eq.(12) it follows that

$$\begin{aligned} (\omega t_1 - k\, D_1) &= (\omega t_2 - k\, D_2) \\ D_2 - D_1 &= \frac{\omega}{k}\,(t_2 - t_1) \end{aligned} \qquad (14)$$

where $D_2 - D_1$ represent the (perpendicular) distance between the two planes. Thus, the velocity of propagation of planes of constant phase, Eq.(13) is expressed by[1]

$$vp = \frac{D_2 - D_1}{t_2 - t_1} = \frac{\omega}{k} \qquad (15)$$

Interference of two plane waves

Consider the interference of two plane wavefronts at a point P in space given by the position vector $\underset{\sim}{r}$, Fig.(4).

Let us assume, for simplicity, the direction of propagation of both wavefronts to be parallel to the plane of the figure.

1. Similar result is obtained substituting Eq.(11) into Eq.(4).

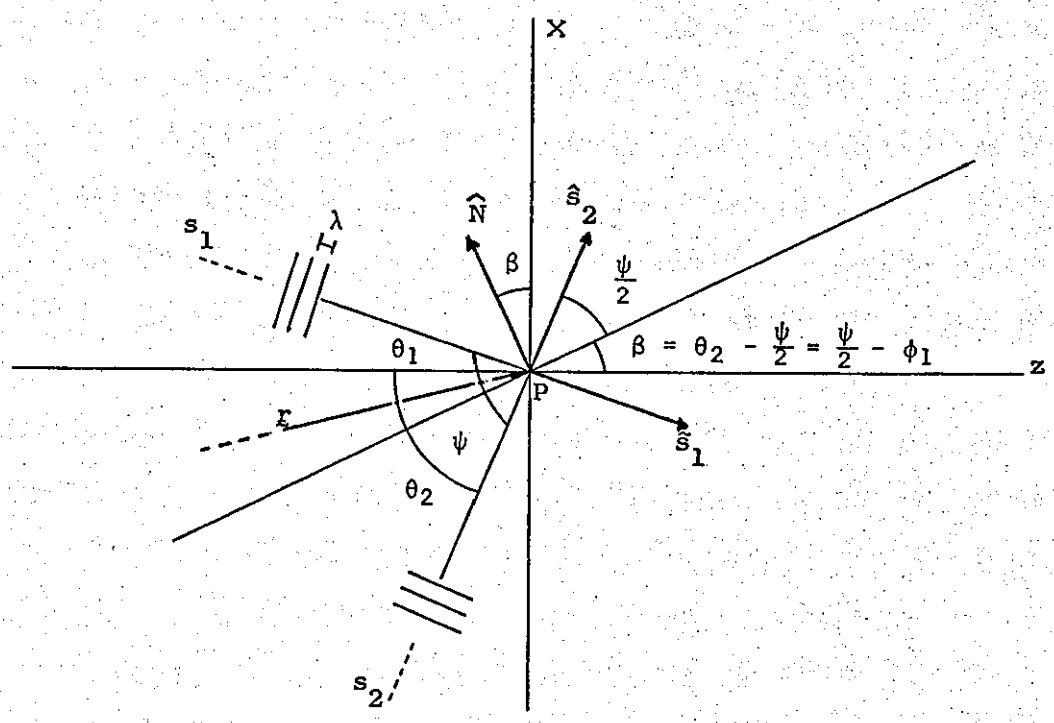

Fig. (4)

The complex amplitude at P is

$$U_p = U_1 + U_2 = A_1 \exp\left[-j(\underset{\sim}{k}_1 . \underset{\sim}{r} - \phi_1)\right] + A_2 \exp\left[-j(\underset{\sim}{k}_2 . \underset{\sim}{r} - \phi_2)\right] \qquad (16)$$

and the intensity

$$I_p = I_1 + I_2 + 2\sqrt{I_1 I_2} \cos\delta \qquad (17)$$

where

$$\delta = \left[(\underset{\sim}{k}_2 - \underset{\sim}{k}_1).\ \underset{\sim}{r} - \phi\right], \qquad \phi = \phi_2 - \phi_1$$

$$= \frac{2\pi}{\lambda} (\hat{s}_2 - \hat{s}_1).\ \underset{\sim}{r} - \phi \qquad (18)$$

According to Fig.5 δ can be written as

$$\delta = \frac{2\pi}{\lambda}\, 2 \sin\frac{\psi}{2}\, \hat{N}.\underline{r} - \phi \qquad (19)$$

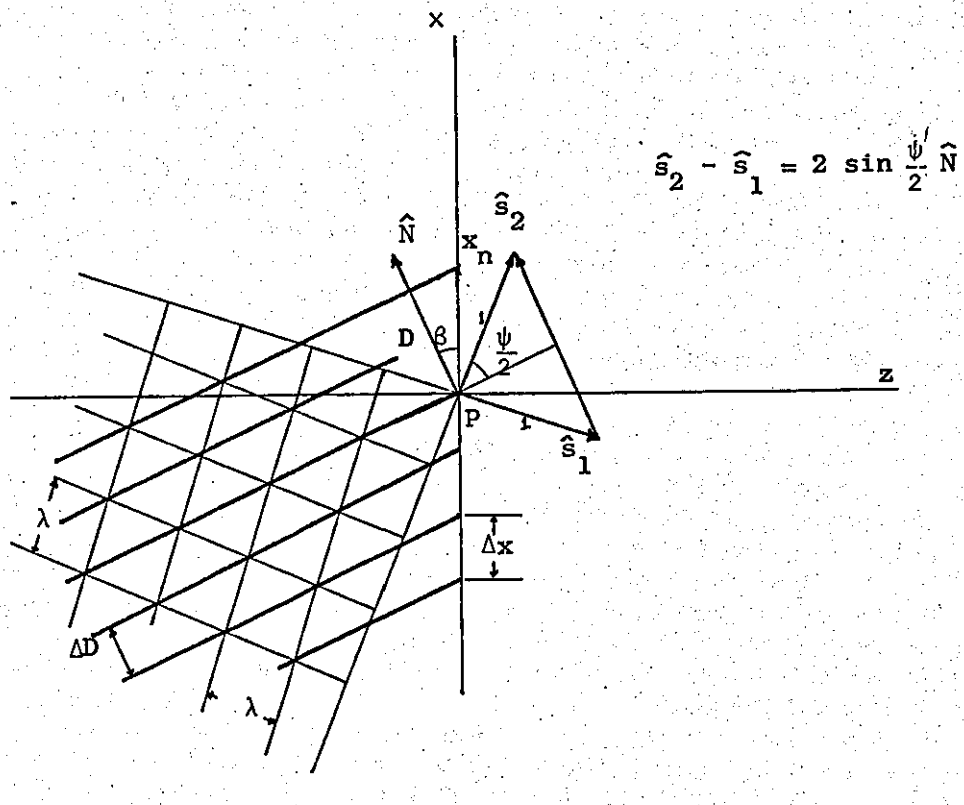

Fig.(5)

The intensity will take, alternatively, maximum and minimum values along the $\hat{N}$ direction[1], generating, in that way, non-localised interference lines.

On Figs.(4) and (5), the location of points P could be at any position along the $\hat{N}$ direction, therefore a projection to the x - y plane is necessary if this plane is to represent the location of a screen or a photodetector. We then obtain for $\delta = n\, 2\pi$, I_{max} and

$$\hat{N}.\underline{r} = \frac{n\,\lambda}{2 \sin\frac{\psi}{2}} + \frac{\phi\,\lambda}{4\pi \sin\frac{\psi}{2}} = D \quad (= \text{constant}) \qquad (20)$$

1. See KOGELNIK, Eq.(8) for $\hat{N} = \underline{K}$, (1967).

The projection on the x axis becomes[1]

$$x_n = \frac{D}{\cos \beta} = \frac{\lambda}{\sin \theta_1 + \sin \theta_2} \left(n + \frac{\phi}{2\pi}\right) \qquad (21)$$

and the separation of the interference lines on the x axis is given by

$$\Delta x = x_{n+1} - x_n = \frac{\lambda}{\sin \theta_1 + \sin \theta_2} \qquad (22)$$

1. β indicates the vector product in KOGELNIK, Eq.(8) (1967).

VECTOR PLANE WAVES - POLARIZATION

Let the electric vector $\underset{\sim}{E}$ represent a wave propagating in the z direction. Then Eq(2) takes the form

$$\underset{\sim}{E}(z,t) = E_x \hat{i} + E_y \hat{j} \tag{23}$$

The harmonic components E_x and E_y are expressed by

$$E_x = A_x \cos(\omega t - kz + \phi_x) \tag{24}$$

$$E_y = A_y \cos(\omega t - kz + \phi_y) \tag{25}$$

where A_x and A_y are independent of z.

At one fixed point on z the locus of the tip of the electric vector $\underset{\sim}{E}$, at time intervals $\frac{2\pi}{\omega}$, is called the polarization of the wave.

Using Eqs.(24) and (25) for $z = 0$, we get the equation of an ellipse[1],

$$\left(\frac{E_x}{A_x}\right)^2 + \left(\frac{E_y}{A_y}\right)^2 - \frac{2 E_x E_y}{A_x A_y} \cos\phi = \sin^2\phi \tag{26}$$

which depends only on ϕ for fixed values of A_x and A_y. Different types[2] of polarization are obtained for fixed amplitude values, namely, linear, circular and elliptical polarization.

1. BORN et al § 1.4 (1970).

2. Called "Polarization figure", see CLARKE (1974), SHURCLIFF, ch.1 (1962).

The use of complex notation simplifies the operations when dealing with polarizing elements, such as, polarizers and quarter wave plates[1]. Thus, Eqs.(24) and (25) become[2]

$$E_x = R_e \left(A_x e^{j\phi_x}\right) e^{j(\omega t - kz)} = \xi_x e^{j(\omega t - kz)} \tag{27}$$

$$E_y = R_e \left(A_y e^{j\phi_y}\right) e^{j(\omega t - kz)} = \xi_y e^{j(\omega t - kz)} \tag{28}$$

which define ξ_x and ξ_y.

Then , Eq.(23) can be written as

$$E = \left(\xi_x i + \xi_y j\right) e^{j(\omega t - kz)} = \underset{\sim}{\xi} e^{j(\omega t - kz)} \tag{29}$$

where $\underset{\sim}{\xi}$ is a complex vector.

The nature of the polarization is determined by the complex polarization vector P.

$$P = \frac{\xi_y}{\xi_x} = \frac{A_y}{A_x} e^{j(\phi_y - \phi_x)} = \frac{A_y}{A_x} e^{j\phi} \tag{30}$$

It is worthwhile to point out the difference in optical and electrical nomenclature with respect to the way the electric vector, acting as a phasor, rotates as it translates through space. Let us consider

1. BORN et al.§ 1.6 (1970). SHURCLIFF, Ch.2 & 8, (1962).
2. Note that the grouping of terms in Eqs.(27) and (28) is different from that in Eqs.(6) and (7). The polarization is considered unchanged throughout the field, see BORN et al., p36 (1970).

circular polarization. Suppose an observer stands on the positive z axis and looks towards the origin, z = 0. The electric vector will be seen rotating about the z axis and moving towards the observer.

Counterclockwise rotation of the electric vector is right handed in Electrical Engineering and left handed in Optics, and clockwise rotation is right handed in Optics and left handed in Electrical Engineering. Figs.(6) and (7) illustrate the way circular polarization advances.

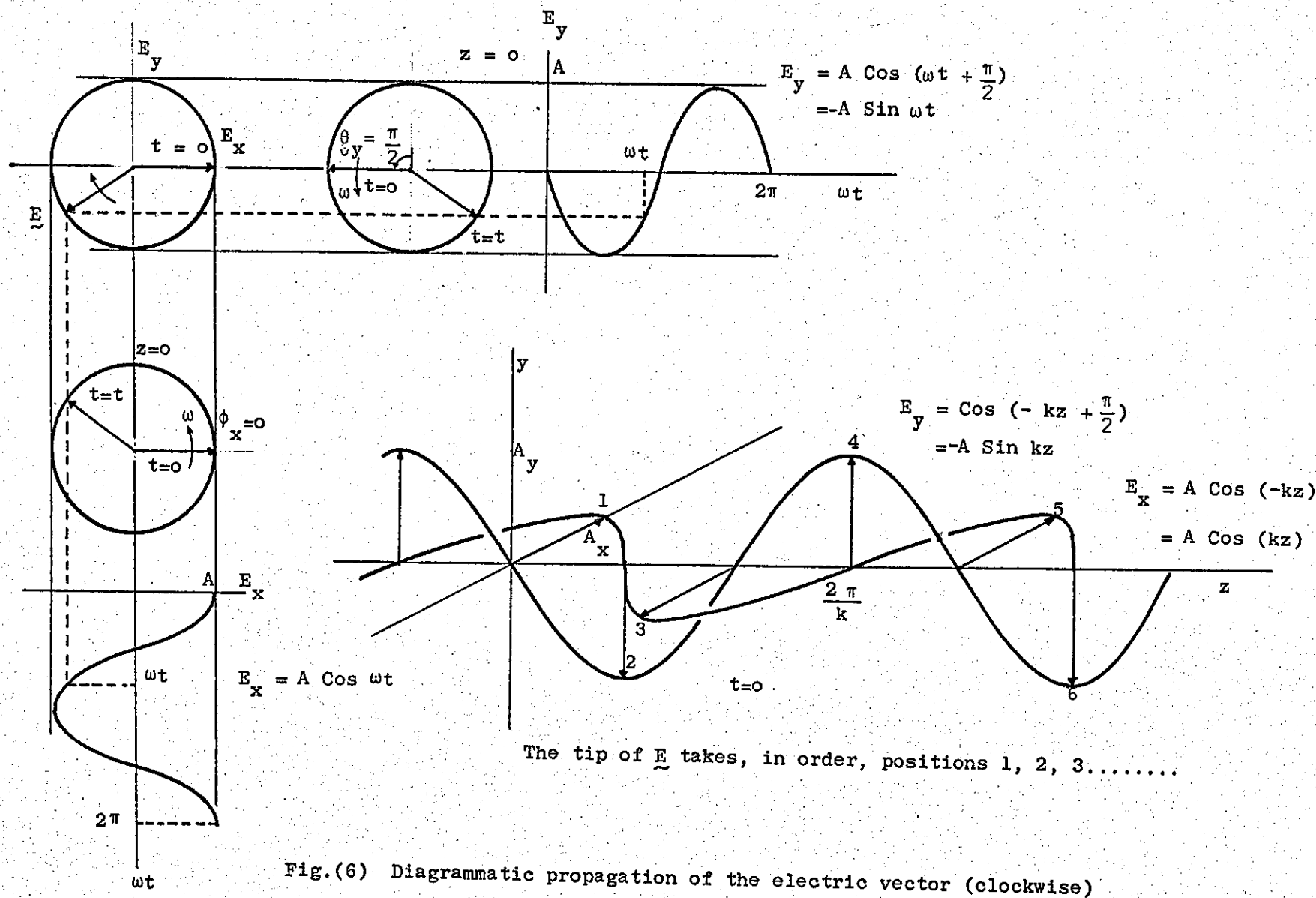

The tip of $\underset{\sim}{E}$ takes, in order, positions 1, 2, 3.....

Fig.(6) Diagrammatic propagation of the electric vector (clockwise)

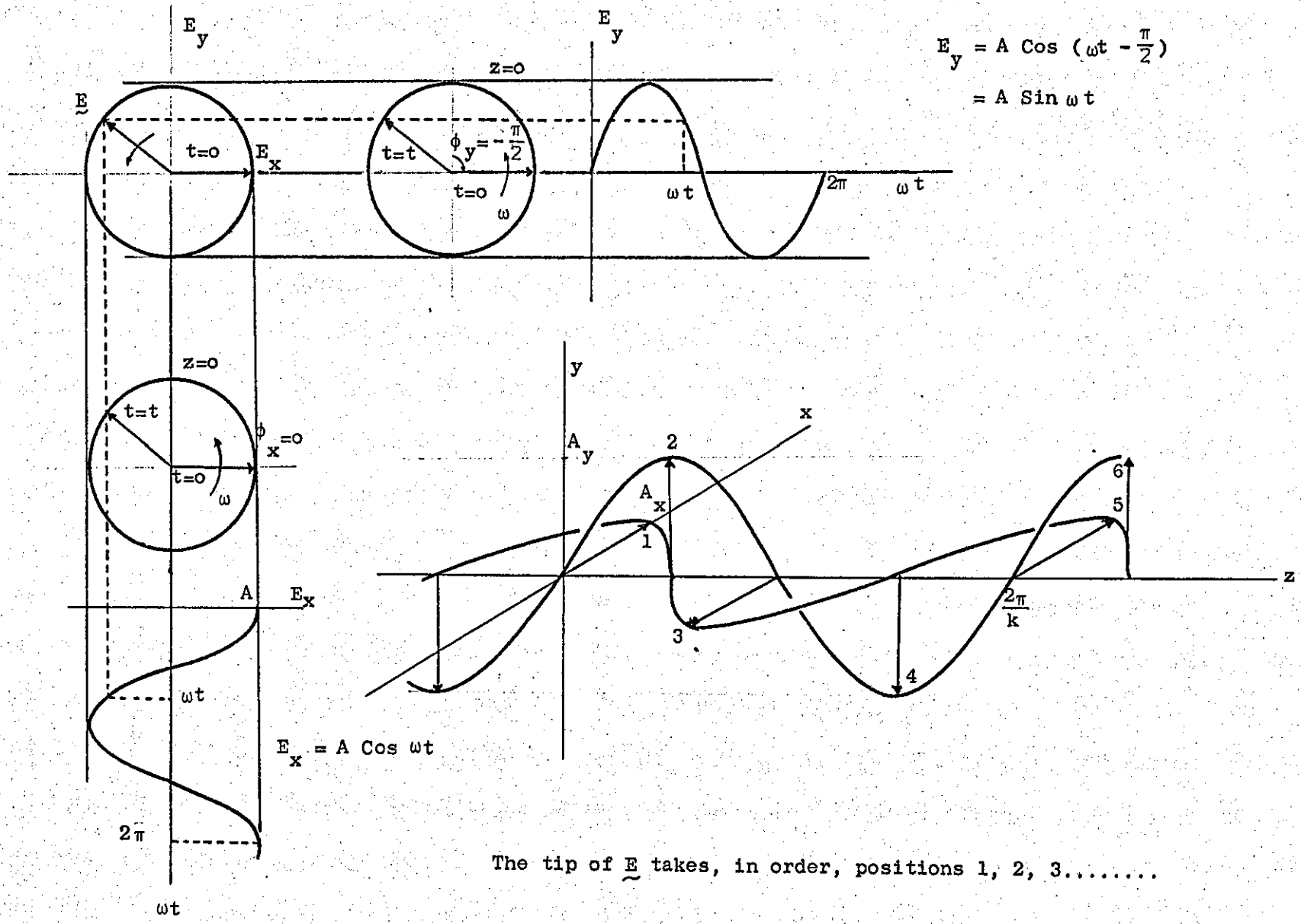

The tip of $\tilde{E}$ takes, in order, positions 1, 2, 3.....

Fig.(7) Diagrammatic propagation of the electric vector (counterclockwise)

Symbols

$\underset{\sim}{E}$	Electric vector
$\underset{\sim}{B}$	Magnetic induction vector
$\underset{\sim}{r}$	Position vector
t	Time
v_p	Phase velocity, BORN et al (1970) footnote ppll and 18. See Appendix A.
∇^2	Differential operator Nabla
E_i	Cartesian components of the electric vector $i = x,y,z$
$\hat{i},\hat{j},\hat{k}$	Unit vectors
ω	Angular frequency of the light vibration
ϕ	Constant phase angle (which specifies the state of polarization, see Appendix A)
$\hat{s}$	Unit vector in the direction of propagation
$k,\underset{\sim}{k}$	Wave number, vector wave number $\underset{\sim}{k} = k\hat{s}$
U	Complex amplitude
R_e	Indicates the real part of the expression
$A(\underset{\sim}{r}), \frac{A_o}{r}$	Plane wave amplitude, spherical wave amplitude
A_o	A constant
j	Complex number, $j = \sqrt{-1}$
I	Intensity
$< >$	Time average
$*$	Complex conjugate operation
C	Constant
n	0,1,2, ...
$\underset{\sim}{\xi}$	Complex vector
P	Complex polarization vector

CHAPTER II

HOLOGRAPHIC INTERFEROMETRY AND ELECTRONIC SPECKLE PATTERN INTERFEROMETRY

INTERFERENCE

Holography is essentially an interferometric phenomenon which can be easily manipulated using scalar wave theory. Let us first analyse the interference process of two coherent, monochromatic, spherical wavefronts at a point P in space, Fig.(8)[1].

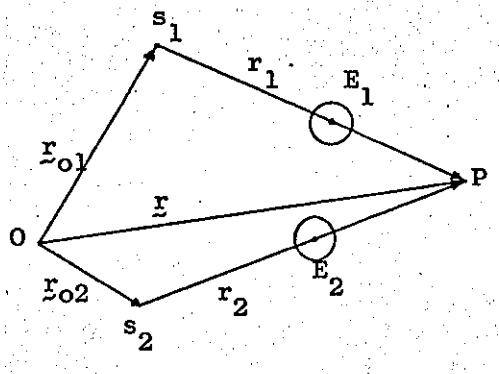

$$U_i = \frac{A_i}{r_i} e^{-j(kr_i - \phi_i)}$$

$$r_1 = |\underline{r} - \underline{r}_{o1}|$$

$$r_2 = |\underline{r} - \underline{r}_{o2}|$$

Fig.(8)

By the superposition principle the complex field at point P is given by

$$U_p = U_1 + U_2 \qquad (31)$$

1. It will be assumed, from now on, that the interfering wavefronts are linearly polarized and that its directions of vibration are parallel to each other, $\Omega = 0$, COLLIER et al, p158 (1971). E_1 and E_2 on Fig.(8) represent two linearly polarized beams having its plane of vibration perpendicular to the plane of the figure. Its direction of vibration are parallel to each other.

   See CLARKE (1974) for the preference to the use of "direction of vibration" or "azimuth of vibration"instead of "plane of polarization". Also see SHURCLIFF, Ch.1 (1962)

and the intensity

$$I = (U_1 + U_2)(U_1^* + U_2^*)$$

$$= \left(\frac{A_1}{r_1}\right)^2 + \left(\frac{A_2}{r_2}\right)^2 + \frac{A_1A_2}{r_1r_2} \exp\, j\left[k(r_2 - r_1) - (\phi_2 - \phi_1)\right]$$

$$+ \frac{A_1A_2}{r_1r_2} \exp\, j\left[k(r_2 - r_1) - (\phi_2 - \phi_1)\right] \qquad (32)$$

$$= I_1 + I_2 + 2\sqrt{I_1I_2} \cos\left[k(r_2 - r_1) - \phi\right] \qquad (33)$$

The expression for intensity, as seen in Eq.(33) includes the interference term $2\sqrt{I_1I_2}\cos\left[k(r_2 - r_1) - \phi\right]$ which causes the intensity to vary from point to point, taking maximum and minimum values,

$$I_{max} = I_1 + I_2 + 2\sqrt{I_1I_2}$$

$$I_{min} = I_1 + I_2 - 2\sqrt{I_1I_2} \qquad (34)$$

To determine the locus of points of maximum intensity[1] let ϕ be constant. Then, for I_{max}

$$\Delta = k(r_2 - r_1) - \phi = n2\pi$$

$$r_2 - r_1 = n\lambda + \frac{\phi\lambda}{2\pi} \qquad (35)$$

n(Integer)

Eq.(35) represents a family of hyperboloids, of two sheets[2], $r_2 - r_1$ = constant, where s_1 and s_2 are the fixed points. Fig.(9) illustrates the intersection of a family of hyperboloids with the plane of the figure. Let us call the lines originated by the intersection of that

1. For I_{min}, $\Delta = (2n + 1)\pi$

2. THOMAS, pp344, 416 (1972).

family of hyperboloids with any plane, interference lines.

Plane 1 on Fig. (9) will contain straight interference lines[1].

Note that if $r_2 - r_1 = 2a$ then the lines on a plane joining the two sources will be spaced by an equal distance, $\frac{\lambda}{2}$.

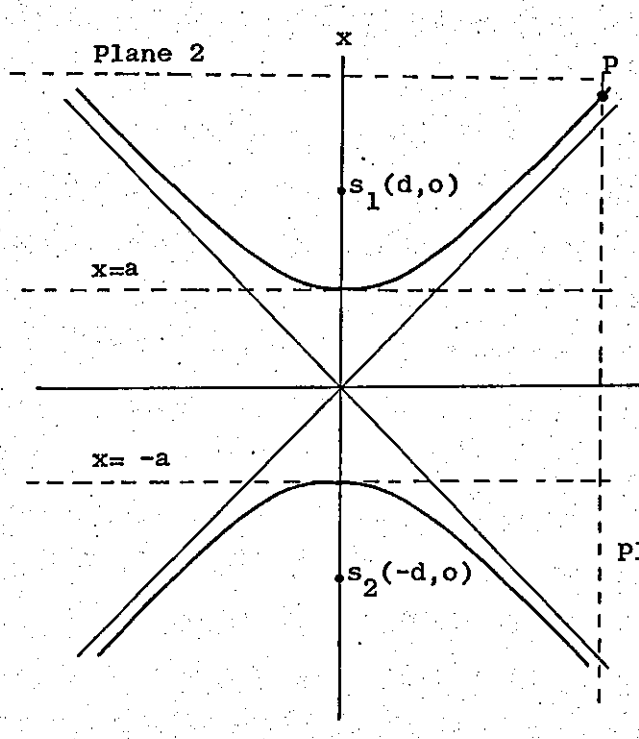

Hyperboloid

$$\frac{x^2}{a^2} - \frac{y^2}{b^2} - \frac{z^2}{c^2} = 1$$

Hyperbola

$$\frac{x^2}{a^2} - \frac{z^2}{c^2} = 1$$

Fig.(9)

The visibility of the interference lines is defined by[2]

$$V = \frac{I_{max} - I_{min}}{I_{max} + I_{min}} \qquad (36)$$

1. See TOLANSKY, p8 (1973).
2. See BORN et al (1970) § 10.4 where quasi-monochromatic light is considered. In this case the expression for visibility becomes

$$V = \frac{2\,|\gamma_{12}|\,\sqrt{R}\,\cos\,\Omega}{R + 1}$$

If we work well inside the limits for spatial coherence and temporal coherence the expression becomes simpler

$$V = \frac{2\sqrt{R}}{R + 1} \qquad \Omega = 0 \qquad \text{(Eq.36)}$$

sometimes referred to as modulation M. See also STROKE, §2.8 (1966) and COLLIER et al § 7.2.1 (1971).

as a quantitative measure of the line's contrast. Fig.(10)[1] shows a plot of the intensity as a function of the argument of the interference term, $\Delta = k(r_2 - r_1) - \phi$.

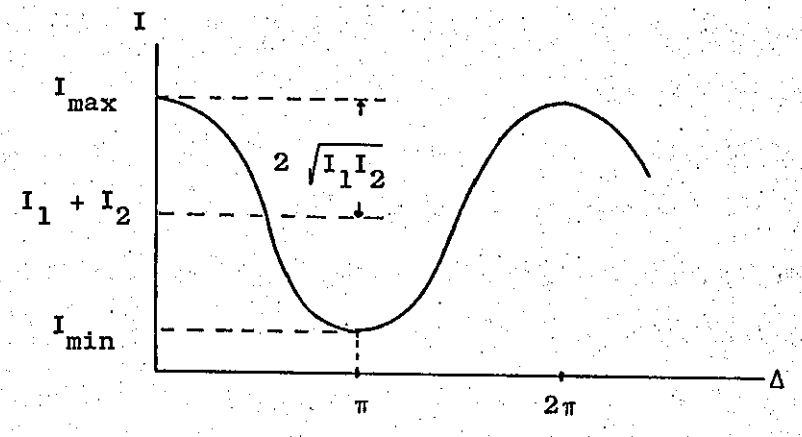

Fig.(10)

As can be seen from this figure maximum contrast, V = 1, is obtained for $I_{min} = 0$, that is, the ratio of the intensities is unity, R = 1.

1. Compare Fig. (10) with Fig. (10.2) in BORN § 10.4

INTRODUCTION TO HOLOGRAPHY

Let us consider the situation shown in Fig.(11) where s represents a point source. The complex amplitude of the electric field vector at a position r in space is expressed by

$$U(\underset{\sim}{r}) = A(\underset{\sim}{r}) \exp\left[jg(\underset{\sim}{r})\right] \qquad (37)$$

where the amplitude A(r) and the phase vary on the recording x-y plane according to the expressions $A(r) = A_o/R$ and $g(\underset{\sim}{r}) = -(\underset{\sim}{k}.\underset{\sim}{r} - \phi)$ respectively. A_o is a constant. The phase g(r) is constant for each point on the recording plane provided the light is coherent, therefore, it is easier to express it with respect to the origin o on that plane.

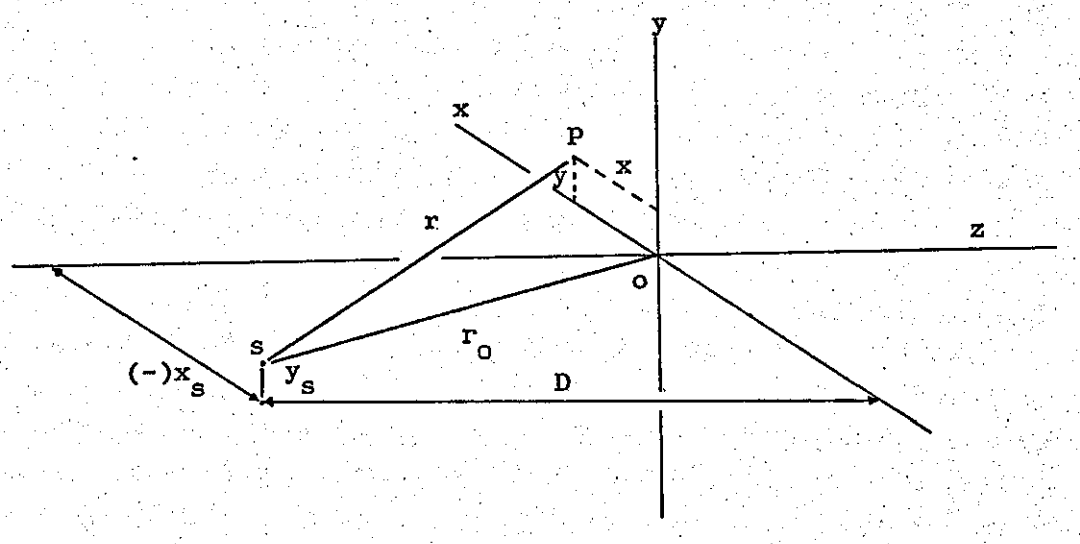

Fig.(11)

Thus the phase at point P in Fig.(11) takes the form

$$g(\underset{\sim}{r}) = g(\underset{\sim}{r}_o) + g(\Delta\underset{\sim}{r}) \tag{38}$$

where $\Delta\underset{\sim}{r} = \underset{\sim}{r} - \underset{\sim}{r}_o$.

If we consider the Fresnel approximation, the distances to the x-y plane may be written as

$$r \simeq D + \frac{(x_s - x)^2}{2D} + \frac{(y_s - y)^2}{2D} \tag{39}$$

$$r_o \simeq D + \frac{(x_s^2 + y_s^2)}{2D}$$

thus,

$$g(\Delta r) = g(r) - g(r_o) \simeq -\frac{2\pi}{\lambda}\,\frac{(x^2 + y^2 - 2\,x\,x_s - 2\,y\,y_s)}{2D}$$

$$= -\frac{2\pi}{\lambda}\left[\frac{x^2 + y^2}{2D} + (\alpha\,x + \beta y)\right] \tag{40}$$

where the expressions for the direction cosines of r_o are approximated by[1]

$$\left.\begin{aligned} \alpha &\simeq -\frac{(-)\,x_s}{D} \\ \beta &\simeq -\frac{y_s}{D} \end{aligned}\right\} \quad \text{for} \quad \begin{aligned} &D >> x, y \\ &D > 0 \\ &r_o \simeq D \end{aligned} \tag{41}$$

Let us refer to $g(\Delta r)$ by $g(x,y)$, the phase of the wavefront at position (x,y) with respect to position $(0,0)$ on the recording plane, so that the complex amplitude at (x,y) may be expressed as

$$U(x,y) = A(x,y)\,\exp\left[j\,g(x,y)\right] \tag{42}$$

1. Depending on the coordinate position: $(\pm)\,x_s$, $(\pm)y_s$.

We will consider now the recording on the x-y plane of the interference pattern produced by two point sources and the subsequent reconstruction process.

The coordinates of the reference and object sources are $(\pm x_r, \pm y_r, D_r)$ and $(\pm x_o, \pm y_o, D_o)$ respectively, and the distance D take positive values to the left of the x-y plane, Fig.(11).

The complex amplitudes of both wavefronts are expressed as:

$$U_o(x,y) = A_o(x,y) \exp(j\, g_o(x,y)) \tag{43}$$

where $$g_o(x,y) \simeq -\frac{2\pi}{\lambda}\left[\frac{x^2 + y^2}{2\, D_o} + (\alpha_o\, x + \beta_o\, y)\right] \tag{44}$$

and $$U_r(x,y) = A_r(x,y) \exp\left[j\, g_r(x,y)\right] \tag{45}$$

where $$g_r(x,y) \simeq -\frac{2\pi}{\lambda}\left[\frac{x^2 + y^2}{2\, D_r} + (\alpha_r\, x + \beta_r\, y)\right] \tag{46}$$

The expression for the spatial intensity distribution on the recording plane is written in the form

$$\begin{aligned} I(x,y) &= (U_o + U_r)\,(U_o + U_r)^* \\ &= I_o + I_r + 2\sqrt{I_o I_r}\ \cos(g_o - g_r) \\ &\simeq I_r\left[1 + 2\sqrt{(I_o/I_r)}\cos(g_o - g_r)\right] \\ &\qquad \text{for } I_r >> I_o \end{aligned} \tag{47}$$

1. Under reconstruction the contribution of the term I_o will be an undesirable background light in the trajectory of the reconstructed object wavefront. For the case of diffuse objects it will represent a speckle pattern formed by self interference of the (coherent) light from the diffuse object. A large reference to object beam ratio, say 4:1, will diminish the contribution of that background noise. See UPATNIEKS (1970) for a treatise of signal to noise ratio in dielectric hologram gratings.

thus we can write

$$\frac{\Delta I}{I_r} = \frac{I - I_r}{I_r} = 2\sqrt{\frac{I_o}{I_r}}\cos(g_o - g_r) = 2\frac{A_o}{A_r}\cos(g_o - g_r) \qquad (48)$$

such that the complex amplitude transmittance, Eq.(139), becomes

$$\dagger = \dagger_o\left(1 - \frac{\gamma}{2}\frac{\Delta I}{I_r}\right) = \dagger_o\left[1 - \gamma\frac{A_o}{A_r}\cos(g_o - g_r)\right] \qquad (49)$$

where I_r represents the bias intensity.

During reconstruction the incident wavefront on the plate is expressed by

$$U_c(x,y) = A_c(x,y)\exp\left[j\, g_c(x,y)\right] \qquad (50)$$

where
$$g_c(x,y) \simeq -\frac{2\pi}{\lambda}\left[\frac{x^2 + y^2}{2\,D_c} + (\alpha_c\, x + \beta_c\, y)\right] \qquad (51)$$

The complex amplitude of the field immediately behind the plate takes the form

$$\begin{aligned} U_\dagger &= U_c\dagger \\ &= \dagger_o A_c \exp(j\, g_c) - \dagger_o \frac{\gamma}{2}\frac{A_o A_c}{A_r}\Big[\exp\left[j(g_o - g_r + g_c)\right] \\ &\qquad + \exp\left[-j(g_o - g_r + g_c)\right]\Big] \\ &= \dagger_o A_c \exp(j\, g_c) - \dagger_o\gamma\frac{A_o A_c}{A_r}\cos(g_o - g_r + g_c) \end{aligned} \qquad (52)$$

The argument of the interference term in the last equation can be written as

$$\begin{aligned} (g_o - g_r + g_c) &\cong -\frac{2\pi}{\lambda}\Big[x(\alpha_o - \alpha_r + \alpha_c) + y(\beta_o - \beta_r + \beta_c) \\ &\qquad + \frac{x^2 + y^2}{2}\left(\frac{1}{D_o} - \frac{1}{D_r} + \frac{1}{D_c}\right)\Big] \\ &= -\frac{2\pi}{\lambda}\left[x\alpha' + y\,\beta' + \frac{x^2 + y^2}{2}\left(\frac{1}{D'}\right)\right] \end{aligned} \qquad (53)$$

where α', β' and D' are the direction cosines and the perpendicular distances from the plate of the reconstructed image respectively.

A particular simple case occurs when $U_c = U_r$, then $\alpha' = \alpha_o$, $\beta' = \beta_o$, $D' = D_o$ and Eq.(52) becomes

$$U_{\dagger} = \dagger_o\left[A_r \exp(j\, g_r)\right] - \dagger_o \frac{\gamma}{2}\left[A_o \exp(j\, g_o)\right] - \dagger_o \frac{\gamma}{2}\left[A_o \exp(-j\, g_o)\right] \quad (54)$$

The second term represents a divergent wavefront and is an exact replica of the object point source except for the constant factor. Because the image is formed to the left of the plate ($D' = D_o$) it is called virtual image. The third term represents a convergent spherical wavefront forming a point source (real image) at the right of the plate, $D' = -D_o$. The first term is a duplicate of the reference wavefront.

The different directions of the three wavefronts are indicated by its respective direction cosines.

HOLOGRAPHIC INTERFEROMETRY

Introduction

The analysis of the previous section for a point source, Fig.(11) can be extended to an infinite number of points as to represent an illuminated diffuse surface. Therefore, under certain conditions, the reconstructed virtual image of an object can be superimposed exactly to the illuminated object in its original state, Eq.(54). In this situation any variation on the object produces a corresponding fringe pattern in the viewing direction[1]. The application of holography to the analysis of the infinitesimal changes undergone by an object subjected to the action of external agents (load, temperature, vibration, shape, say) is known as Holographic Interferometry[2]. The object is analysed according to the effects of the external agents on its surface if it is opaque, or according to the refractive index changes if the object is translucid and homogeneous.

As a preamble to Electronic Speckle Pattern Interferometry (ESPI) an introduction to the theory of Real Time (RT), Double Exposure (DE), and Time Average (TA) Holographic Interferometry applied to opaque objects is considered in this section. We will only be concerned with the formation process of the fringes taking into account the photographic plate characteristics.

1. We will refer to these interference fringes as "fringes" to differentiate them from the "Interference lines" on the hologram, see Fig.(5) and Chapter III.

2. Only cw lasers as the light source will be considered here.

The application of holographic interferometry to the analysis of strain and amplitude of vibration in practical problems makes it possible to get information which is difficult to obtain otherwise, BURCH (1975). Its application to strain analysis was first reported by HILDEBRAND and HAINES (1965-1966). Subsequent improvements to the theory were made by ALEKSANDROV et al (1967), ENNOS (1968) and SOLLID (1969) - VEST (1973)[1]. The difficulty of obtaining the desired information from the fringe pattern, in most applications, has been clearly explained by BURCH (1974)[2], and a number of practical applications have appeared in the literature[3]. Lately efforts have been made to ease the obtaining of fringe data and its mathematical manipulation by means of optical, electronic and digital processing, VARNER, (b),(ERF, Ed.(1974)), BELLANI et al (1974), BRUNNING et al (1974), CHAMPAGNE (1972), LÄNDLIKER et al (1975).

Equally to strain the literature about applications of holography to the analysis of small amplitude[4] of vibration is considerable. A review of the main aspects of the subject is found in FRYER (1970) and ERF (1974)[5].

1. Rigid body motion and deformation have been analysed by STETSON (1975, 1974, 1970).

2. See also BOONE (1975), KING (1974), ENNOS (ERF, Ed. (1974)).

3. See: ERF, Ed. (1974) for examples of applications, ABRAMSON (1972) for a convenient way to deal with the fringes, ADAMS, et al (1974) for the combined use of holography and speckle in image-plane holography for the determination of 3-D displacements, MATSUMOTO et al (1973), VIENOT et al Eds. Section 17 (1970), ARCHBOLD (1975).

4. FRYER, p518 (1970).

5. Articles of special interest, POWELL and STETSON (1965), ARCHBOLD et al (1968), POWELL (1970), WALL (1970), STETSON and WATERS, ERF Ed. (1974), HUGES (1975).

Single exposure hologram (Real Time)

Let the object wavefront U_o and the plane reference[1] wavefront U_r be expressed by

$$U_o(x,y) = A_o(x,y) \exp\left[j\, g_o(x,y) \right]$$

$$U_r(x,y) = A_r(x,y) \exp\left[j\, g_r(x,y) \right] \qquad (55)$$

where $g_o(x,y)$ are defined by Eqs.(44) and (46) respectively, and $\beta_r = 0$.

The complex amplitude of the electric field at P, Fig.(11) and the corresponding intensity are

$$U_p = U_o + U_r \qquad (56)$$

$$I = U_p U_p^* = I_o + I_r + U_o U_r^* + U_o^* U_r$$

Rearranging the last equation to obtain $(I - I_r)/ I_r$ and using Eq.(139) we can express the complex amplitude transmittance as

$$\dagger = \frac{\dagger_o}{2\, I_r} \left[2\, I_r - \gamma I_o - \gamma\, (U_o\, U_r^* + U_o^*\, U_r) \right] \qquad (57)$$

During reconstruction the reference wavefront U_r reconstructs the object wavefront U_o which is superimposed to the modified object wavefront U_o'. This is defined as

$$U_o' = A_o'(x,y) \exp\left[j\, g_o'(x,y) \right] \qquad (58)$$

1. Except for the control in the spatial frequency on the photographic plate (resolution) there is no difference in using either a plane or spherical reference wavefront. This is only a carrier of the information contained in the object wavefront. The interpretation of localisation of the reconstructed images is simplified using a plane reference wavefront, GOODMAN, p214 (1968), but this is irrelevant in the interpretation of the fringes.

The complex amplitude of the field before the hologram, U_H, is written as

$$U_H = U_o' + U_r \tag{59}$$

and the complex amplitude after the hologram as

$$U_\dagger = \dagger U_H \tag{60}$$

Substituting the above equations into Eq.(60) and after some operations it becomes

$$U_\dagger = \frac{\dagger_o}{2 I_r} \{ U_r (2 I_r - \gamma I_o) - [\gamma U_o'(U_o U_r^* + U_o^* U_r) + U_o^* \gamma U_r^2] + [U_o' (2 I_r - \gamma I_o) - U_o \gamma I_r] \} \tag{61}$$

Only the third term of Eq.(61) possesses the exact information about the original and final states of the object, and its intensity is written as

$$\text{Intensity} = (\frac{\dagger_o}{2 I_r}) \{ I_o' [2 I_r - \gamma I_o]^2 - [(2 I_r - \gamma I_o)(\gamma I_r) (U_o' U_o^* + U_o'^* U_o)] + I_o [\gamma I_r]^2 \} \tag{62}$$

The second term is called the interference term W and can be expressed as

$$W = \frac{\gamma \dagger_o}{2} (2 A_r^2 - \gamma A_o^2)(A_o A_o') \left\{ \exp[-j((g_o - g_o') + \pi)] + \exp[j((g_o - g_o') + \pi)] \right\}$$

$$= \gamma \dagger_o (2 A_r^2 - \gamma A_o^2)(A_o A_o') \cos[g_o(x,y) - g_o'(x,y) + \pi] \tag{63}$$

The interference term represents a spatial distribution of light intensity in space forming bright and dark bands referred to as interference fringes. Thus;

$$g_o(x,y) - g_o'(x,y) = n\pi \qquad \begin{matrix} n = 0,2,4 \ldots & \text{Dark fringe} \\ n = 1,3,5 \ldots & \text{Bright fringe} \end{matrix} \tag{64}$$

Double exposure hologram

The total exposure E_t of the holographic plate consists of a first exposure E (object in this original state) and a second exposure E' in which the object is in its final state.

The intensity at point P, Fig.(11) during the first exposure is given by:

$$I = \left|U_o\right|^2 + \left|U_r\right|^2 + U_o U_r^* + U_o^* U_r \tag{65}$$

and

$$E = I\ t \tag{66}$$

For the second exposure we have

$$I' = \left|U_o'\right|^2 + \left|U_r\right|^2 + U_o' U_r^* + U_o'^* U_r \tag{67}$$

and

$$E' = I'\ t \tag{68}$$

where t represents an equal time for the two exposures.

The complex amplitude transmittance, Eq.(138), then becomes

$$\dagger = \dagger_o \left(\frac{E_t}{E_o}\right)^{-\frac{\gamma}{2}} \tag{69}$$

where $E_t = E + E'$ and E_o is the bias exposure,

E_o = (Bias Intensity) t = (BI)t.

Substituting the above equations into Eq.(69) taking $2\left|U_r\right|^2$ as a factor and the remaining binomial series approximated to the first order term, we have

$$\dagger = C\left\{4\left|U_r\right|^2 - \left|\gamma\left[U_o\right|^2 + \left|U_o'\right|^2 + (U_o U_r^* + U_o^* U_r) + (U_o' U_r^* + U_o'^* U_r)\right]\right\} \quad (70)$$

where C is a complex constant and $I_r > I_o$, $I_r > I_o'$.

During reconstruction the hologram is illuminated by the original reference wavefront U_r, and the complex amplitude of the field after the hologram is

$$U_\dagger = \dagger U_r$$

$$= C\{U_r\ 4\left[U_r\right|^2 - \gamma(U_o^{\,2} + U_o'^{\,2})] - \gamma\left|U_r\right|^2\left[U_o + U_o'\right]$$

$$- \gamma U_r^{\,2}\left[U_o^* + U_o'^*\right]\} \quad (71)$$

Only the second term of Eq.(71) possesses the exact information about the original and final states of the object, and its intensity is written as

$$\text{Intensity} = (C\gamma U_r^{\,2})^2\left[\left|U_o\right|^2 + \left|U_o'\right|^2 + (U_o U_o'^* + U_o^* U_o')\right] \quad (72)$$

The third term is called the interference term W and can be expressed as

$$W = C A_o(x,y) A_o'(x;y) \cos\left[g_o(x,y) - g_o'(x,y)\right] \quad (73)$$

where extra constant terms have been included in C.

The interference term represents a spatial distribution of light intensity forming bright and dark bands referred to as interference fringes. Thus

$$g_o(x,y) - g'_o(x,y) = n\pi \qquad \begin{matrix} n = 0,2,4 \ldots \text{ Bright fringe} \\ n = 1,3,5 \ldots \text{ Dark fringe} \end{matrix} \qquad (74)$$

The phase difference of π between Eqs. (64) and (74) is illustrated in Figs.(14a) and (b), where (a) shows the fringes due to displacement of a cantilever beam, real time on the left and double exposure on the right, and (b) shows the fringes corresponding to a displacement undergone by a circular plate clamped by its edge[1] when a concentrated load was applied at its centre, real time on the top half and double exposure on the bottom.

Interpretation of the fringes

Fig.(12) illustrates the original and final positions of a point on the surface of an object[2], q and f respectively, a light source s, a point p on the photographic plate (in the viewing direction) and an arbitrary reference point o.

$\hat{r}_1$, $\hat{r}_2$, $\hat{r}_3$, $\hat{r}_4$ are unit vectors.

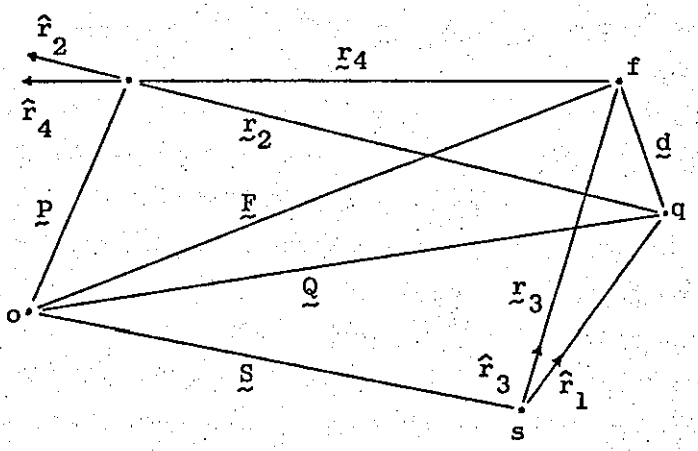

Fig.(12)

1. BOONE et al (1969).
2. In practice $\overline{qf}$ is an infinitesimal displacement.

We are interested in the change of phase due to the displacement of a point on the object surface from position q to position f, i.e. $\Delta g = g_q - g_f$.

According to Figs. (8) and (12) the phase associated to the optical paths sqp and sfp take the form

$$g_q = -\frac{2\pi}{\lambda}(\underset{\sim}{r}_1.\hat{r}_1 + \underset{\sim}{r}_2.\hat{r}_2 + \phi) \tag{75}$$

and

$$g_f = -\frac{2\pi}{\lambda}(\underset{\sim}{r}_3.\hat{r}_3 + \underset{\sim}{r}_4.\hat{r}_4 + \phi) \tag{76}$$

From Fig.(12) we have

$$\underset{\sim}{r}_1 = \underset{\sim}{Q} - \underset{\sim}{S} \tag{77}$$

$$\underset{\sim}{r}_2 = \underset{\sim}{P} - \underset{\sim}{Q} \tag{78}$$

$$\underset{\sim}{r}_3 = \underset{\sim}{F} - \underset{\sim}{S} \tag{79}$$

$$\underset{\sim}{r}_4 = \underset{\sim}{P} - \underset{\sim}{F} \tag{80}$$

$$\hat{r}_3 = \hat{r}_1 + \Delta r_1 \tag{81}$$

$$\hat{r}_4 = \hat{r}_2 + \Delta r_2 \tag{82}$$

Substituting the above equations into Eqs.(75) and (76) we obtain

$$g_q = -\frac{2\pi}{\lambda}\left[(\underset{\sim}{Q} - \underset{\sim}{S}).\hat{r}_1 + (\underset{\sim}{P} - \underset{\sim}{Q}).\hat{r}_2 + \phi\right] \tag{83}$$

$$g_f = -\frac{2\pi}{\lambda}\left[(\underset{\sim}{F} - \underset{\sim}{S}).(\hat{r}_1 + \Delta\hat{r}_1) + (\underset{\sim}{P} - \underset{\sim}{F}).(\hat{r}_2 + \Delta\hat{r}_2) + \phi\right] \tag{84}$$

thus,

$$\Delta g = g_q - g_f = -\frac{2\pi}{\lambda}\left[(\underset{\sim}{Q} - \underset{\sim}{F}).(\hat{r}_1 - \hat{r}_2) - (\underset{\sim}{F} - \underset{\sim}{s})\Delta\hat{r}_1 - (\underset{\sim}{P} - \underset{\sim}{F})\Delta\hat{r}_2\right] \tag{85}$$

If we assume that infinitesimal displacements take place

$$\left|\underset{\sim}{r}_1\right| \simeq \left|\underset{\sim}{r}_3\right|$$

$$\left|\underset{\sim}{r}_2\right| \simeq \left|\underset{\sim}{r}_4\right| \qquad \therefore \left|\underset{\sim}{r}_1\right|, \left|\underset{\sim}{r}_2\right| >> \left|\underset{\sim}{Q} - \underset{\sim}{F}\right| \tag{86}$$

then

$$(\underset{\sim}{F} - \underset{\sim}{S}).\,\Delta\hat{r}_1 = 0 \quad , \quad (\underset{\sim}{P} - \underset{\sim}{F}).\,\Delta\hat{r}_2 = 0 \tag{87}$$

and Eq. (85) can be written as

$$\Delta g = -\frac{2\pi}{\lambda}\left[(\underset{\sim}{Q} - \underset{\sim}{F}).(\hat{r}_1 - \hat{r}_2)\right] \tag{88}$$

The vector $\hat{r}_1 - \hat{r}_2$ is called the sensitivity vector[1].

Therefore, comparing Eq. (88) with Eqs. (64) and (74), where g_q and q_f correspond to g_o and g'_o, it can be readily seen that the fringes represent the loci of points of equal vector displacement $\underset{\sim}{d} = (\underset{\sim}{Q} - \underset{\sim}{F})$.

Time average hologram

Fig. (13) shows a lateral cross section of a circular plate[2] where the solid line indicates its equilibrium position, and the dotted lines indicate the two extreme positions of a sinusoidal vibrating motion. For simplicity let us consider the positions of q and f on the plane of the figure.

Because only one exposure is necessary the interest now is to find the expression for the phase time-variation of the object wavefront U'_o.

1. BURCH, Eq.(2), (1974).

2. COLLIER et al. p439, (1971)

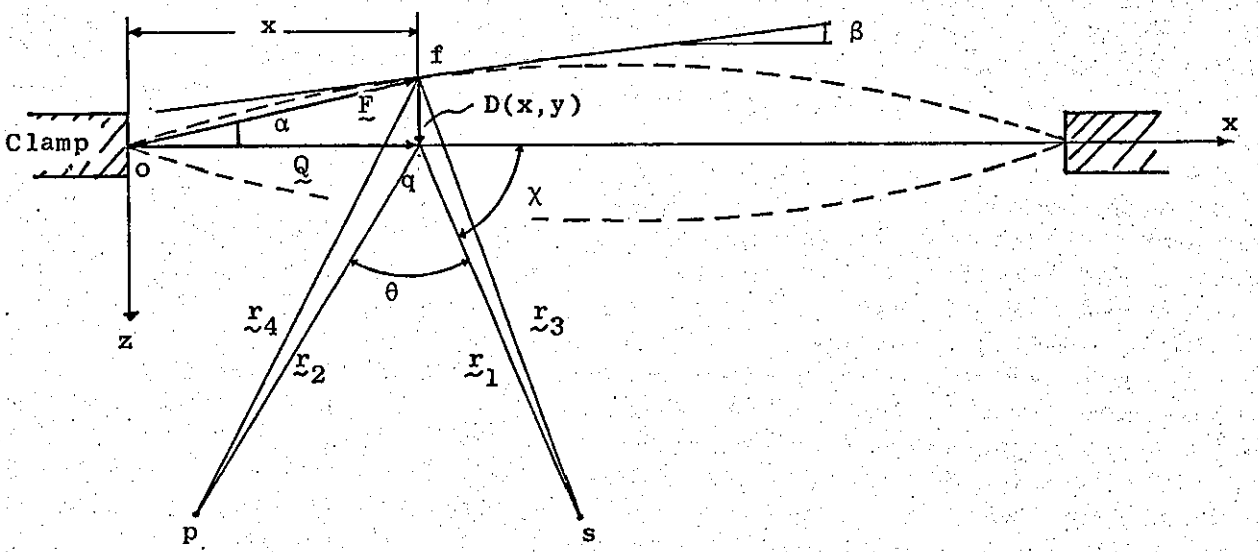

Fig.(13)

According to Figs. (12) and (13) the rectangular components of vectors $\underset{\sim}{Q}$ and $\underset{\sim}{F}$ are $Q_x = x$, $Q_y = Q_z = 0$ and $F_x = x$, $F_y = 0$, $F_z = D(x,t)$ respectively, and

$$D(x,t) = D(x) \cos(\omega t + \phi) \tag{89}$$

where $D(x)$ is the amplitude, ω the angular frequency and ϕ is the phase.

The coordinates of points s and p are $(x_s, 0, z_s)$ and $(x_p, 0, z_p)$ respectively. The position vectors $\underset{\sim}{r}_1$ and $\underset{\sim}{r}_2$ are expressed by

$$\begin{aligned} \underset{\sim}{r}_1 &= \left| x_s - x \right| \hat{i} - z_s \hat{k} \\ \underset{\sim}{r}_2 &= \left| x_p - x \right| \hat{i} - z_p \hat{k} \end{aligned} \tag{90}$$

so that

$$\hat{r}_1 = \frac{|x_s - x|}{R_s}\hat{i} - \frac{z_s}{R_s}\hat{k} = \cos\chi\,\hat{i} - \sin\chi\,\hat{k}$$

$$\hat{r}_2 = \frac{|x_p - x|}{R_p}\hat{i} + \frac{z_s}{R_p}\hat{k} = -\cos(\chi + \theta) + \sin(\chi + \theta) \qquad (91)$$

where $R_s = \sqrt{(|x_s - x|^2 + z_s^2)}$ and $R_p = \sqrt{(|x_p - x|^2 + z_p^2)}$

The instantaneous phase difference can be expressed by Eq.(88), so that after substitition of the above equations we obtain[1]

$$\Delta g(x,t) = -\frac{2\pi}{\lambda}\left[\underset{\sim}{Q}.\hat{r}_1 - \underset{\sim}{Q}.\hat{r}_2 - \underset{\sim}{F}.\hat{r}_1 + \underset{\sim}{F}.\hat{r}_2\right]$$

$$= -\frac{2\pi}{\lambda} D(x)\cos(\omega t + \phi)\left[\sin\chi + \sin(\theta + \chi)\right] \qquad (92)$$

The total instantaneous complex amplitude at the photographic plate during exposure is

$$U_p(x,t) = U_r + U_o' = A\exp\left[j\,g_r(x)\right] + U_o(x)\exp\left[j^{\Delta}\,g_o(x,t)\right] \qquad (93)$$

where $U_o(x)$ is the object complex amplitude in the equilibrium position, and $^{\Delta}g_o(x,t)$ is the phase shift introduced to take into account the variations of the optical path while the object is vibrating, Eq.(92).

Each position of the vibrating object will contribute to the total exposure which will be proportional to the time average of the intensity over the exposure time, then

1. Notice that $\Delta g(x,t)$ represents, in this case, an instantaneous value.

$$\langle I(x,t)\rangle = \langle\langle U_p\, U_p^{*}\rangle = \frac{1}{T}\int_0^T I(x,t)\,dt$$

$$= \frac{1}{T}\int_0^T \left[\,|U_o'|^2 + |U_r|^2 + U_o'^{*}\,U_r + U_o'\,U_r^{*}\,\right] \tag{94}$$

For simplicity T is chosen to be equal to the period of the harmonic motion,[1] $\frac{2\pi}{\omega}$.

Only the last term of the integrand has the information about the object, thus using Eqs.(92),(93) and (94) we can write[2]

$$\langle I(x,t)\rangle \propto \frac{1}{T}\int_0 (U_o'\,U_r^{*})\,dt = \frac{U_r^{*}}{2\pi}\int_0^{2\pi} U_o'\,d(\omega t)$$

$$= \frac{U_r^{*}\,U_o(x)}{2\pi}\int_0^{2\pi} \exp\left\{-j\left[\frac{2\pi}{\lambda}D(x)\left(\sin\chi + \sin(\theta+\chi)\right)\right]\right.$$

$$\left.\cos(\omega t + \phi)\right\}\,d(\omega t)$$

$$= U_r^{*}\,U_o(x)\,J_o\left[\frac{2\pi}{\lambda}D(x)\left(\sin\chi + \sin(\theta+\chi)\right)\right] \tag{95}$$

1. An alternative could be to consider T as the exposure time.

2. $J_n(z) = \frac{1}{\pi}\int_0^{\pi}\cos(z\sin p - np)\,dp = \frac{1}{2\pi}\int_{-\pi}^{\pi}\exp\left[j\,(z\sin p - np)\right]dp$

for $n = 0,1,2\ldots$.

If $p = \frac{\pi}{2} + (\omega t + \phi)$ and $n = 0$, we have

$$J_o(z) = \frac{1}{\pi}\int_0^{\pi}\cos\left[z\cos(\omega t + \phi)\right]\,d(\omega t)$$

$$= \frac{1}{2\pi}\int_0^{\pi}\exp\left[j\,(z\cos(\omega t + \phi))\right]\,d(\omega t)$$

where $d\left[\frac{\pi}{2} + (\omega t + \phi)\right] = d(\omega t)$

For $z = -\frac{2\pi}{\lambda}D(x)\left[\sin\chi + \sin(\theta+\chi)\right]$

$$J_o(z) = \frac{1}{2\pi}\int_0\exp\left\{-j\left[\frac{2\pi}{\lambda}D(x)\left(\sin\chi + \sin(\theta+\chi)\right)\cos(\omega t + \phi)\right]\right\}d(\omega t)$$

$J_o(z) = J_o(-z)$ See JAHNKE et al (1960)

During reconstruction the complex amplitude after the hologram is given by

$$U_{\dagger} = U_r \dagger \propto U_r < I(x,t) > \tag{96}$$

Therefore the complex amplitude and the intensity at the observation point are expressed by

$$U_{\dagger} \propto U_o(x)\, J_o \left[\frac{2\pi}{\lambda} D(x) \left(\sin \chi + \sin (\theta + \chi) \right) \right] \tag{97}$$

and

$$I(x) = U_{\dagger}\, U_{\dagger}^{*} \propto \left| U_o(x) \right|^2 \left\{ J_o \left[\frac{2\pi}{\lambda} D(x) \left(\sin \chi + \sin (\theta + \chi) \right) \right] \right\}^2 \tag{98}$$

It can be seen from the last equation that the intensity of the object in the equilibrium position $\left| U_o(x) \right|^2$ is modulated by the function $J_o^{\,2}$, therefore a bright fringe will correspond to a maxima of the $J_o^{\,2}$ function and a dark fringe to the zero values of that function.

$$D(x) = \frac{n \lambda}{2(\sin \chi + \sin (\theta + \chi))} \qquad \begin{array}{l} n = 0,2,4 \ldots \text{ Bright fringe. Node} \\ n = 1,3,5 \ldots \text{ Dark fringe} \end{array} \tag{99}$$

The clamped region of the vibrating square plate illustrated in Fig.(14)(c) is at its centre.* Therefore, only the interference of the two wavefronts corresponding to the extreme positions is observed and the fringes are interpreted as contour lines of equal displacement of the object surface. Notice that ω and ϕ are lost during the time average operation and the contrast of the fringes is sharply reduced by increasing the amplitude of vibration, POWELL (1970), FRYER (1970).

* During reconstruction all the instantaneous positions of the object are reconstructed according to a weighting factor proportional to their contribution to the total exposure[1].

1. BUTTERS, ch.7 (1971)

Real time hologram (vibration)

We start the derivation from Eq.(63), (real time, static), thus

$$W \propto 2|U_o|^2 \cos[\Delta g(x,t) + \pi] \qquad (100)$$

where $\Delta g(x,t)$ is defined by Eq.(92).

During observation, the photographic film or the eye will respond to the average intensity, therefore

$$I = \langle W \rangle = 2|U_o|^2 \{1 - J_o[\frac{2\pi}{\lambda} D(x) (\sin\chi + \sin(\theta+\chi)) \ldots]\}^{\frac{1}{2}} \qquad (101)$$

and

$$D(x) = \frac{n\lambda}{2(\sin\chi + \sin(\theta+\chi))} \qquad \begin{array}{l} n = 0,2,4 \ldots \text{Dark fringe. Node} \\ n = 1,3,5 \ldots \text{Bright fringe} \end{array} \qquad (102)$$

In practice the above condition is difficult to obtain and generally the "fixed" parts of the object appear bright as can be seen from Fig.(14) (c) and (d). It shows the time average (c) and real time (d) holographic pattern of a square thin metal plate vibrating at a frequency 22.7 kHz due to the action of a piezoelectric crystal placed in the back of the plate. Both show the fixed centre portion bright.

Observations[1]

According to the footnotes on pages 16 and 18 the use of a polarizer between the hologram and observation point was a common practice, as it improves the fringe contrast.[2] Also to control the

1. The results of Fig. (14) were obtained using amplitude holograms. 8E75 AGFA plates.
2. RUDDER (1967).

beam ratio two polarizers were used in the unexpanded reference beam. The first polarizer in the path of the beam decreases the beam intensity a certain amount and the other restores the original polarization and fixes the required beam intensity. This arrangement works as a variable neutral density filter. If during real time reconstruction[1] the first polarizer is rotated to increase the light intensity, and therefore increase the virtual image intensity to match that of the object, the interference fringe pattern translates periodically by an amount corresponding to a phase shift of π. The number and shape of the fringes remains the same.[2]

The rotation of the polarizer during reconstruction (real time) was needed because with an exposure ratio of 5:1 (reference to object beam) there is always the need for increasing the image intensity. An equalization of intensities, object and virtual image, was obtained for a ratio of about 20:1 without rotating the polarizer.

A beam ratio of nearly 20:1 (modulation 0.42) was found to be the most suitable for real time, a ratio of 2:1 for double exposure, and a ratio of 4:1 for time average.

1. The plates were processed in-situ, BUTTERS et al (1969).
2. STETSON et al (1965) suggests the use of an attenuator in the object beam. It was noticed that if a polarizer is used in this way the interference pattern is altered.

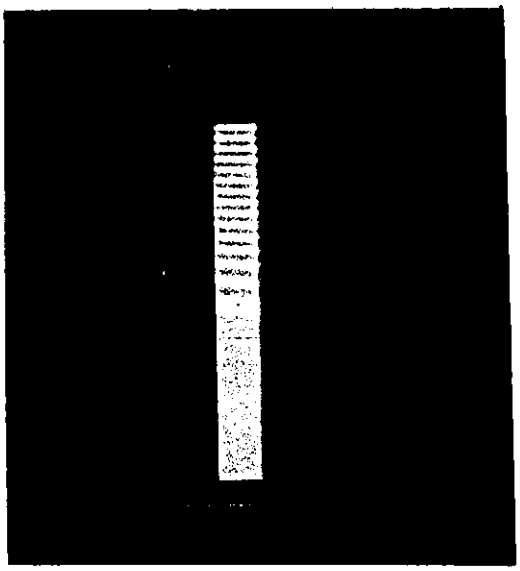

a

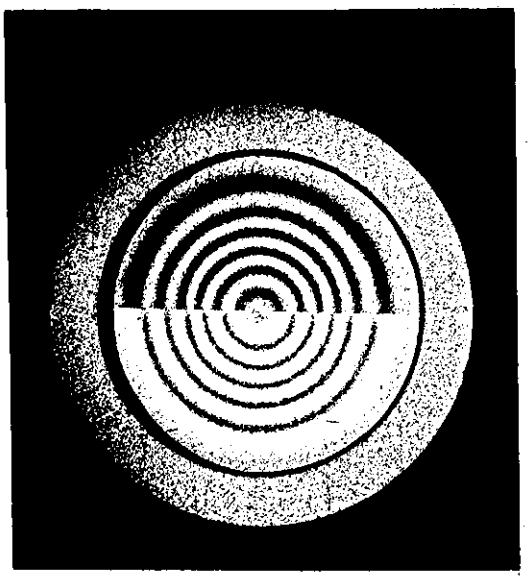

b

c

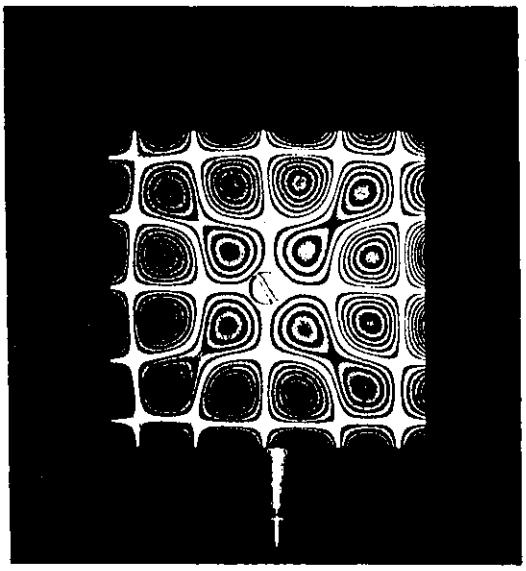

d

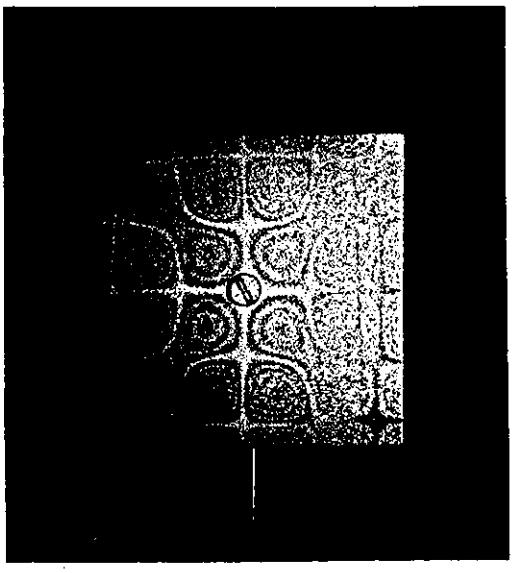

Fig. 14 (a) and (b) show the π phase difference between Eqs.(64) and (74). (c) and (d) show modes of vibration of the same object at the same frequency for time average and real time holography respectively.

UNIVERSITY OF TECHNOLOGY
LOUGHBOROUGH,
MECHANICAL ENGINEERING.

ELECTRONIC SPECKLE PATTERN INTERFEROMETRY

Introduction

Speckle interferometry embraces a diversity of applications in the NDT and NDI fields. While in some fields of coherent optics research is carried out to find ways of eliminating or reducing the speckle[1], in others the speckle is used as a metrological tool, ENNOS (1975)[2]. The roughness assessment of surfaces and decorrelation phenomenon related to wavelength, WYKES (1975), LEGER et al (1975), and the possibility of 3-D strain analysis in transparent and homogeneous models, CHIANG (1975), extends even further the potentials of speckle analysis and applications.

We have already referred to the information obtained by Holographic Interferometry techniques in strain analysis, and the difficulty in transforming that information into quantitative strain data.

Speckle interferometry discriminates between normal and in-plane displacement components, therefore providing an easier way to relate the fringe pattern to the strain configuration, ENNOS (ERF. Ed.(1974)). The low speckle spatial frequency allows for the use of television systems and so dispenses with the photographic recording, BUTTERS (1975), and also sets the conditions for a desensitized speckle photographic method, ARCHBOLD et al (1972).

1. McKECHNIE (1974), BURCH et al (1970).
2. Also see BURCH (1971) and (1974) for a review of the literature about the applications and mathematical formulation of speckle theory.

Electronic Speckle Pattern Interferometry

This subject has already been covered in various articles by BUTTERS, LEENDERTZ and DENBY[1] in its application to strain analysis, being the purpose here to add some comments on the optical and electronic (speckle) signal processing in conjunction with speckle pattern interferometry that will be useful in the discussions in the next Chapter.

In the space between a scattering surface illuminated with coherent light and the observer (image plane) a random interference phenomenon occurs by the contributions of the light scattered from different parts of the surface. Consider Fig.(15) where p is a point in a parallel plane between the scattering surface s and the image plane o, and l represents the imaging system.

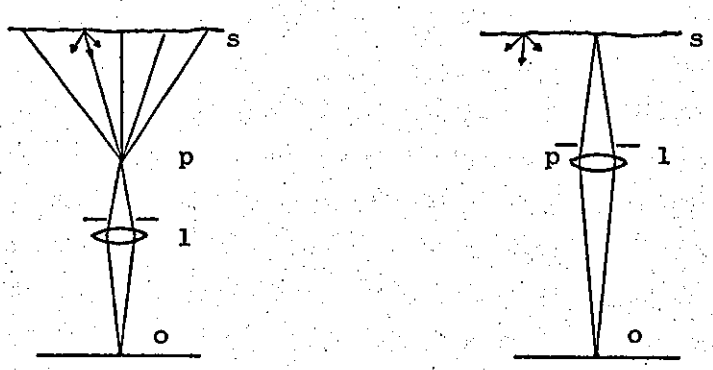

Fig.(15)

1. BUTTERS et al (1971-1972), DENBY et al (1974-1975).

In Fig. (15)(a), l images p on o. The random spatial frequency of the light intensity at p is not resolvable by the imaging system, only that determined by the Rayleigh Criterion, the speckle pattern.

To relate the speckle pattern to a point by point basis with the surface, an imaging system similar to the one illustrated in Fig. (15)(b) is used. Under this condition the speckle is of the same size than that portion of the surface whose scattered light contributes to the formation of the speckle in the first place, the size being determined by the Rayleigh Criterion.

Let us analyse the speckle at the surface, imaged on plane o. A speckle is formed by the random contributions of the light scattered by the surface. Fig. (16)(a) illustrates the vectorial representation of the formation of the speckle, where the small arrows represent random light vectors, A_s the amplitude of the resultant vector (the speckle amplitude) and ϕ its total phase.

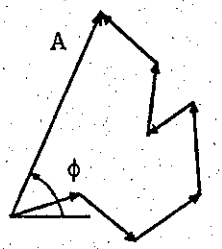

$I = A^2$

(a)

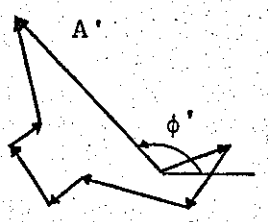

$I = A'^2$

(b)

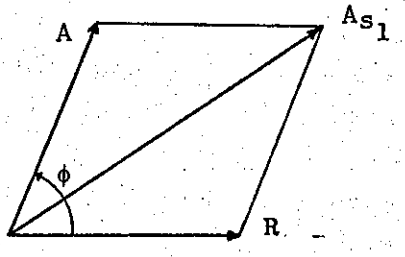

$I_1 = A_{s_1}^2 = A^2 + R^2 + 2AR \cos \phi$

(c)

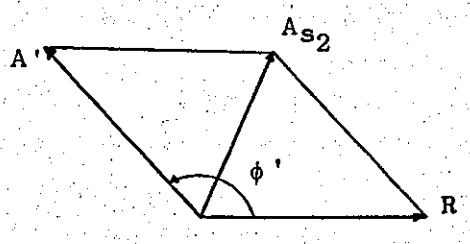

$I = A_{s_2}^2 = A'^2 + R^2 + 2AR \cos \phi'$

(d)

Fig.(16)

Assume now that the surface experiences a non-uniform infinitesimal change and the phases of the random vectors change accordingly, so that the final speckle amplitude is A', Fig.(16)(b). Neither of these two speckles (or speckle patterns), (a) and (b), give information about their phases, ϕ and ϕ'.

If a reference beam is made to interfere with the speckle patterns in the image plane, their amplitudes are modified according to their respective phases, ϕ and ϕ', giving new speckle patterns whose intensities are expressed in Figs.(16)(b) and (c).

The vidicon tube will scan the image at plane o, Fig. (15) (b) and the signal will be electronically processed as is illustrated in Appendix B. During the electronic subtraction the two speckle patterns corresponding to the original and final states of the object will behave as random moire grids, and the fringes will be formed by moire effect, "figure interference". The final signal is displayed on a television monitor, and its appearance is described below.

Let us assume that the resolution of the vidicon tube is approximately 25μ and its screen area 125 mm^2, also that the image area of the television screen is 3850 mm^2. Then we will have an approximate magnification of 30. Therefore the speckle size on the television screen will be about 3/4 of a millimetre. The image of the surface appears to be covered by a globule formation formed by sets of speckles. Therefore, for the fringes to be clearly distinct from the globules, the spatial distribution of surface displacement must be sufficiently gradual for a fringe period to be spread over several globules, a number of speckles.

When the surface is polished to a degree that produces almost no speckles, or none at all, the information is carried in the interference lines produced by the in-line superposition of the object and reference beams before the vidicon tube of the electronic speckle interferometer. There will be a family of interference lines for each of the two states of the surface. Any local phase change produced by some effect on the surface object (if opaque) will produce a corresponding local change in the interference lines, and fringes will appear by moire effect. This subject will be extended in the next Chapter.

The ESPI system includes a high-pass filter circuit that eliminates slowly varying brightness levels, and by differentiation doubles the number of globules or lines, improving, in this way, the fringe contrast, although good results are obtained without this step. The system also offers a range of magnification depending on the amount of light being returned into the system (from the object), the size of the object and the distinct number of fringes on the television screen. About 50 fringes can be clearly seen across the screen. If, for example, we consider about 30 fringes across the image on the television monitor, of an actual object size of 60 mm, and as the period of the fringe corresponds to a $\lambda/2$ displacement, then an intermediate value for the measurable strain will be about 125 microstrains.

Experiments have been carried out to process two speckle patterns, corresponding to the initial and final states of the object, using the ESPI system without the reference beam. The experiments were repeated exactly, using the reference beam, as a manner of control test.

When a silver sprayed surface was used, fringes of very poor contrast appeared identical to the fringes obtained using a reference beam. Actually, it was the specular light coming from the object surface itself which acted as a reference, (local reference beam, WATERS (ERF, Ed. 1974)). When the surface was tilted, as to cause the specular light not to enter the system, the fringes remained equal to the control ones, but the contrast was even worse. This suggests that in the small region of the surface that contributes to the formation of the speckle, exists tiny parts that reflect the light specularly. Furthermore, because the fringe contrast decreases as the surface is tilted, it is assumed that this specularly reflecting part has an angular distribution.

When a matt white sprayed surface was used, the fringes were imperceptible when static, and extremely difficult to observe while in motion, without knowing in advance, by the control test, its position and distribution. This indicates that very weak reflections in the system are acting as reference beams. Because both fringe patterns (test and control) were identical they correspond to displacement of the surface of $\lambda/2$. For a speckle pattern to act as a moire grating without reference beam, the displacement would have to be at least of the size of the grid pitch (size of the speckle) and the fringes would not be detected by simple inspection.

SYMBOLS

V	Visibility
R	Beam intensity ratio
γ_{12}	Degree of coherence or partial coherence factor
Ω	Angle between the directions of polarization of the interfering beams
BI	Bias intensity
W	Interference term
$\underset{\sim}{F},\underset{\sim}{Q},\underset{\sim}{S},\underset{\sim}{P}$	Position vectors of points f, q, s, and p respectively
$\underset{\sim}{d}$	Displacement vector
χ	See Fig.(13)

CHAPTER III

CONTOURING BY ELECTRONIC SPECKLE INTERFEROMETRY

INTRODUCTION

The preceding Chapter dealt with the applications of holographic and speckle interferometry to the analysis of infintesimal displacements, and the difficulty presented in measuring large displacements due to the high sensitivity of those interferometric methods. Ways of circumventing, to some extent, that difficulty in holographic and speckle methods have appeared in the literature, FRYER (1970), VARNER (b) and ENNOS (ERF Ed. (1974)). Moiré methods provide an alternative to finding the solution to the problem of high sensitivity; methods whose potential applications and limitations have been studied in comparison with holographic and speckle interferometry have been made by VARNER (a) (ERF Ed. (1974)), LUXMOORE (1975) and BURCH (1975).

The purpose of this Chapter is to present some new holographic and speckle interferometric techniques which may be referred to the group of reduced sensitivity contouring methods. These techniques are used in conjunction with the ESPI system already described, and the main feature is that of finding the contour difference between an object and master surfaces in a production line. The reduced sensitivity is obtained by matching the master surface shape to that of the object, although that sensitivity corresponds to an interferometric one, ESPI sensitivity.

In specialised cases, the matching of surface shapes could be done by moiré and holographic methods, within their own limitations and practicability. It will be attempted, in the remainder of this section, to give some insight into the need for the proposed contouring methods. In doing so we will consider first, as a simple and representative example, the single-grid-projection contouring method proposed by HOVANESIAN, et al (1971)[1]. It consists in the projection of a grid of regularly spaced straight lines onto both a flat reference plane and the object surface. The reference plane and the object take alternatively the same place in space and their images are superimposed, by double exposure, on a photographic plate. The moiré effect (figure interference) between the regular and distorted lines of the imaged reference plane and object surface respectively, resulting in contour fringes, is shown in Fig.(17)(a) and (b). This figure shows the contour fringes of an ordinary light bulb and a turbine blade, over a background of unwanted high frequency (projected) lines that can be observed on the flat screen and at the left half of the bulb. These lines may be eliminated by optical filtering, or by grid motion, ALLEN et al (1971). Another problem is that of specular reflections that obstruct the information over a portion of the object surface as it can be seen in Fig.(17)(b), where a long vertical band of bright specular light, along the middle of the blade, makes it impossible to distinguish the contour fringes in this region.[2] The use of photographic film is, at the moment, an inconvenient factor in production line applications.

1. See also HOVANESIAN (1975) for contouring by a scanned ruling method, which we will refer to in the holographic illumination contouring section, MACOVSKI et al (1971) and BENOIT et al (1974).

2. The common practice of spraying the surface with matt paint to reduce the specular light limits the scope of the techniques. The light bulb shown in Fig.(17)(a) was sprayed with white matt paint to eliminate specular reflections.

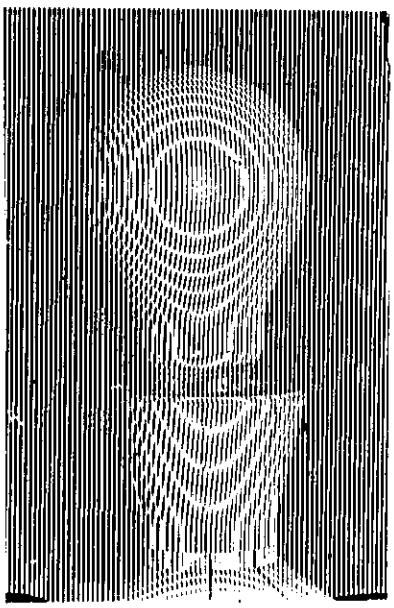

a

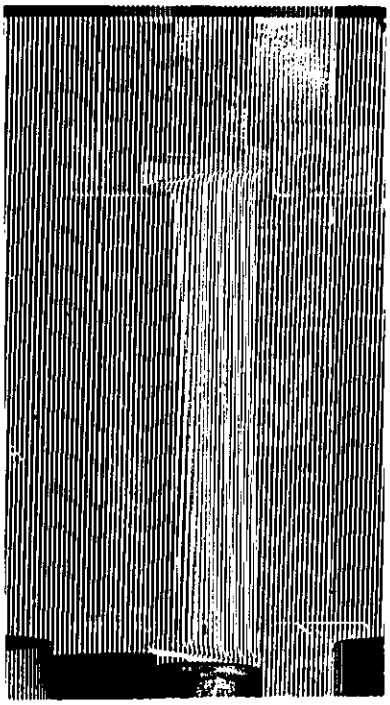

b

Fig. 17 Moire contour fringes of a: (a) light bulb, (b) turbine blade.

UNIVERSITY OF TECHNOLOGY
LOUGHBOROUGH,
MECHANICAL ENGINEERING.

Moiré contouring methods find acceptance when low sensitivity is required, with the extra advantage of using incoherent light. Fig.(17)(a) shows one of the possible cases where low sensitivity is required. Let us now analyse in more detail the case shown in Fig.(17)(b). A transparency with a 11.81 lines/mm grating was used to project the lines on to the reference screen, the frequency of the lines on it being 0.86 lines/mm and the angle between the projecting and viewing direction was $\alpha = 45^{o}$. Therefore according to HOVANESIAN, Eq.(2), (1971) the height difference, parallel to the viewing direction, gives

$$\Delta Z = \frac{P}{2 \tan \alpha} = 1.22 \text{ mm} \qquad (103)$$

where ΔZ is the contour difference per fringe interval, P = 1.16 lines/mm and $\alpha = 45^{o}$. To be able to measure height differences[1] of 25.4 μm (1 thou) a resolution of 12.7 μm (0.5 thou) is needed, which can be obtained from a grid of 47.24 lines/mm for $\alpha = 45^{o}$. Diffraction will be a great problem besides the difficulty of obtaining a square grid of that frequency. The method can be used as a non-destructive evaluation method and, using a divergent projection beam, it could be used for larger objects;[2] even so the variations of the grid pitch on the reference surface and the variation in the contrast of the projected lines due to the surface finish will create more problems.

A variation of the single-grid method is also presented in the aforementioned article by HOVANESIAN whereby two surface shapes are compared against each other by the use of a beam splitter, this time only one exposure is necessary. Following a similar line of action we may dispense with the use of the beam splitter by means of a double

1. "height difference", "contour interval" or "depth change per fringe".
2. See also TAKASAKI (1970-1973).

exposure placing, consecutively, the object and the master object exactly in the same place.

It must be recalled at this point that the above mentioned moiré methods rely on "figure interference"[1], the formation of fringes by obstruction of light, and that there is no phase information available. Therefore the information obtained by moiré methods is limited by the pitch of the grating.

Moiré methods, in general, are easy to apply and provide a useful continuous range of sensitivity. Moiré sensitivity can be selected over a range from 5 mm (for which great depth of field, i.e. 1 m, is provided) TAKASAKI (1973), to a maximum of 3 μm, for flatness testing JAERISCH et al (1973). Equally fringe projection is simple to use, and offers a real time information and a large range of sensitivity, ROWE et al (1967), DESSUS et al (1973), WAY (1972). Shadowing, in the case of undulating surfaces, presents a great limitation to the technique, due to the necessary large angle between the illumination and viewing directions.

The methods described in the next Sections are based on two holographic contouring methods; the two-wavelength method, HAINES et al (1965) and the immersion method, TSURUTA et al (1967)[2]. The first of these methods uses the phenomenon of beats between two (laser) wavelengths whereas the second method uses the changes of refractive index of the liquid in which the test object is immersed to give similar results, with the advantage of using only one wavelength.

1. THEOCARIS, p4 (1969). See also p92.
2. Both methods later improved by ZELENKA et al (1968-1969) and VARNER (1970-1971).

These methods offer a greater sensitivity when compared with moire methods, and turn the condition of operating through small apertures into an advantageous characteristic. Usually the direction of illumination and viewing are both in-line, thus preventing shadowing. However, the holographic methods are more complex, they require high quality - large aperture optical apparatus, and the experimental procedures are lengthy (for real time operation) due to the photographic recording step. In particular, restrictions apply to the distance between the object (or its image) and the hologram, and to the slope of the object surface relative to the viewing axis, as discussed by VARNER (a) (ERF Ed. (1974)).

The main advantage of the aforementioned optical contouring methods, when compared with transducer probes, is the amount of information over the full field of view at one go, which provides both a rapid assessment of the overall features of the surface and a detailed measurement. Furthermore, generally no physical contact is made with the object surface and the methods work in rough surfaces.

The contouring methods described below are based on the optical contouring methods already mentioned, but offer advantages over moire and holographic methods in terms of extended scope, simplicity and practicability.

Principles

Because the proposed contouring methods are also based on the use of the ESPI system, let us recall some characteristics of speckle interferometry as we go into the mathematical derivation and experimental conditions for contouring.

Consider the interference between an isolated speckle in a speckled image (i.e. vidicon tube screen) and a coherent (in-line) reference wavefront. The total complex amplitude is given by

$$U = A_r \exp(-j\phi_r) + A_s \exp(-j\phi_s) \tag{104}$$

where A is the amplitude and ϕ the phase, and the subscripts r and s refer to the reference and signal wavefronts respectively. The intensity is expressed by

$$I = |U|^2 = A_r^2 + A_s^2 + 2A_rA_s\cos(\phi_r - \phi_s) \tag{105}$$

Suppose the reference wavefront remains constant, but the phase of the signal wavefront is slightly altered an amount $\Delta\phi_s$, due for example, to an infinitesimal displacement of the object surface which produces the signal. As the surface is altered the phase change ($\Delta\phi_s$) takes periodically multiple values of 2π, returning the intensity I to its original value. Thus by monitoring the resultant intensity the change in optical path via the object surface can be interferometrically measured. The reference wavefront can be a conventional smooth wavefront[1] or an independently produced speckle.

1. By "smooth wavefront" is understood to be a wavefront produced by an optical element so as to have the same phase across it; also the wavefront that having been produced this way is reflected and directed by optically polished surfaces.

We can generalise the above equations to represent the speckle pattern wavefront of the deformed surface so that, for practical purposes, it can be compared with the initial pattern corresponding to its original state. In this way those parts of the object surface that have remained unaltered or those which have contributed with multiple phase changes of 2π give, after subtraction, zero intensity. Those parts of the object that contribute with intermediate phase change values produce a variation of intensity which results, after subtraction, in a fringe pattern, where the zero order fringe is a dark fringe. So the fringes represent the loci of points of equal phase change and are localised on the surface.

Since the fringes are formed by obstruction of light (figure interference) they are not strictly interference fringes, though can be interpreted as such. Let us extend our discussion to the performance of the reference wavefront in the ESPI system. Let us consider a speckle pattern (without reference wavefront) to be a grid of randomly distributed lines, therefore when subtracted from the final speckle pattern, after the surface has experienced a change, it is expected to find moire fringes due to a surface change corresponding to the pitch of the grating, speckle size. On the other hand, the ESPI system controls the size of the speckle so that it can be resolved by the vidicon tube. If now a reference beam is introduced, in-line with the speckle pattern wavefronts, it will change accordingly the speckle pattern of the latter, Eq.(105). When both speckle patterns are subtracted electronically by the ESPI system, a zero intensity condition is obtained; any departure from it will this time be due, not to a pitch size variation (random grating) of the surface, but to a variation

corresponding to changes in phase. An important condition being that the phase change of 2π be spread over a number of speckles and so the fringe period, such that the fringes are perceptible. We will return to this subject later in the Chapter where smooth surfaces are analysed by the ESPI system.

Mathematical derivation

The mathematical model for two-wavelength contouring is as follows. Fig. (18)(a) represents two optical paths, $ABC = s_1 \lambda_1 = s_2 \lambda_2$ and $AC = r_1 \lambda_1 = r_2 \lambda_2$, where λ_1, λ_2 are the wavelengths and A,B,C are the points on the beam splitter, object and vidicon tube (image plane) respectively. According to Eq.(104) the complex amplitude of the field at the image plane is

$$U_i = A_r \exp(-j k_i r_i \lambda_i) + A_s \exp(-j k_i s_i \lambda_i) \qquad (106)$$

where A_r and A_s are the amplitudes of the reference and object wavefronts respectively and K is the wave number. The subtraction of the intensities for the two wavelengths made by the ESPI system, assuming its response to be linear, is expressed by

$$I = |U_2|^2 - |U_1|^2 = \{[A_r^2 + A_s^2 + 2 A_r A_s \cos k_2(r_2 \lambda_2 - s_2 \lambda_2)]$$

$$- [A_r^2 + A_s^2 + 2 A_r A_s \cos k_1(r_1 \lambda_1 - s_1 \lambda_1)]\}$$

$$= 2 A_r A_s \{2 \sin [2\pi (\frac{\lambda_2 - \lambda_1}{2 \lambda_1 \lambda_2}) (r_1 - s_1) \lambda_1]\}$$

$$x\{ \sin [2\pi (\frac{\lambda_1 + \lambda_2}{2 \lambda_1 \lambda_2}) (r_1 - s_1) \lambda_1]\} \qquad (107)$$

which represents the beat phenomenon. The intensity pattern has a period

$$(r_1 - s_1)\,\lambda_1 = \frac{2\,\lambda_1\,\lambda_2}{\lambda_1 + \lambda_2} \tag{108}$$

and is modulated by the amplitude term $2\,\lambda_1\,\lambda_2/(\lambda_2 - \lambda_1)$, see Fig.(18)(b).

The maximum value for the amplitude (beats) of I occurs twice in a cycle, therefore two consecutive beats represent a change in path given by

$$(r_1 - s_1)\,\lambda_1 = \frac{\lambda_1\,\lambda_2}{\lambda_2 - \lambda_1} \tag{109}$$

The period $2\,\lambda_1\,\lambda_2/(\lambda_1 + \lambda_2)$ shows that unwanted variation in the optical path produces a shift in the position of the beats, that is, the system possesses interferometric sensitivity and must be properly isolated. This term manifests itself as an interference pattern (interference lines) in the case of two smooth wavefronts, as it will be seen later. When applied to ESPI contouring this term, the carrier in Eq.(107), is given by the random character of a speckled wavefront.

The interference at the image plane between the reference and speckled wavefronts, produced by a small area on the object surface, can be expressed by Eq.(106). It is understood that a variation in path will result in fringes provided it occurs over a number of speckles, as it was established before. In the interference of two speckled wavefronts it is random character of both the reference and object wavefronts which results in poor contrast fringes.

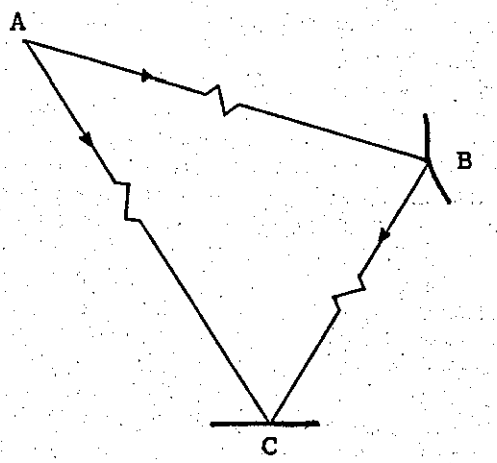

(a)

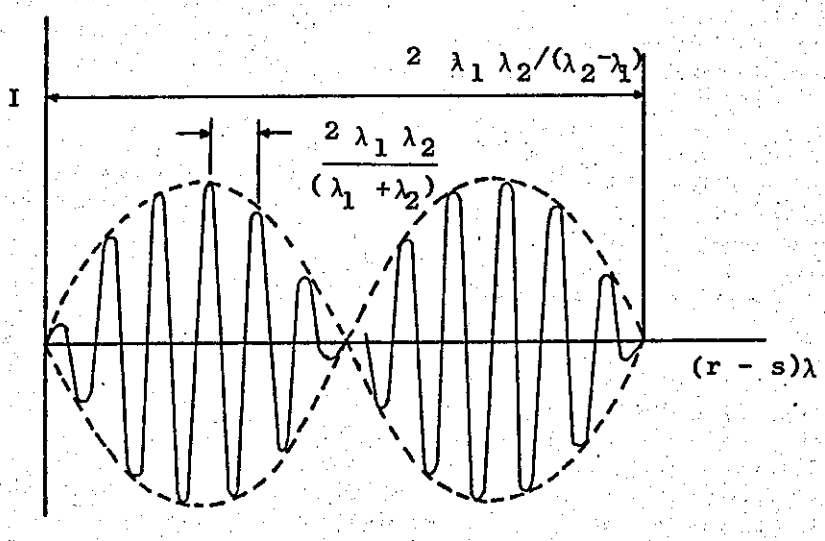

(b)

Fig.(18) (a) Reference and signal paths of a contouring system. A beam splitter; B object surface; C image plane.

(b) Illustration of the beats described by Eq.(107)

Experimental conditions for contouring

It is clear from the above equations that a variation of optical path length ABC (via the object surface), Fig.(18)(a), with respect to the reference beam path AC will produce contour fringes. This of course is designed to produce fringes over undulations in test surfaces, but at the same time imposes tolerances on all wavefront shapes and optical components used to form the optical paths.

Consider an idealized speckle pattern contouring system described by Fig.(19)(a), which shows the illumination of an object surface and the arrangement for the superposition of the reference beam. The reference beam is expanded at R such that all rays between A and the spherical wavefront DCE have the same optical path length, (it constitutes a smooth wavefront). The light via the object is collected through a point (ideal) aperture Q which is a mirror image of the reference beam point R. Thus the signal wavefront exactly matches the spherical reference wavefront DCE. Therefore when the wavelength is changed there is no relative change of phase over the paths from R and Q between corresponding points of the reference and signal wavefronts incident at the image plane. Consequently it is only between P and Q that a relative phase change, due to differences in optical path, occurs on changing wavelength, thus producing contour fringes. These relative phase changes occur in the varying gap between the illumination (and viewing) wavefront LBK and the object surface. Since the contour fringes represent constant range[1] from this wavefront, absolute measurements of surface shape can

1. Definition: "Constant range" - constant phase change due to a change in optical path as expressed by Eq.(109).

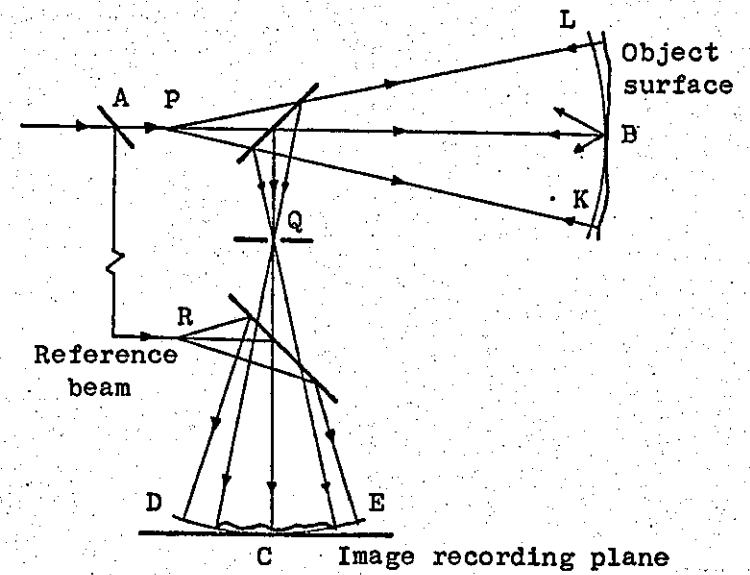

(a)

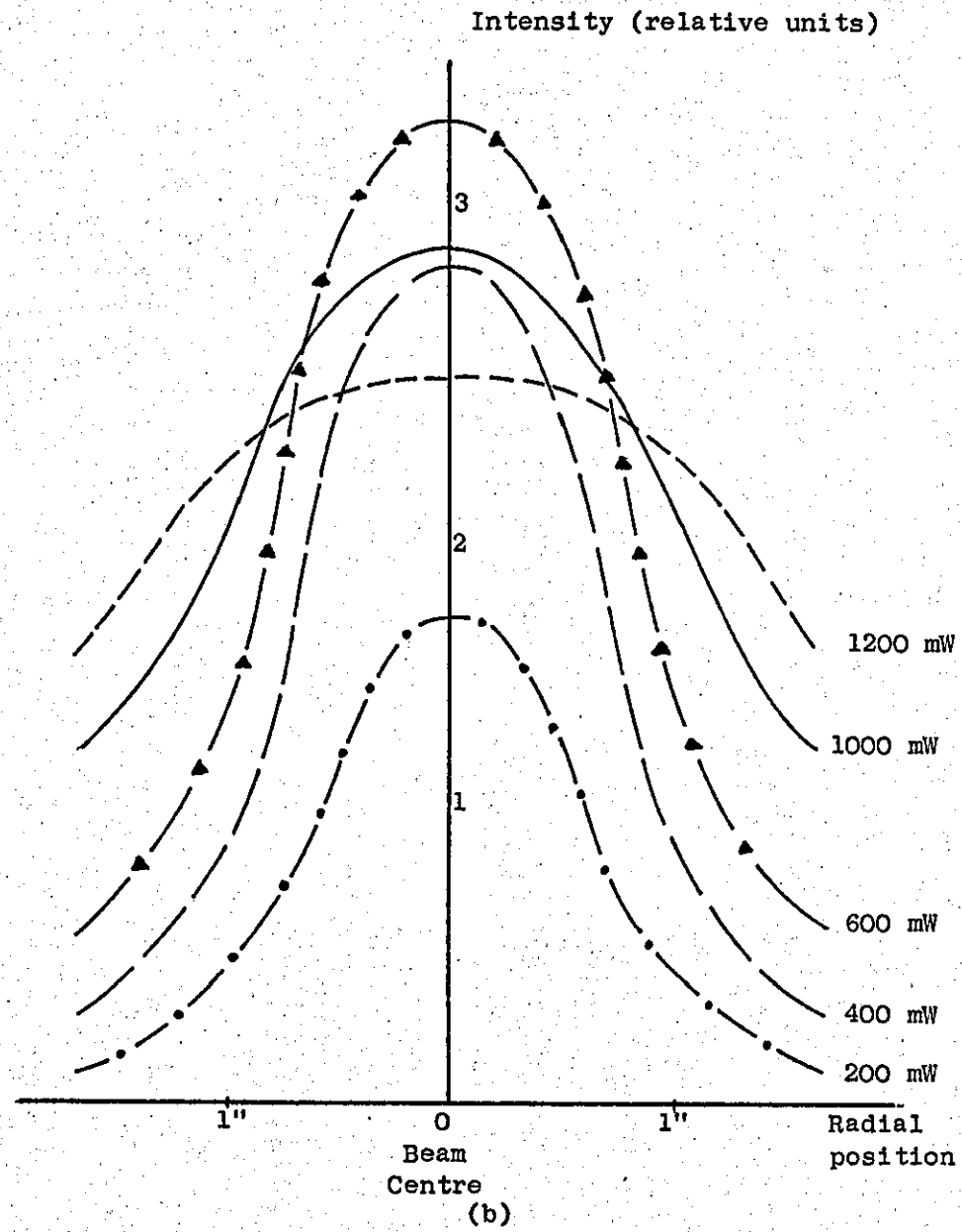

(b)

Fig.(19) (a) An idealized speckle pattern contouring system. (b) Argon laser itensity profiles across an expanded beam for various power outputs, at 4965Å.

be made only if the wavefront shape is known. Further, the wavefront shape must be true to within the accuracy of measurement required. Also the surface must be located according to the same accuracy, and the location of different components as in a production line, requires jigging. If the object surface wavefront is smooth, then at the image plane, resolvable "interference lines"[1] appear due to its in-line interference with the also smooth reference wavefront.

Let us introduce a list of the contour intervals[2] obtained by the wavelength pairs of a Spectra-Physics Argon laser model 171 and the specified output power in watts (without etalon), Table I.

Optical elements may introduce error in wavefront shapes. In the case of reflecting optical components (mirrors) successive beams of different wavelength follow the same path, and therefore errors in wavefront shape simply accumulate. Assume for example, a series of four (steering) mirrors whose normals make an angle of 45^{o} with respect to the signal wavefront path, and also have a hollow in the area of illumination 2.5λ deep. Therefore the deviation from perfect mirror flatness will produce a wavefront error of 28λ ($\simeq$ 14 μm) that corresponds, according to Table I and Eq.(109), to half residual fringe for the wavelength pair 4880Å and 4965Å. For refracting components (in particular lenses) not only must the emergent wavefront be true to the same tolerance than for mirrors (within 1λ at one wavelength), but chromatic aberrations must be limited such that the change of wavefront shape at the second wavelength is also within the tolerance (a fraction of a wavelength). Consider the case of a

1. Definition: "Interference lines" - Bright and dark bands produced in the region of interference of two smooth wavefronts. See Chapter I.
2. Definition: "Contour interval" or "contour fringe" - same as " constant range".

TABLE I

Output power (watts)	λ Å	5145	5017	4965	4880	4765	4727
4.0	5145	$\frac{\lambda_1 \lambda_2}{(\lambda_1 - \lambda_2)}$ (μm)					
0.5	5017	20.16					
1.2	4965	14.18	47.90				
3.2	4880	9.46	17.86	28.50			
1.0	4765	6.44	9.48	11.82	20.22		
0.2	4727	5.80	8.16	9.86	15.06	59.26	
0.3	4579	4.16	5.24	5.88	7.42	11.72	14.62

thin lens made of crown-glass of refractive indexes n_D = 1.51534 and n_F = 1.51690 for the Fraunhofer lines 5086Å and 4861Å respectively[1]. For a focal length of 130 mm the longitudinal chromatic aberration will be 392.340 μm that corresponds, for an intermediate wavelength value of 5000Å to 784.680 λ(wavelength). The wavelength pair 4861Å and 5086Å give a contour interval of 56 λ/fringe, therefore the wavefront error at the optical axis gives approximately 14 fringes. The wavefront distortion increases with increasing aperture values.

The resolution given by the ESPI system is about 50 distinct fringes across the television screen. This is as a result of the condition that the fringes must be spread over a number of speckles.

1. See BORN et al § 4.7 (1970) and JENKINS et al, p465 (1957).

A standard television camera can resolve less than 400 bits per line (3.2 bits/mm), compared with spatial frequencies in excess of 1000 lines/mm, in holographic recording. In order that the speckle information is resolved by the camera, a small aperture must be used, and the reference beam is arranged to be in line. Since speckle intensities vary from zero to some maximum in any speckle pattern, it is not possible to achieve interference of maximum visibility for all the speckles. The reference beam intensity must therefore be set at some intermediate value. It has been found that a reference beam intensity slightly greater than the average intensity of the speckle image produces good fringe contrast by ESPI, and that the beam ratio is not critical. So, if we consider that the image of a flat object (100 mm^2) fills the television screen, then the maximum tilt that can be measured is about $\frac{1}{2}^o$ for the wavelength pair 4880Å and 4965Å. Greater contour intervals allow for larger angles.

It has already been mentioned about the need for a normal interferometric stability as in holography (high frequency term in Eq.(107)) apart from matching the path lengths of the reference and signal beams within the coherence length of each of the wavelengths used.

Optical arrangement

A Michelson interferometer was built into the optical arrangement in order to monitor the coherence of the laser light.[1] It was noticed

1. The light reflected by optical components was used for this purpose.

that a loss of coherence occurred for certain wavelengths at particular power outputs. The optical arrangement for combining the reference and signal wavefronts in the ESPI system is shown in Fig.(20). Instead of a conventional beam splitter for bringing the signal rays (approximately) into line with the reference beam, a mirror with a small hole (1 mm diameter) is used. Compared with a conventional glass plate beam splitter, this means of combining the beams uses the light more efficiently and avoids secondary reflections. The setting of a lens to generate a specified wavefront shape is achieved by using a perfectly true reflector to reverse the light through the optical system, OST et al (1969). When the lens is correctly positioned the light is passed back strongly through the pinhole filter (25 μm diameter). The number of optical elements and the vidicon tube response impose a minimum of laser output power. For a situation in which the laser power was reduced until it was just being obtained, useful information (from the television screen) for contouring, it was found that a power output of about 30 mW is needed[1] to contour a diffuse surface area of about 6500 mm^2. The distribution of light intensity across the laser beam (at 900 mm from the point source) for various power outputs is illustrated in Fig.(19)(b). It gives the relative intensity profiles across an expanded beam, at 4965Å. The profiles take a maximum and then flatten down for higher power output values. This means that at higher power outputs (1W, say) there is a more uniform distribution of energy across the beam, but not necessarily greater intensity.

1. The surface was placed near a lens to collect the light. Without this lens or at a greater separation a power output of at least 100 mW is needed to perform the contour techniques established here.

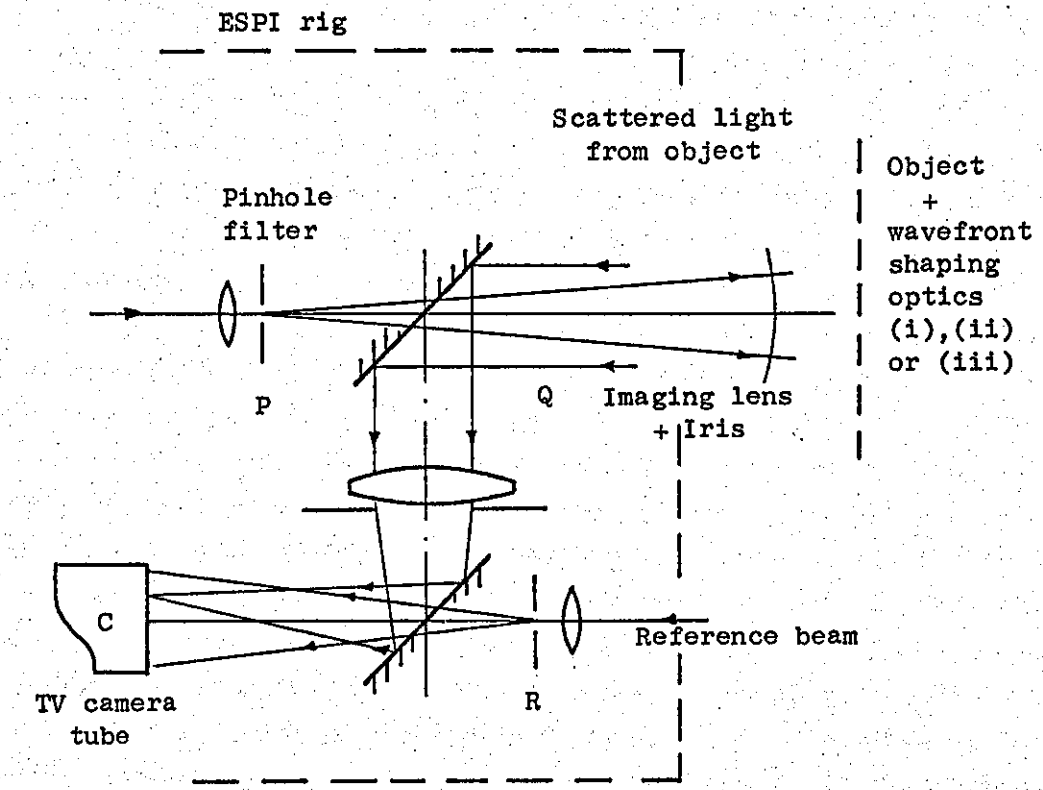

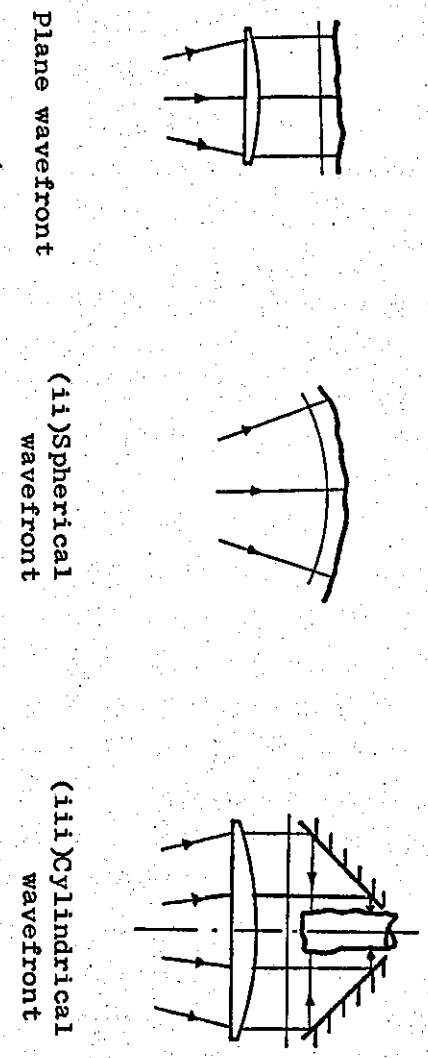

Fig.(20) Optical arrangements for contouring regular shaped components, by means of conventionally generated wavefronts: Method I.

CONTOURING OF REGULAR SHAPES

Contouring by conventionally generated wavefronts: Method I

The most straightforward contouring scheme (as used in the holographic two-wavelength method), uses conventional optical components to generate a wavefront that matches the general shape of the object surface. Optical arrangements for contouring surfaces that are nominally plane, spherical or cylindrical are shown in Fig.(20)[1]. In each of the three cases the surface is (in general) illuminated normally, and of the light scattered from the surface only that close to the wavefront direction is collected by the imaging lens. Thus, from Eq.(109), the optical paths over which phase changes can occur, for all surface points, are folded back on themselves, and the contour interval, Δ, is given by

$$\Delta = 2\delta = \frac{\lambda_1 \lambda_2}{\lambda_2 - \lambda_1} \qquad (110)$$

where δ represents the depth change per fringe, measured along the master wavefront direction, Fig.(21). It is seen that the entire surface is viewed in (or close to) the specular direction of reflection from the surface.

The procedure for making a contouring measurement is as described in ESPI measurements and Appendix B, except that phase changes are produced by a change of wavelength as opposed to object deformation. Thus the first interference speckle pattern is recorded

1. BUTTERS et al (1974). Also, notice that an achromatic imaging lens and an aperture, illustrated in Fig.(20), have been substituted for the aperture R in Fig.(19)(a).

using λ_1, and then subtracted from the live camera picture of the modified pattern formed by λ_2.

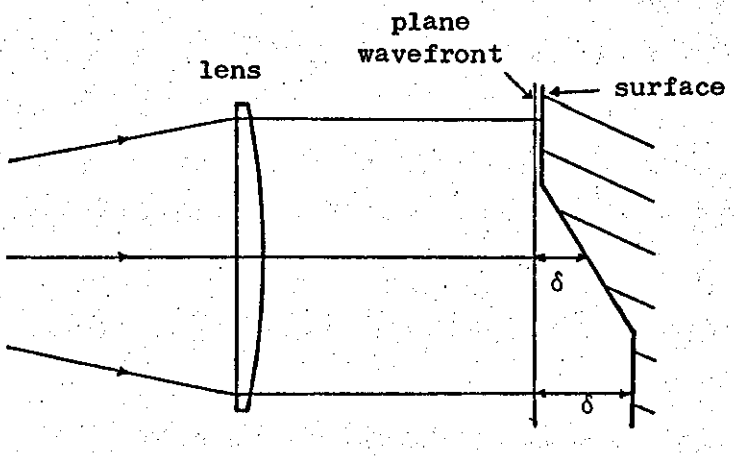

Fig.(21)

In order to confirm the contouring principles, a flat steel disc of 63 mm diameter was machined, having a flat incline with one end protruding from the disc surface and the other end recessed, as shown in Fig.(22).

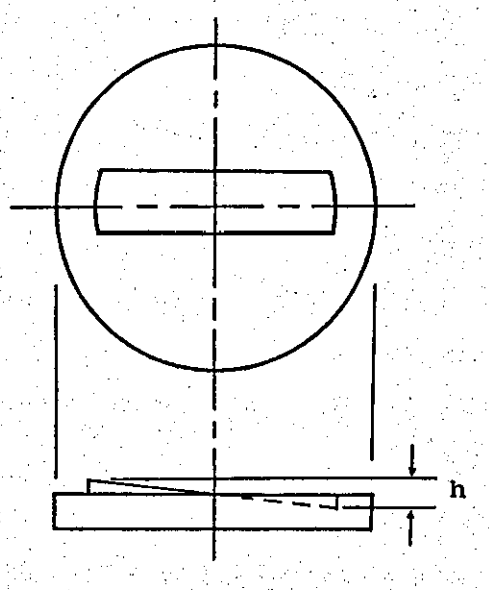

Fig.(22)

The overall depth h of the incline was measured by dial gauge calibrated in inches, to be 0.0042 in (106 μm) ±2%, relative to the surrounding face[1]. For contouring, the disc was illuminated by a collimated beam, and was adjusted so that no fringes formed on the surrounding face. The resulting fringe patterns over the incline for two wavelength pairs, photographed from the television screen, are shown in Fig.(23). The wavefront pairs were 4880Å and 4965Å in (a), and 4965Å and 5017Å in (b), producing depth changes δ of 14.25 μm and 23.95 μm respectively. Measurement of the incline depth from the fringe patterns, compared with the dial gauge reading, as tabulated below:

Depth of incline by dial gauge	Depth of incline by contour fringes	Wavelength pair used
106 μm(± 2)	106 μm ± 4	4880Å & 4965Å
	108 μm ± 6	4965Å & 5017Å

There is agreement within the experimental error (the accuracy of the fringe measurements is based on an error of ¼ fringe in estimating the number of fringes). The pendulum-shaped shadow over these images was due to a mask inserted to stop bright reflections from the faces of the collimating lens.

1. The surface was in its machine-finished state, although in particular cases (different machining operations cause different surface reflectances), the surface is lightly sprayed with aluminium paint so as to produce a uniform brightness over the image. Matt white paint, thinly sprayed onto shiny surfaces, is useful in general speckle pattern interferometry as a means of producing even scattering of light, and hence an image of uniform brightness. However for contouring it does not work, unless sanded very smooth, because its roughness causes the speckle patterns to decorrelate on changing wavelength.

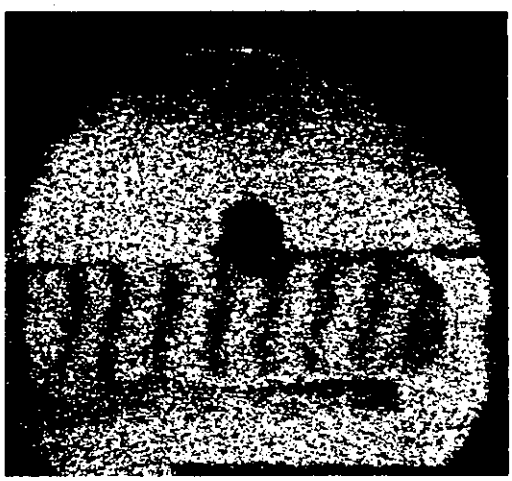

a

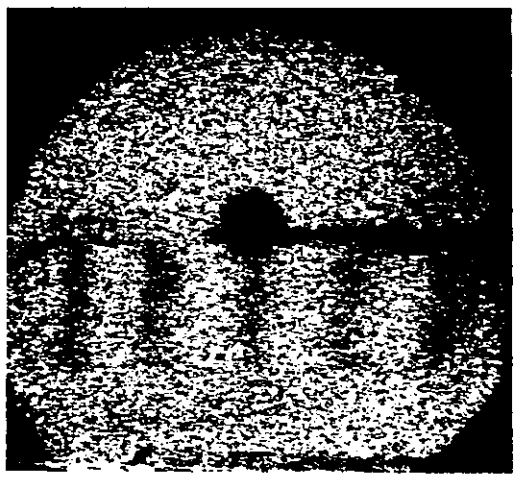

b

Fig. 23 Contour fringes over the flat incline object (Method I) Photographs taken from the television screen. (a) Contour interval of 28.5 μm; (b) Contour interval of 47.9 μm.

UNIVERSITY OF TECHNOLOGY
LOUGHBOROUGH,
MECHANICAL ENGINEERING.

When contouring various surfaces it has been noticed that the contour fringe visibility varies considerably. This is directly related to surface roughness and its effect on changing the form of a speckle pattern on changing wavelength. As a consequence the degree of correlation between two interference speckle patterns in a contouring measurement decreases as the surface becomes rougher. Fig.(24) shows contour fringes obtained over three different surfaces using the 4880Å and 4965Å pair. The first (a), was surface ground steel having a centre line average (CLA) roughness value of 0.35 μm in one direction and a value of 0.65 μm in the perpendicular direction. The second (b) and third (c) surfaces were ground glass, (aluminium vacuum coated to increase its reflectance), having CLA values of 0.62 μm and 1.20 μm respectively. The fringe visibility for the smoother surface ground steel was more noticeable, though the difference in visibility has partly been lost in video tape and photographic reproduction, and also due to different brightness and contrast settings of the television monitor. The fringes over the ground steel disc reveal indentations in the surface, while the ground glass is seen to be approximately flat, though tilted with respect to the illumination beam. A more coarsely ground glass plate having a CLA value of 3.12 μm was tried, again using the 4880Å and 4965Å wavelengths, but produced no recognisable contour fringes. This roughness represents an unacceptable degree of decorrelation at this wavelength difference. However, low contrast fringes were obtained when a smaller wavelength difference, namely 4965Å and 5017Å, was used. This decorrelation also becomes greater as the difference between the wavelengths increases. Fig.(25) shows the contour fringes on a brass faced disc (.42 5 μm CLA) for the wavelength pairs; (a) 4880Å and 4965Å, δ = 14.25 μm, (b) 5145Å and 4965Å, δ = 7.90 μm, (c) 4880Å and 5145Å, δ = 4.73 μm.

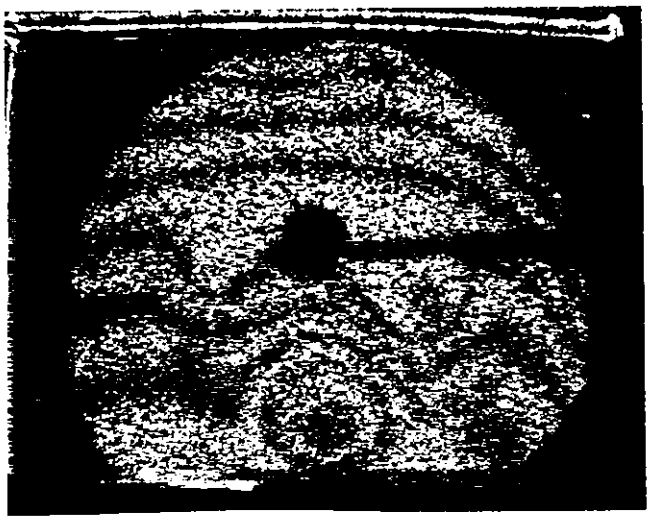

a

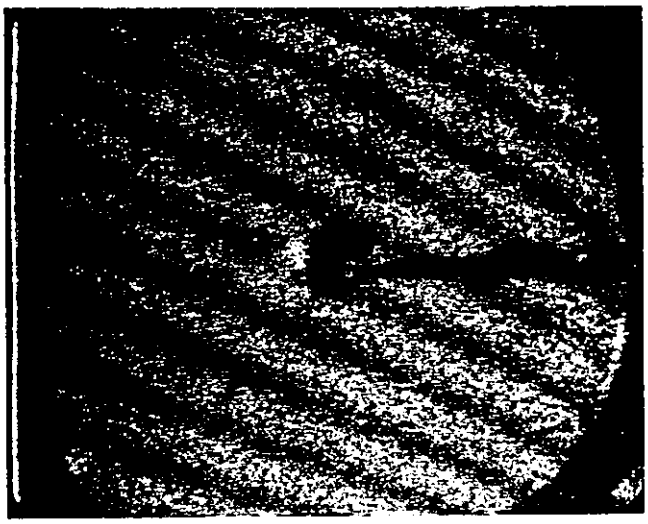

b

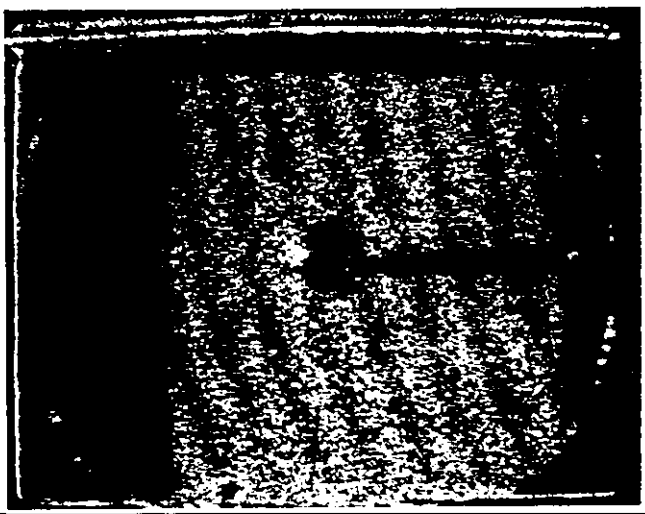

c

Fig. 24 Contour fringes over surfaces of different roughness for a contour interval of 28.5 μm. (a) Surface ground steel, CLA values of 0.35 μm and 0.65 μm in perpendicular directions; (b) and (c) ground glass, CLA values of 0.62 μm and 1.20 μm respectively.

UNIVERSITY OF TECHNOLOGY
LOUGHBOROUGH,
MECHANICAL ENGINEERING.

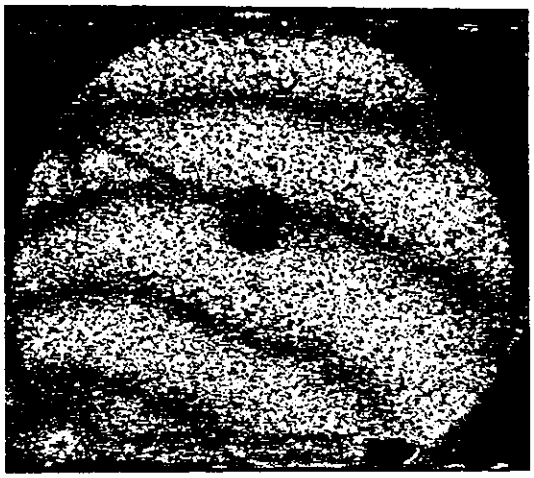

a

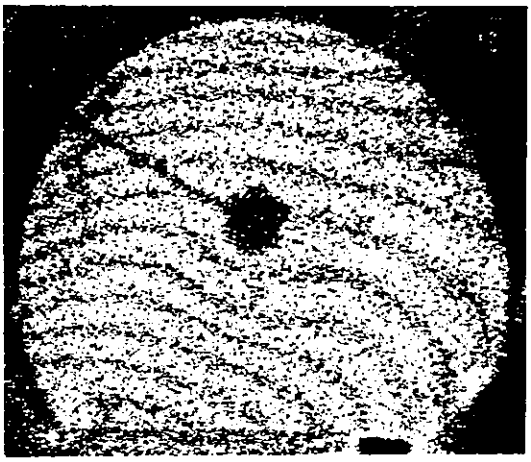

b

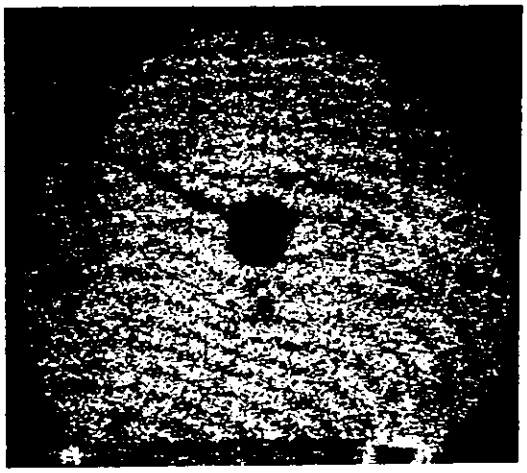

c

Fig. 25 Contour fringes on a brass faced disc, CIA values of 0.42.5 μm for different contour intervals. (a) 28.5 μm, (b) 14.18 μm, (c) 9.46 μm.

UNIVERSITY OF TECHNOLOGY
LOUGHBOROUGH,
MECHANICAL ENGINEERING.

The decorrelation is more apparent as the wavelength difference increases. In addition to flat surfaces, spheres and cylinders have also been contoured by method I, DENBY et al (1975).

Distinction between hills and valleys

This is a subject of present research since differentiation between hills and valleys requires extra information, besides that given by the contour fringes. It has been noticed, in ESPI applied to two-wavelength (and multiple-index) contouring, that the contour fringes, obtained when setting the laser light from a wavelength to a shorter one, move in one direction as the object is moved a determined amount. The fringes in turn move in the opposite direction for the same object movement, when the laser is tuned from the short to the larger wavelength. The signal corresponding to the first wavelength is stored and subtracted from the signal corresponding to the second wavelength. The object does not need to be moved, only a uniform variation of the optical path is necessary.

Fig.(26) illustrates some observations in which a preliminary analysis can be based. (a) represents a flat surface contoured at position C. Position r represents the position (or part) of the surface which is parallel to the illuminating wavefront, and the top wavelength of the pair indicates the first one used (stored). The surface is slightly moved to position f about a fixed axis, as it is indicated by the arrow P. The intersection of this axis with the plane of the figure is indicated by the point o. The horizontal arrows indicate the direction in which the fringes move. Looking in

the direction of illumination the fringes move downhill in (a) and (b) for a reduction of the optical path and the wavelength sequence λ_1, λ_2 for $\lambda_1 > \lambda_2$, and uphill for the sequence λ_2, λ_1.

At this point only information about the slope can be obtained. To be able to distinguish between hills and valleys, it is necessary to know that portion of the surface which is parallel to the illuminating wavefront or the axis about which the object is rotated. Such an axis is represented in Fig.(26) by o. Fig.(26)(a) and (b) show a hill and valley situation respectively, and (c) and (d) a combination of both for different axis. For a situation corresponding to an axis located at infinity, Fig.(26)(d) for example, the fringes will still move as are shown in the figure. This corresponds to a translation of the object or to a uniform change in the illuminating beam phase.

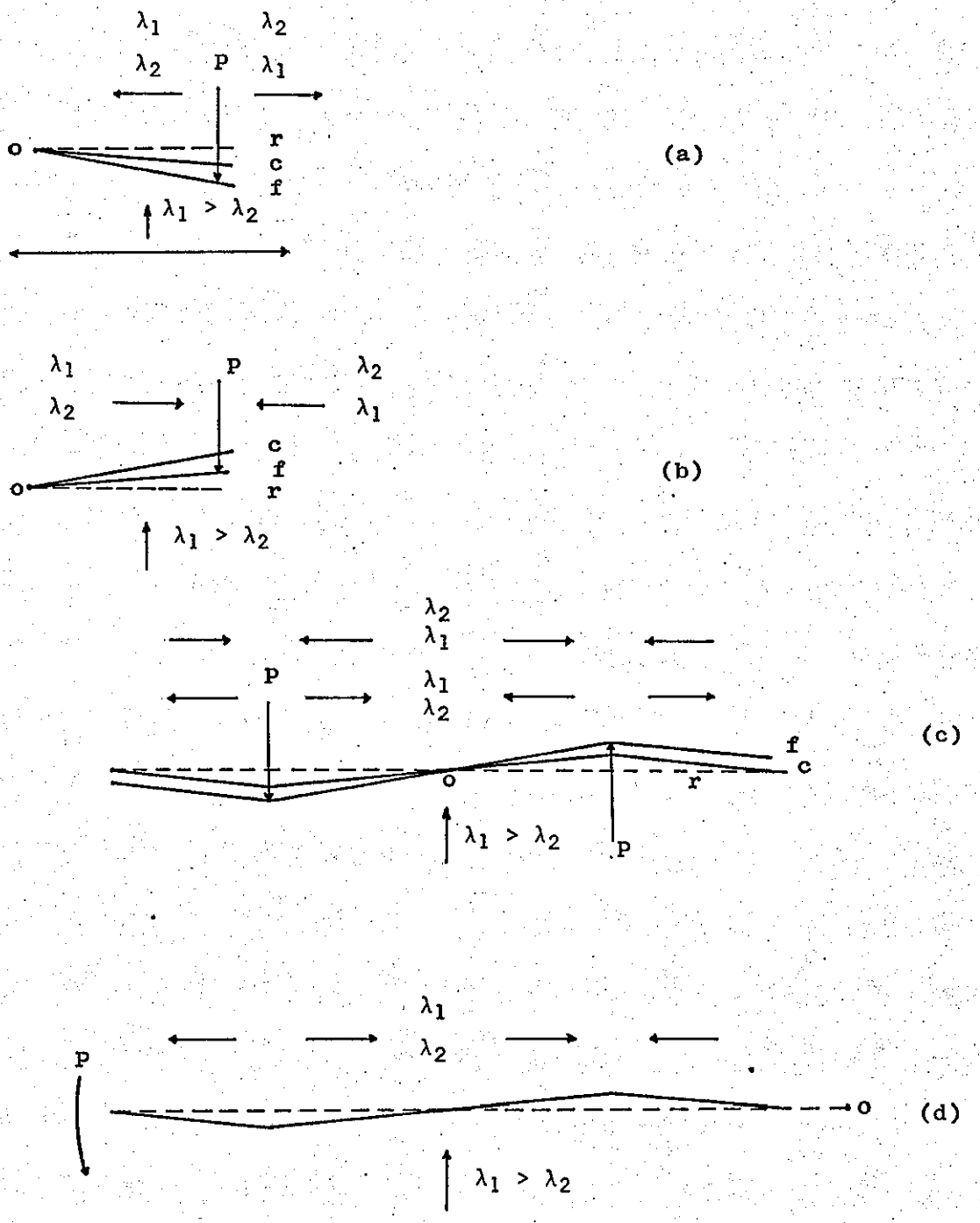

Fig.(26) Hill and valley distinction. (a) a hill situation, (b) a valley situation, (c) and (d) hill and valley situations for different axis of rotation.

CONTOURING OF IRREGULAR SHAPES

Direct comparison of two similar surfaces: Method II

A method was sought to enable irregularly curved surfaces with deep features to be contoured. A Michelson interferometer arrangement provides the means for the comparison of two similar scattering (or almost flat polished) surfaces which replace the conventional mirrors in that interferometer[1]. A beam splitting cube is used to bring the two surfaces in line and they are imaged on to the vidicon tube of the ESPI system. There they interfere acting as a reference and object wavefront for each other simultaneously, to produce contour fringes that represent points of equal constant interval between the surfaces[2], that is, $\Delta/2 = \lambda_1 \lambda_2/2(\lambda_2 - \lambda_1)$. Fig.(27) shows various optical arrangements for the beam splitting cube and test surfaces.

1. See LEENDERTZ (1970), CHIANG (1974), BERGGREN (1970).
2. The depth change per fringe δ, for the case in which the slope of the test surface is parallel to the reference wavefront, takes the form

$$\delta = \frac{\lambda_1 \lambda_2}{2(\lambda_2 - \lambda_1)} \cdot \cos \alpha \qquad (111)$$

where α is the angle between the normal to the reference wavefront (and surface) and the direction of propagation (illumination and viewing). This equation is the same as FRIESEM Eq.(16) for $\theta_o = 0$.

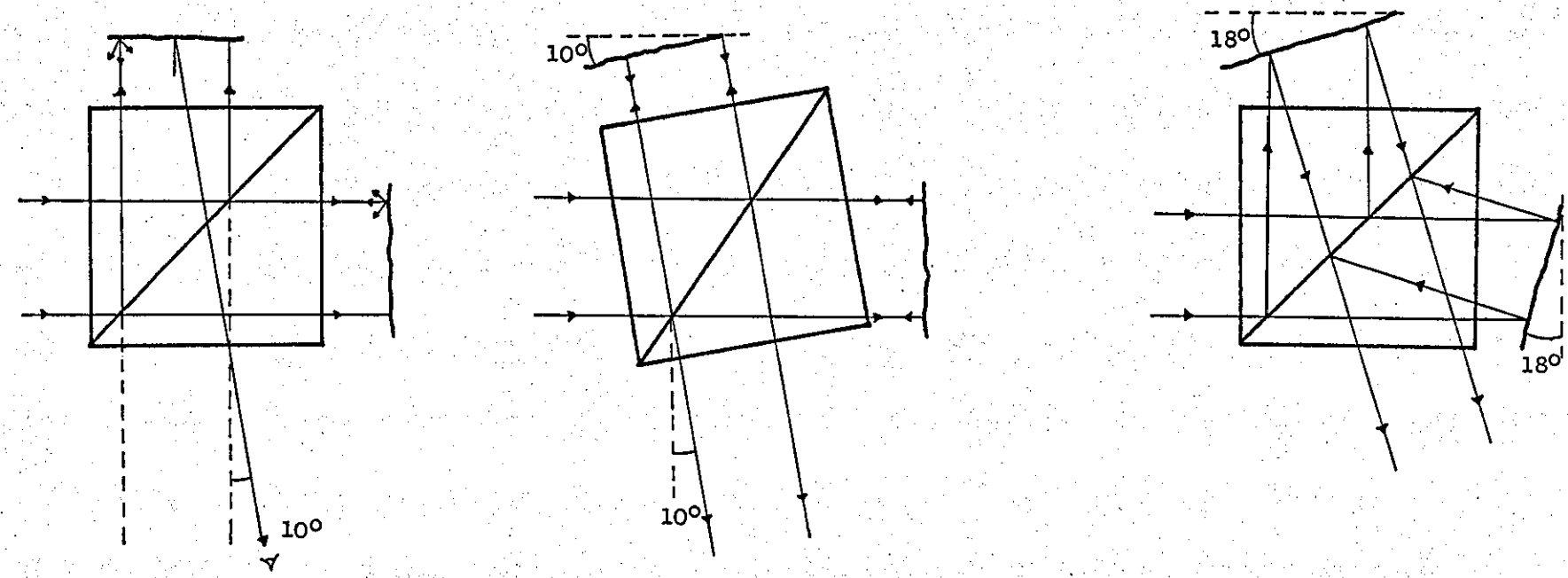

Fig.(27) Optical arrangements for beam splitting cube and test surfaces. (a) normal illumination and viewing directions; (b) normal illumination and viewing (specular); (c) oblique illumination and viewing in the specular direction.

(a) shows the situation for normal illumination and viewing direction (10° from the specular direction). For this case the specularly reflected light from the surface follows the direction of unwanted reflection originated in the internal faces of the beam splitting cube. The test objects were flat mirrors, a portion of them silver spray painted, Fig.(46)(b). The mirror surfaces were used to align the Michelson interferometer arrangement for zero path difference condition using white light. As scattering surfaces, the silver spray painted portion of the objects (mirrors) were used. In this position less than one contour fringe was obtained for the wavelength pair 4880Å and 4965Å. One of the objects was then tilted an amount corresponding to 150 fringes for normal speckle pattern interferometry at 4880Å. This was done in steps of about 30 fringes each. After contouring, with the same wavelength pair, $2\frac{1}{2}$ fringes were obtained as expected, Fig.(28)(a). It was observed that the contour pattern remained unaltered as the same contouring procedure was repeated for different positions of one of the objects, away from its original position, keeping the original orientation with respect to the reference object (and the same tilt). Even at a distance of 2.5 mm from the original position there was no noticeable change in the contour pattern. When a lens of 275 mm focal length was placed in the path of the beam (25 mm diameter), before the beam splitting cube a distance 115 mm away from the object (thus making a maximum angle of illumination with the surface normal of 2.5°), there was, again, not a noticeable change in the contour pattern. Therefore the alignment of the objects along a longitudinal direction is not as critical (nor the collimation of the beam) as the setting of the object in its other five degrees of freedom.

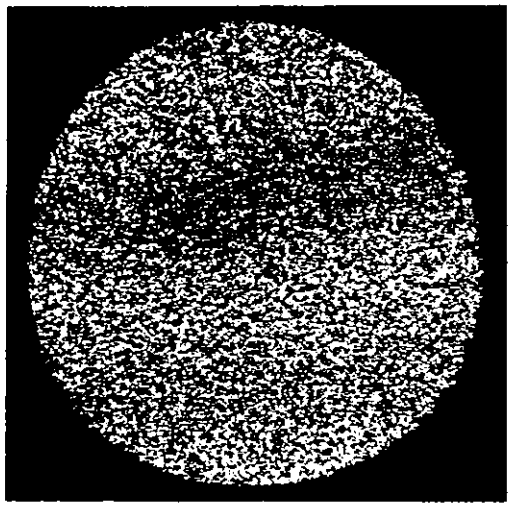

a

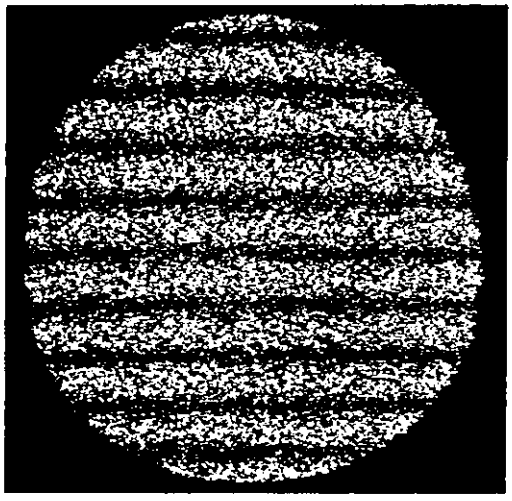

b

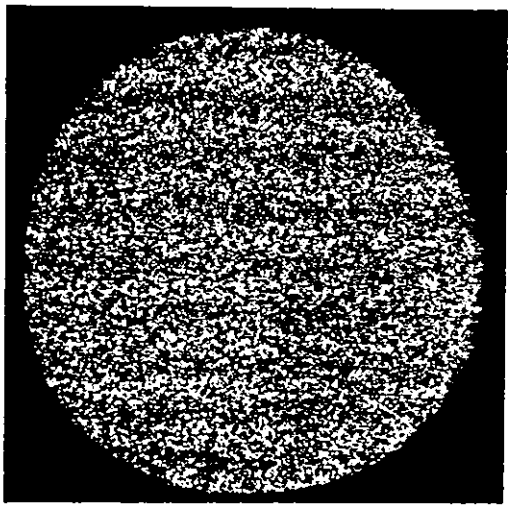

c

Fig. 28 Contour fring s over (a) a silver spray pained mirror (28.5 μm contour interval) Method II, (b) and (c) interferometric (ESPI) fringes for 4880Å and 4880Å and 4965Å respectively.

UNIVERSITY OF TECHNOLOGY
LOUGHBOROUGH,
MECHANICAL ENGINEERING.

It was noticed that the fringe contrast was better when viewed in the specular direction, as for arrangements (b) and (c). Arrangement (c) shows an oblique illumination, and viewed in the specular direction[1]. Fig. (28)(b) and (c) show normal speckle interferometric fringes (ESPI) due to a tilt of one of the objects. (b) shows the situation in which the two states of the object (before and after tilting) were recorded at one wavelength, in this case 4880Å. For (c) the first recording was made at 4880Å, the wavelength was changed to 4965Å and then the object was tilted. The poor fringe contrast, due to speckle de-correlation, is apparent on changing wavelengths. Even so, the fringe contrast for case (b) is not as good if compared with the contrast obtained using a smooth reference wavefront.

The use of a mirror in one of the paths is required if the surfaces are irregular or, if they are flat or symmetric about a vertical axis, it is important to have a one to one point correspondence. The poor contrast obtained by the superposition of two speckle wavefronts is aggravated by the difficulty in collecting the specular light from all parts of the surface. A cap-like surface for example, produces a strong reflection in the specular viewing direction. As a consequence those points of the surface that are inclined and therefore are not viewed in the specular direction form a very dim image. This is because a vidicon tube has a limited dynamic range.

1. This arrangement is similar in principle (oblique illumination and viewing directions) to holographic illumination contouring (Method III). The angle (in this case 18°) was limited by the size of the beam splitting cube.

The system could be used as a desensitized interferometric contouring method applied to almost flat polished surfaces, as will be seen later.

Holographic illumination contouring: Method III

This novel method incorporates holographic reconstruction of a "master" wavefront[1] which is used to illuminate test components, such that effectively, components are compared against the master shape. As shown in Fig.(29)(a), two superimposed holograms, one at each wavelength used, are recorded of the wavefront shaped by the master component. Both holograms are superimposed on one plate, with separated reference beams. The angles between the plane reference wavefronts and the master wavefront for each wavelength are different, to reduce crosstalk during reconstruction. The two reference beams are directed by means of one good quality mirror kinematically mounted successively in the two positions shown. This is considered the best arrangement, to use all the light for each reference beam and to minimise the number of (high quality) optical components.

1. Gara et al (1973) have developed an automatic surface mapping system that when compared with holographic illumination contouring possess the following advantages:

   only one wavelength is used; automatic data processing; does not require interferometric stability; contouring of large objects.

   disadvantages: photographic process for each component; accurate relocation (components - real image) and focus determination; less sensitivity.

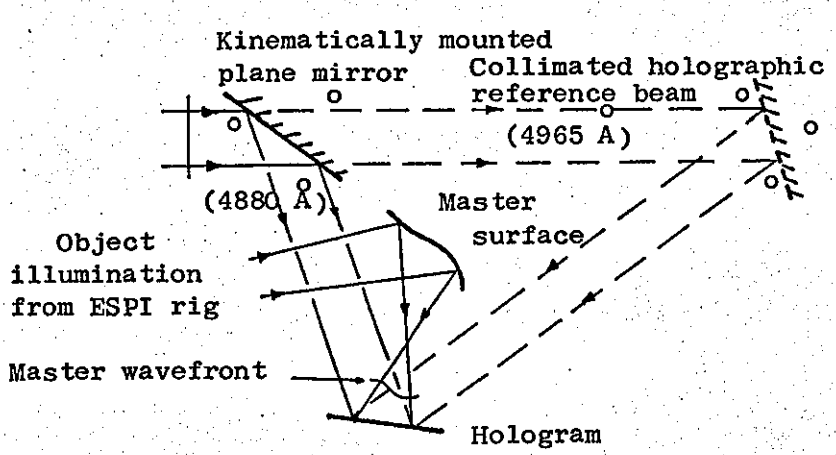

(a)

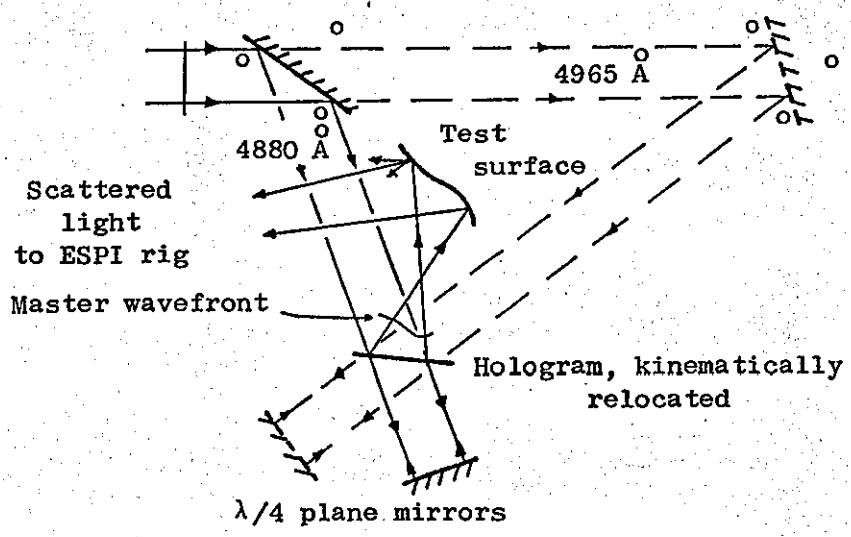

(b)

Fig.(29) The optical arrangements for holographic illumination contouring: (a) recording of the holograms, (b) reconstruction and contouring

The master component surface must have a finish approaching the specular quality of a mirror. This is because the wavefront that illuminates a test surface needs to provide (i) a unique illumination direction for each surface point, and (ii) strong specular reflection back along the path of the original object illumination beam[1].

The turbine blade used in this experiment as the master component had to be further polished with $\frac{1}{4}$ μm particle size diamond paste, in order to produce a wavefront comparable in smoothness with those from conventional optical components. The object illumination beam wavefront does not need to be spherical; it can be any shape. The simplest arrangement is to use the spherical wavefront emitted from the ESPI rig, shown in Fig.(20).

After exposure the hologram plate is developed and bleached (see the holographic recording section) and kinematically relocated, as for real-time holographic interferometry. The master component is replaced (kinematically) by the test component. Fig.(29)(b) shows the optical arrangement for reconstruction and contouring. In order to illuminate the test component with the reconstructed master wavefront,[2] the two holographic reference beams are accurately reversed. The mirrors used for this purpose must be flat to within at least $\lambda/4$ (preferably $\lambda/10$), otherwise error fringes may be introduced[3]. Fine adjustments are (sometimes) made as necessary to these two $\lambda/4$ mirrors to compensate for reference path displacements caused by introducing

1. ARCHBOLD et al, p494 (1967).
2. Real (pseudoscopic) image.
3. The tolerance on the mirror flatness is not simply 1 λ as was the case stated for method I, because these reference beams do not follow a common path.

the hologram plate. The procedure is then as described for the other contouring methods using ESPI, with the addition of re-positioning the reference beam mirror when changing wavelength. Fig.(30) shows the contour fringes so obtained, for the wavelength pair 4880Å and 4965Å, representing the difference in shape between the master blade and the blade being inspected (two in the figure). The area shown (246 mm^2) corresponds to a small portion of the turbine blade. This limitation was imposed by the aperture of the system, being the reference beam diameter 25.4 mm.[1] Fig.(31) shows more examples of contoured turbine blades. Fig. (32) shows the contours of (a) a surface ground steel flat, 0.60 μm CLA, (b) a brass faced flat, 0.40 μm CLA, and (c) the disc shown in Fig.(22), in a tilted position with respect to the illumination wavefront. The flat incline surface can easily be detected (bottom half). The diameter of the round area shown in Fig.(32) is about 25.4 mm.

The contour interval equation for holographic illumination contouring becomes

$$\Delta = 2\ \delta \cos\ \alpha = \frac{\lambda_1 \lambda_2}{\lambda_2 - \lambda_1} \qquad (112)$$

as seen from Fig.(33)(a). This equation indicates that the sensitivity varies as the value of α changes over the surface, as explained by reference to Fig.(33)(b). This diagram shows the positions of master and test surfaces to produce the same fringe order for different gaps.

1. Having now established the principle, the aperture can be increased as required. At present, research is being done about the possibility of using a combination of a divergent reference beam-spherical mirror and the holographic plate without introducing spurious fringes.

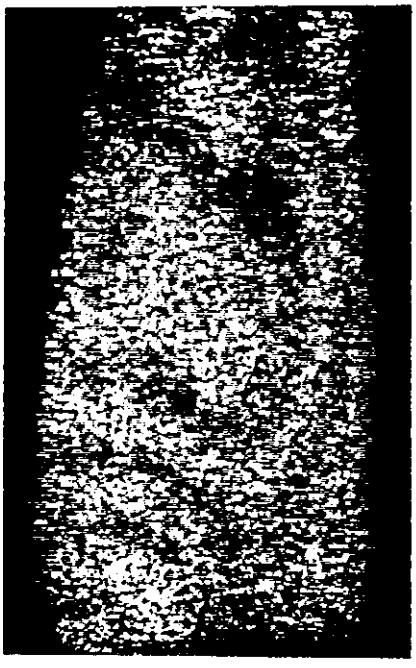

Fig. 30 Contour fringes of two turbine blades by holographic illumination contouring (28.5 μm contour interval)

UNIVERSITY OF TECHNOLOGY
LOUGHBOROUGH,
MECHANICAL ENGINEERING.

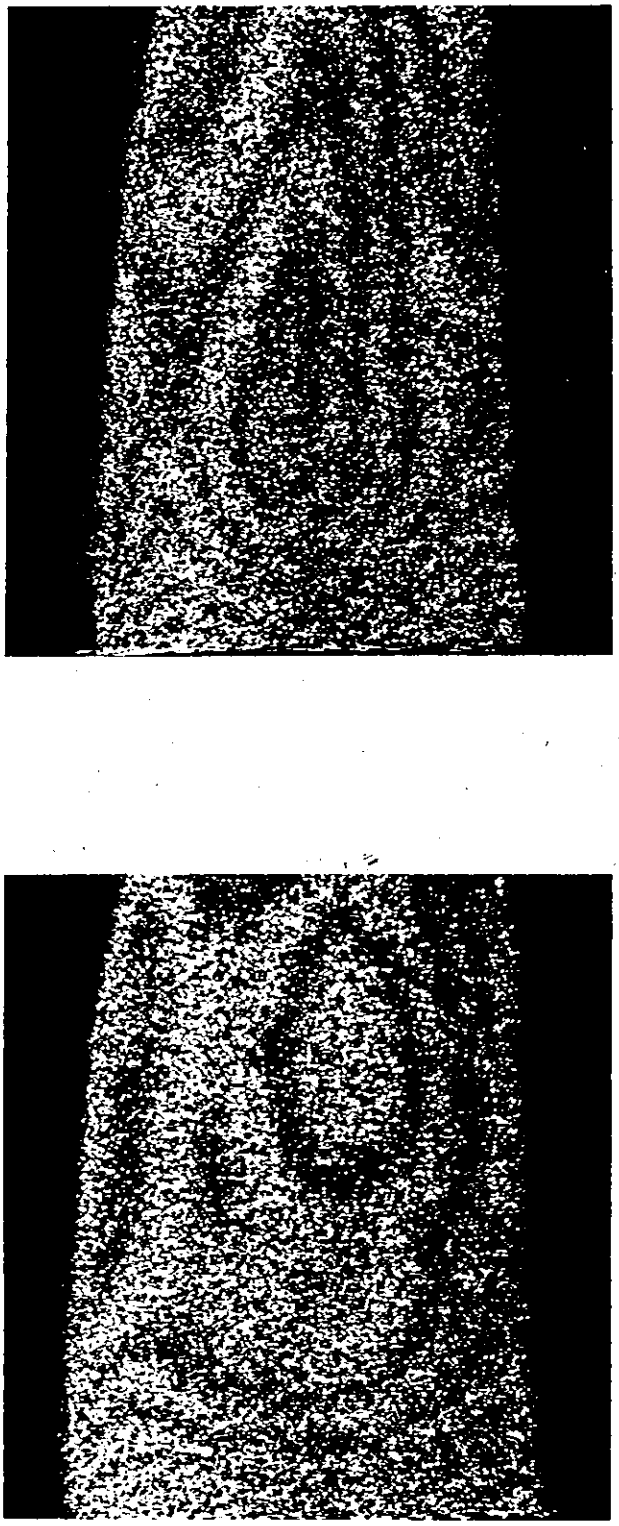

Fig. 31 Contour fringes of two turbine blades by holographic illumination contouring (28.5 μm contour interval).

UNIVERSITY OF TECHNOLOGY.
LOUGHBOROUGH,
MECHANICAL ENGINEERING.

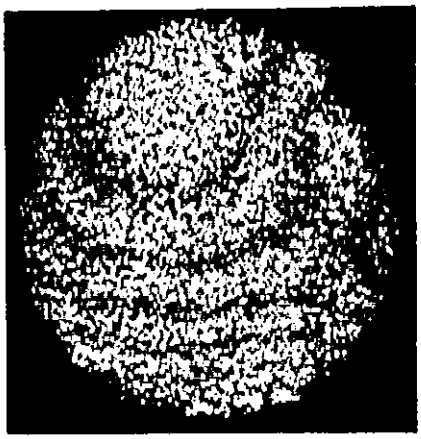

a

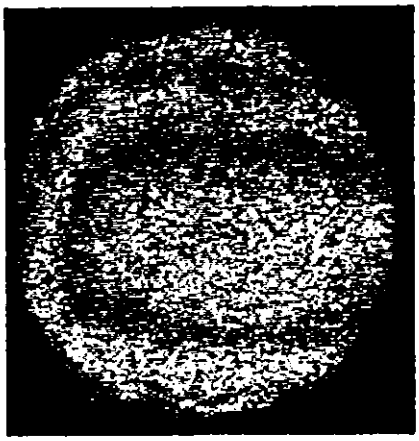

b

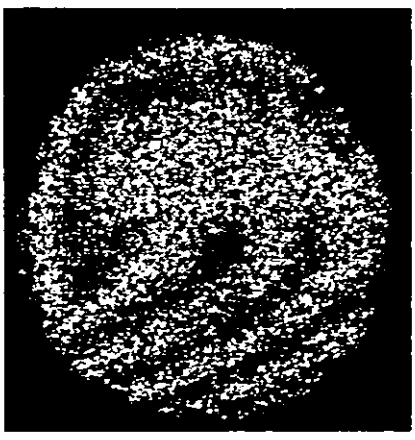

c

Fig. 32 Contour fringes by holographic illumination contouring. (a) surface ground steel, CLA 0.60 μm, (b) brass faced flat, CLA 0.40 μm, (c) flat incline object tilted with respect to the illuminating wavefront.

UNIVERSITY OF TECHNOLOGY.
LOUGHBOROUGH,
MECHANICAL ENGINEERING.

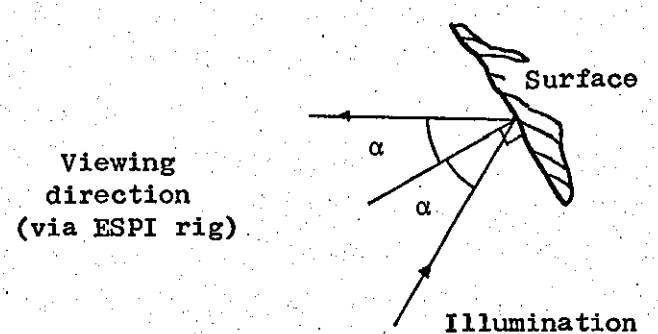

$$2 \cos \alpha \cdot \delta = \frac{\lambda_1 \lambda_2}{(\lambda_2 - \lambda_1)}$$

(a)

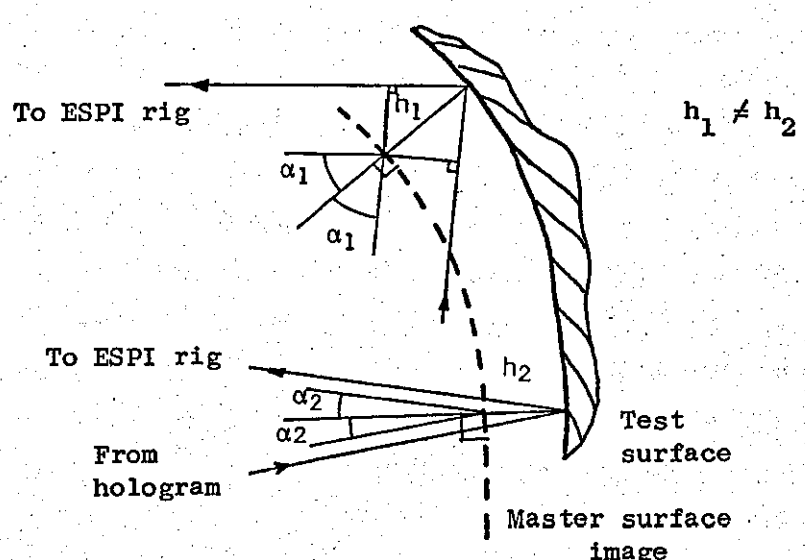

$h_1 \neq h_2$

(b)

Fig.(33) (a) The contour interval equation for holographic illumination contouring.

(b) Diagram showing equal path changes for different depth changes.

If the total change in $(r_1 - s_1)\,\lambda_1$ produces exactly one fringe at both positions, then the gaps shown both correspond to δ. Thus for irregularly curved surfaces the analysis is not so straightforward as for regular component shapes that are contoured by Method I.

Observations

From the points of view of simplicity of reference beam arrangement and elimination of crosstalk between images of different wavelength, one would record each hologram on a separate plate. However this is unacceptable because any thickness difference between the two plates would then introduce error fringes. This is illustrated in Fig.(34); (a) and (b) show the contour fringes (of the same object) obtained using one and two holographic plates respectively, for the wavelength pair 4965Å and 5017Å. The introduction of spurious fringes using two holographic plates is apparent.

The repositioning of the holographic plate is critical[1], therefor a diffuse flat control surface is placed besides the master surface in the area of illumination. Under reconstruction the repositioning of the plate is performed for zero spurious fringes over the scattering surface. This procedure might be used to align an optical system that

1. See the holographic recording section.

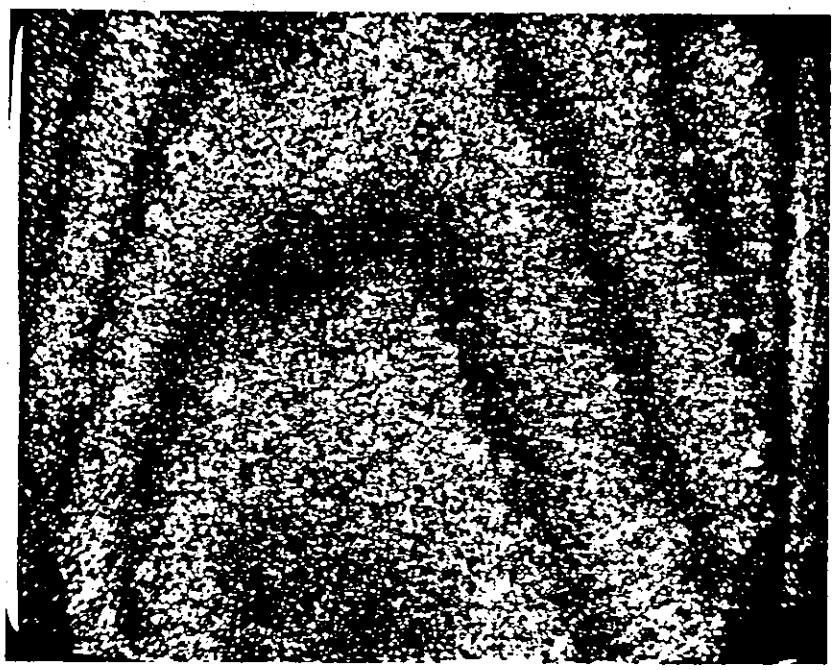

a

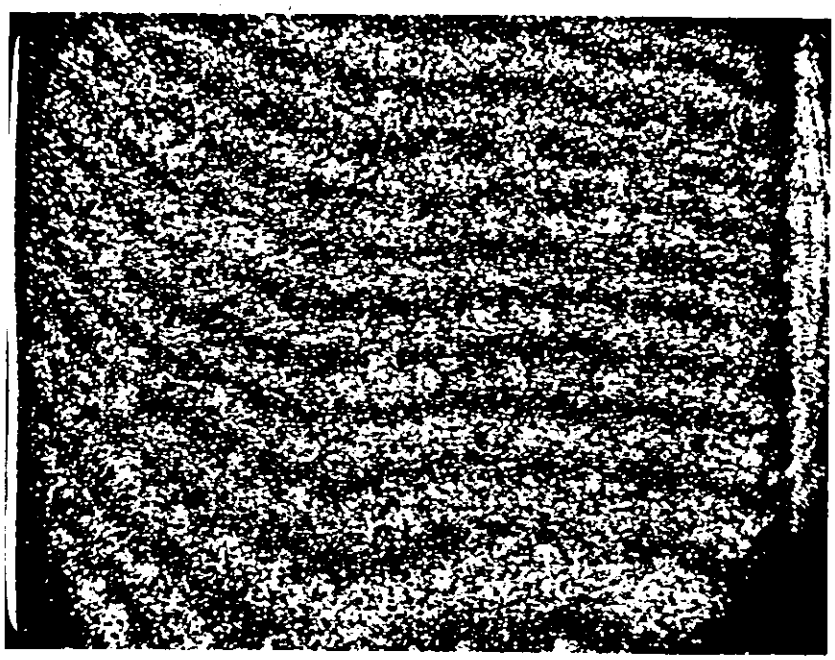

b

Fig. 34 Holographic illumination contour fringes of the same object using: (a) one, (b) two holographic plates.

UNIVERSITY OF TECHNOLOGY.
LOUGHBOROUGH,
MECHANICAL ENGINEERING.

would send the light through the back of the photographic plate so as to use the light more effectively, higher diffraction efficiency. This system of course would need high quality optical components and would be limited by the aperture of the collimating lenses.

The size and shape of the test surface is mainly limited by two factors, namely, the need of having two separated reference beams and the photographic plate area illuminated by the reference beam.

CONTOURING OF SMOOTH SURFACES

All three contouring methods described previously apply also to smooth surfaces, the principles are the same as those for scattering surfaces. This can be deduced from Eq.(107) in which the last term

$$\sin\left[2\pi \frac{\lambda_1 + \lambda_2}{2\,\lambda_1\,\lambda_2}\,(r_1 - s_1)\,\lambda_1\right] \tag{113}$$

represents a carrier which is modulated by the first sine term:

$$\sin\left[2\pi \frac{\lambda_2 - \lambda_1}{2\,\lambda_1\,\lambda_2}\,(r_1 - s_1)\,\lambda_1\right] \tag{114}$$

In the case of smooth wavefronts the carrier is a regular interference pattern (as opposed to the random speckle pattern carrier considered up to now). Fig.(36)(c) shows the nature of this carrier as produced by in-line interference between a reference beam and a smooth wavefront from the front surface of a glass plate. When the contouring process is completed, the contour fringes are "produced" by moiré effect (figure interference), but "caused" by local phase changes. A portion of a dark line (interference line) becomes bright when there is a local phase change of π due to a surface change, and not to a change of the surface of half the pitch grating on Fig.(36)(c) as in moiré techniques. Fig.(35) shows two superimposed sets of interference lines corresponding to each of the two wavelengths (or to

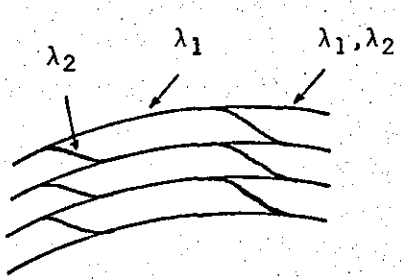

Fig.(35)

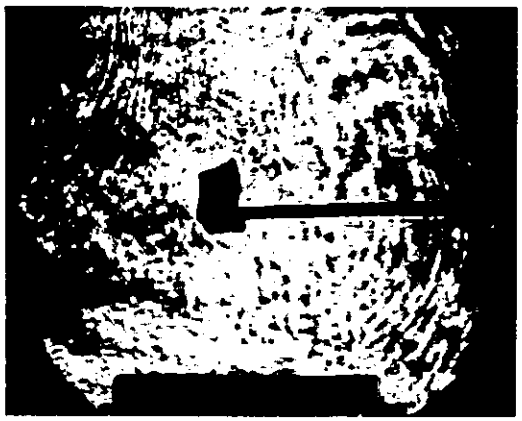

a

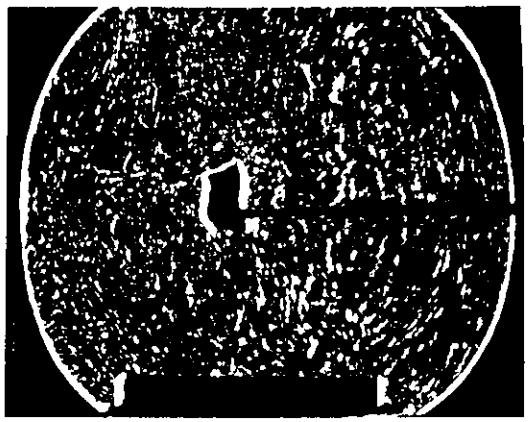

b

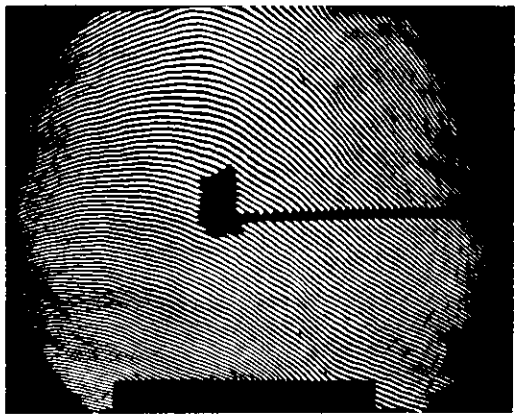

c

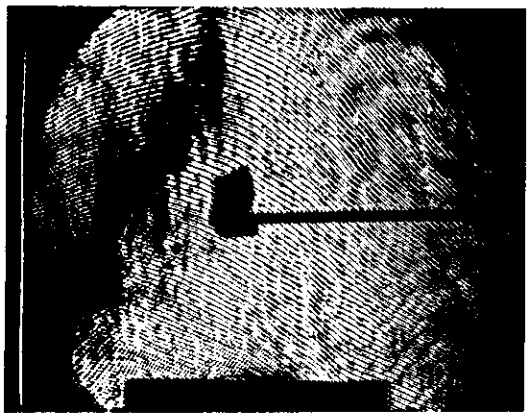

d

Fig. 36 ESPI steps: object, (a) direct, (b) filter. Object + reference, (c) direct, (d) filter.

UNIVERSITY OF TECHNOLOGY,
LOUGHBOROUGH,
MECHANICAL ENGINEERING.

the two states of the test object under normal (addition) ESPI operation); λ_1 for the "stored" information and λ_2 for the "live" information. When phase changes occur the interference lines for λ_2 change, and this change is made visible as a pattern of bright and dark fringes due to the figure interference between the interference lines of both wavelengths. This effect can be observed in Figs.(38) and (39).

Thus ESPI contouring can be applied to certain surfaces, for example, lapped air bearings, which are not smooth enough to allow reliable interferometric inspection. At the same time the degree of roughness is so slight that little scattering takes place and the speckle pattern is consequently very weak relative to the specularly reflected light. For such surfaces the method can be regarded as reduced sensitivity interferometry.

Observations

The aperture that controls the size of the speckle in ESPI does not affect the formation of interference lines, and is used to control the object wavefront intensity.

Sometimes the interference lines and the television lines generate unwanted fringes due to figure interference. These fringes are in continuous vibration due to image flickering from the television; they are enhanced in filter position (see below) Figs.36(d) and (37)(a), (b) and not quite as distinct in direct position, Figs.(37)(d),(c), (38),(39).

As an illustration of the formation of the fringes (for smooth surfaces), in ESPI, let us consider the television images for the different electronic steps with the help of Appendix B, Figs. (50) and (51).

		Switch A	Switch B position
Fig.36(a)	Illuminated object	direct	1
" (b)	Illuminated object	filter	1
" (c)	Illuminated object + Reference wavefront	direct	1
" (d)	Illuminated object + Reference wavefront	filter	1
Fig.37(a)	Normal interferometric fringes (ESPI). Object tilted about a horizontal axis. Subtraction	filter	2
" (b)	Object tilted about a vertical axis. Subtraction	filter	2
" (c)	Same as (a)	direct	2
" (d)	Same as (b)	direct	2
Fig.38(a)	Interferometric fringes (ESPI). Object tilted about a horizontal axis. Addition	direct	3
" (b)	Object tilted about a vertical axis. Addition	direct	3
" (c)	Same as (b) for an incorrect superposition of the interference lines. Line phase control not properly adjusted. Addition	direct	3
Fig.39(a)	Contour fringes of a flat glass plate contoured by method III. Addition. One channel	direct	3
" (b)	Same as (a). Addition. Two channels	direct	3

Fig.(38)(a) shows the video and camera images displaced with respect to one another due to an incorrect line-phase control adjustment. The corresponding interference lines can be seen at the extreme end of each image where they do not overlap. The fringes, that continue to be present, are distorted by the uniform displacement of the individual interference-line gratings with respect to one another.

The use of two channels, Fig.(39)(b), that is, the information of each of the two states of the object (or the object state for two wavelengths) is stored in separate channels of the disc so as to have an equivalent in double exposure holography.

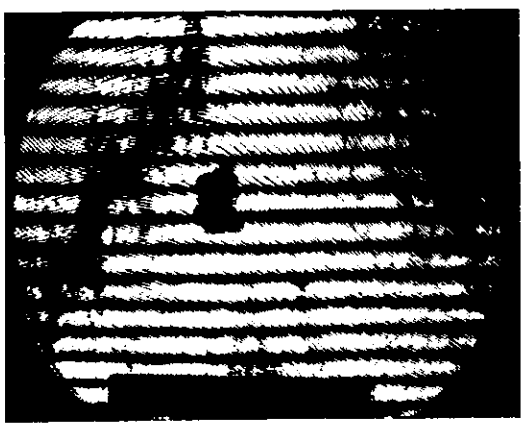

a

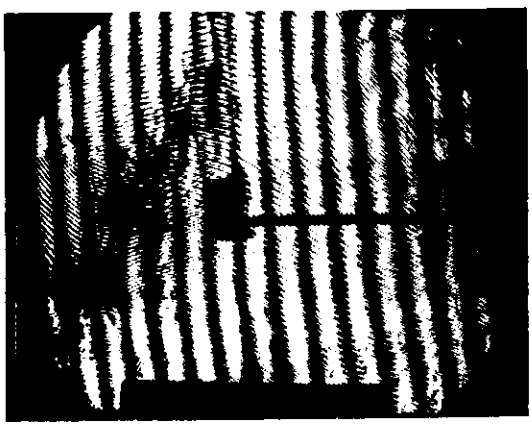

b

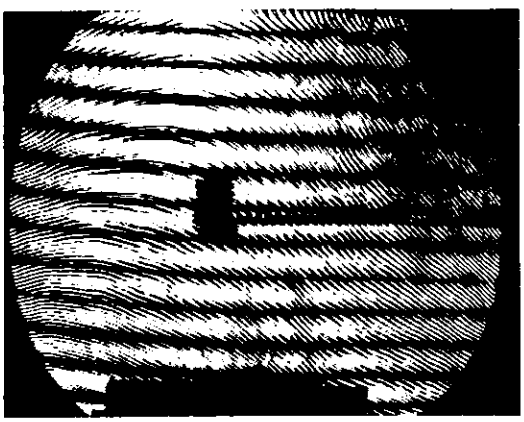

c

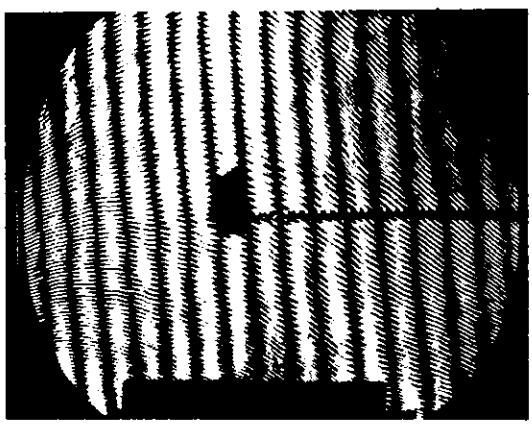

d

Fig. 37 Object tilted about: a horizontal axis (a) filter, (c) direct; a vertical axis, (b) filter, (d) direct. Subtraction.

UNIVERSITY OF TECHNOLOGY.
LOUGHBOROUGH,
MECHANICAL ENGINEERING.

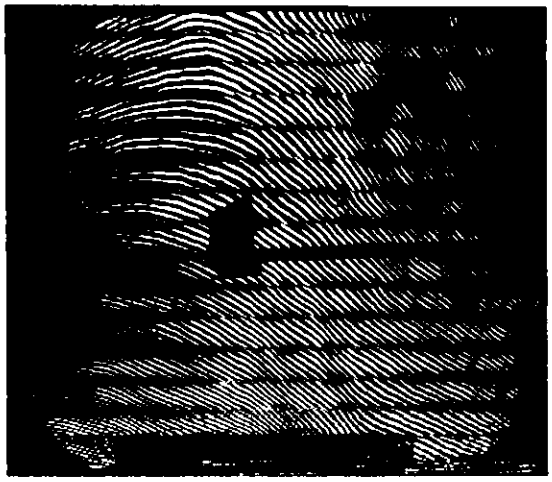

a

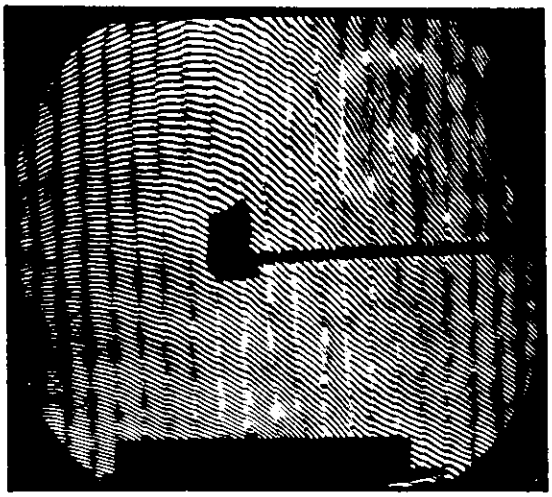

b

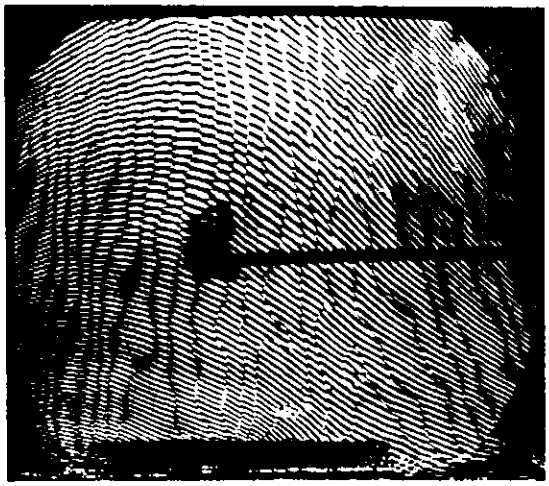

c

Fig. 38 ESPI addition (direct). Object tilted about: (a) a horizontal, (b) a vertical axis, (c) normal ESPI fringes as for (b), for an incorrect line-phase control adjustment.

UNIVERSITY OF TECHNOLOGY,
LOUGHBOROUGH,
MECHANICAL ENGINEERING.

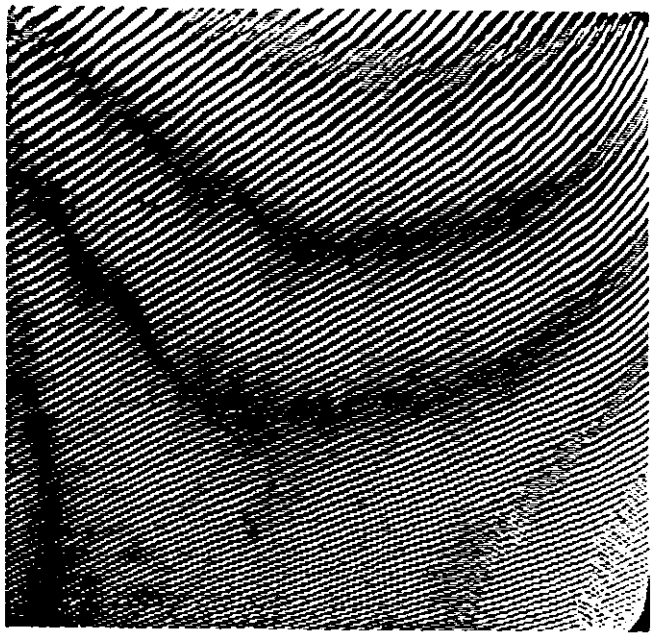

a

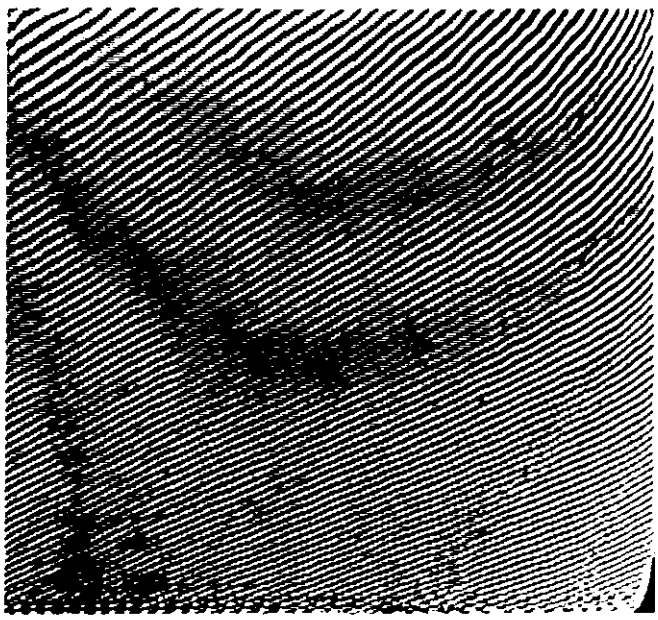

b

Fig. 39 Holographic illumination contour fringes of a smooth surface using: (a) one channel (b) two channels of the disc.

UNIVERSITY OF TECHNOLOGY
LOUGHBOROUGH,
MECHANICAL ENGINEERING.

DIFFUSE SCREEN ESPI METHODS

The analysis by holographic processes of the convection currents of the gas inside incandescent lamps, and contouring by refractive index changes has been the subject of an extensive research[1]. The main difficulty is the interpretation of the fringes to give the local change values of refractive index for a non-uniform isotropic refractive index field. The problem is accentuated by the refractive index changes of the external medium, in both sides of the point under analysis, in the viewing direction.

The ESPI system can be applied to the analysis of refractive index changes undergone by a transparent medium (solid, liquid or gas) when subjected to external agents or, knowing the uniform and isotropic refractive index change it can be applied to contour the container of the medium.

Fig.(40) shows the fringe pattern generated by a variation in refractive index of the gas medium of an incandescent bulb produced by the heat of the filament. The black fringes represent a total phase change of 0 or 2 π, but do not give information about local refractive index changes.

The ESPI methods offers a real time analysis of the propagation of those total refractive index changes without the need of photographic recording processes, and the convenience of using any transient state of the medium (object) as the initial state (provided it is static during a television frame period). This method is sensitive to

1. ENNOS (1967), GATES (1968), SWEENEY et al (1972), PHILLIPS et al (1973), WUERKER (1975), TSURUTA et al (1967) FITZGERALD et al (1969)

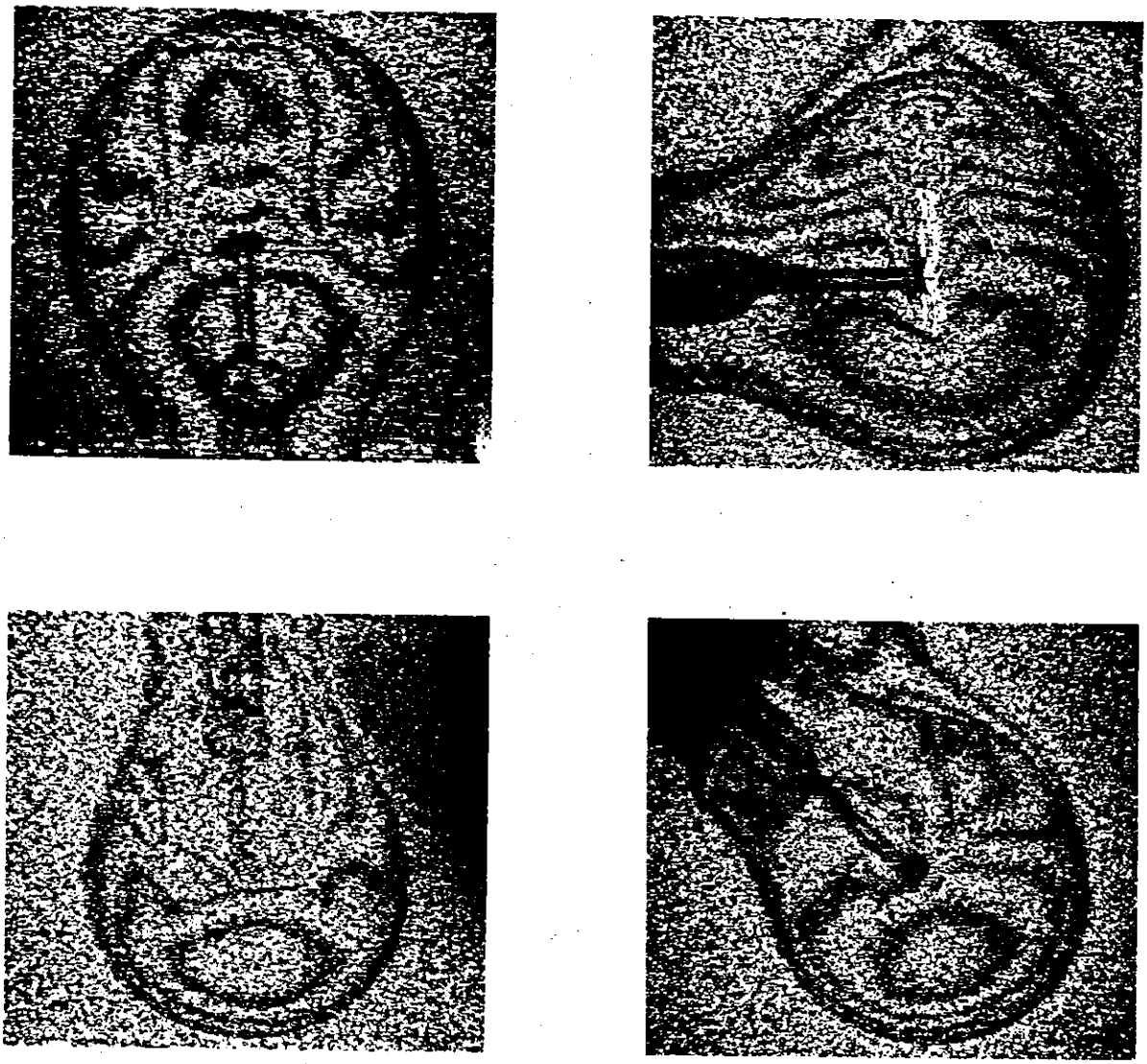

Fig. 40 Fringe pattern for different attitudes of an incandescent bulb, generated by a variation in refractive index of the gas medium.

UNIVERSITY OF TECHNOLOGY
LOUGHBOROUGH,
MECHANICAL ENGINEERING.

variations in air temperature along the light paths, therefore precautions must be taken (especially if the external agent is a heat source) to avoid those changes. This effect, on the other hand, could be useful in the study of the cooling processes of lamps and lighting assemblies, Fig.(41)(a),(b). The speckle pattern was obtained by placing a diffuse screen (ground glass) before the object, and the camera lens was stopped down to $f/16$ to increase speckle size and allow rays within a narrow departure angle from the optical axis direction to be focussed on the vidicon tube.

Fig.(41)(c) shows the contour fringes of a glass due to an isotropic change on the refractive index of the liquid contained in it. The principle is the same as for the immersion method. The diagram on Fig.(42) serves to the mathematical analysis.

Consider z to be the optical axis, and $d(x)$ a parallel line to z bounded by the walls of the container.

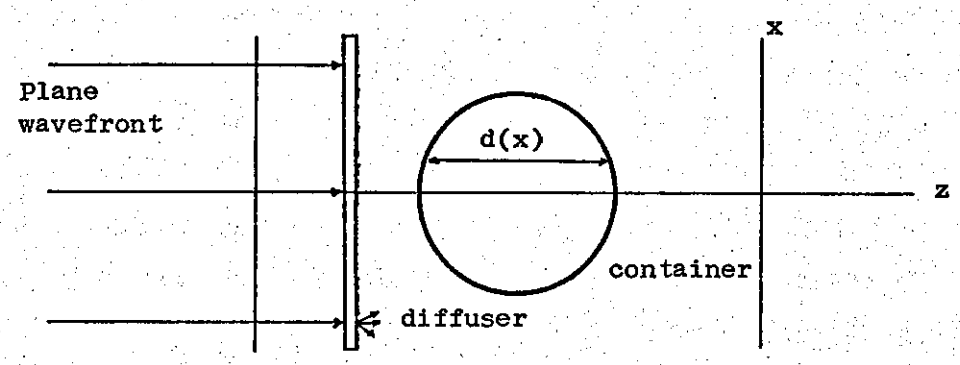

Fig.(42)

The phase change produced by a refractive index change of the liquid, $n_2 - n_1$, is expressed by

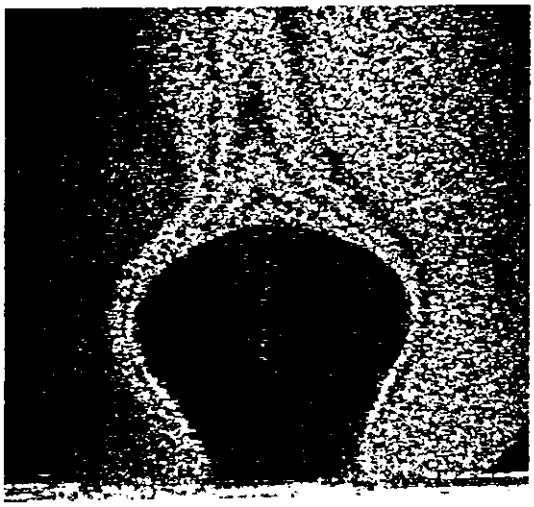

a

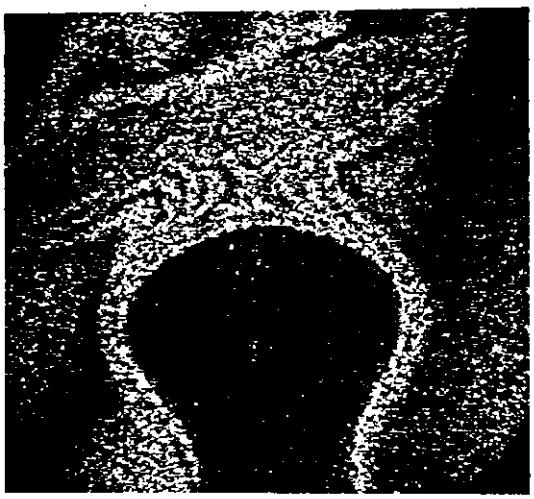

b

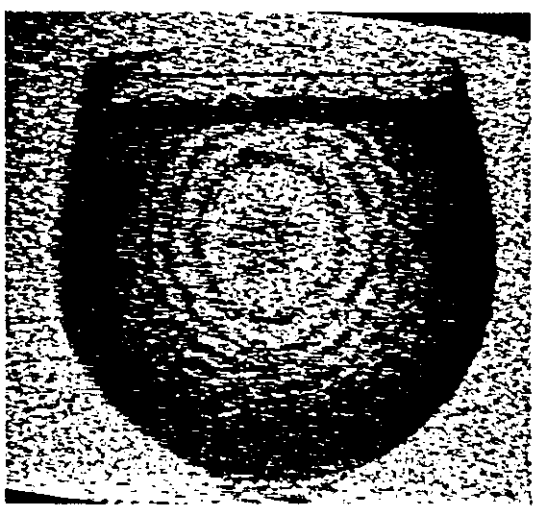

c

Fig. 41 (a) and (b) show the cooling process of a lamp, (c) contour fringes of a glass due to an isotropic change on the refractive index of the liquid contained in it.

UNIVERSITY OF TECHNOLOGY.
LOUGHBOROUGH,
MECHANICAL ENGINEERING.

$$\Delta\phi = \frac{2\pi}{\lambda} (n_2 - n_1)\, d(x) \qquad (115)$$

A phase change of $2n\pi$ gives

$$\Delta\, d(x) = \frac{n\,\lambda}{n_2 - n_1} \qquad (116)$$

where n is the fringe order (integer). Eq.(116) is the same equation derived by TSURUTA et al (1967) for normal illumination and viewing directions. The system range goes from few microns to several millimetres for combinations of liquids and gases, ZELENKA et al (1969), VARNER (ERF. Ed. (1974)).

HOLOGRAPHIC RECORDING TECHNIQUES FOR HOLOGRAPHIC ILLUMINATION CONTOURING

The most reliable recording technique in Holographic Interferometry, at present, is based on the use of silver-halide high resolution photographic emulsion. Other optical recording techniques have been developed to suit particular applications of holography although their use in Holographic Interferometry is under study[1].

Bleaching processes have been a major topic in holography since phase holograms were first reported by CATHEY (1965). The aim of those techniques have been the development of phase holograms of optimum characteristics, namely: high diffraction efficiency, low noise-high resolution and low wavefront distortion.

1. An extensive guide to these techniques, up to 1971 is found in BUTTERS, Ch.9 (1971), COLLIER et al, Ch.10 (1971) and in the "Proceedings of the International Symposium of Holography" VIENOT, et al, Eds. Besancon (1970). Interesting reading, as a comparison, for the bleaching of photographic plates, discussed later are: SHANKOFF (1968) (grating spacing, air-gelatin index differential, exposure values, etching) and LIN (1969), (chemical hardener, absorption spectra).
   For the use of photoplastic material in holography see LIN et al (1970), LEE (1974) FRIESEM (1975).
   For an appraisal of the material and devices for Holographic data storage and optical storage of digital data see the Applied Optics issue of April 1974, Vol.13, No. 4 and VANDER LUGT (1975).

The holograms in general, may be divided according to the type of "hologram grating"[1] formed after the bleaching process: absorption hologram grating (silver image). The emulsion thickness varies proportional to the original silver density of the grating, creating a silver emulsion relief; pure relief hologram grating (pure relief image). The emulsion is transformed to a transparent compound of varying thickness proportional to the original silver density, where effects on the reconstructed wavefront due to changes in the refractive index of the emulsion are negligible, ALTMAN (1966)[2]; dielectric hologram grating (dielectric image). The emulsion is transformed to a transparent compound whose refractive index variation is proportional to the original silver density, and where emulsion relief effects are negligible, UPATNIEKS et al (1970), PENNINGTON et al (1970).

In practice both emulsion effects, relief and refractive index, are present in any bleaching process, and a reduction in one of them results in an improvement of the hologram characteristics. Furthermore it has been shown[3] that the noise and unwanted distortion of the emulsion, products of the recording and bleaching processes, may be reduced by the proper choice of holographic processing parameters.

The selection of dielectric bleaching techniques in holographic illumination contouring satisfies the need for a high-diffraction-efficiency hologram grating besides the almost uniform wavefront response,

1. After KOGELNIK (1967), also frequently called "image". See p133.
2. See also RUSSO et al (1968) for a discussion on resolution.
3. LAMBERTZ et al (1971), UPATNIEKS et al (1970), FRIESEM et al (1967), BIEDERMANN et al (1974), URBACH et al (1969), HAMALAINEN et al (1974).

required from the holographic plate, to argon laser light[1]. The use of Millimask "ultra flat" Agfa plates satisfies this requirement[2]. The modification of two bleaching techniques, besides high exposure values, were found to give satisfactory results in their application to holographic illumination contouring. Both techniques are described below.

It was found that a modification of the Agfa reversal bleaching (Agfa Gevaert Technical Information)[3] gave a satisfactory diffraction efficiency, low wavefront distortion and great hologram stability to ordinary ambient laboratory conditions, ie. light and humidity. The processing of the holographic plates was carried out as described below:

i) Stress relief. The plate was immersed in industrial methylated spirit for 2 minutes, BUTTERS et al (1969). The plate was then slowly removed from the spirit by one edge to prevent a non-uniform drying and then left to stand on its opposite edge, to dry in a nitrogen atmosphere, BURCKHARDT et al (1969) for 15-20 minutes.

ii) Exposure, $D > 4$, See Appendix A.

iii) Developed for 5 minutes in Agfa Gevaert G3P.

iv) Stop. 1% solution of acetic acid, 2 minutes.

v) Washed in running water for 5 minutes.

1. Intensity of at least 100 mW is required from the laser.
2. All bleaching experiments were conducted using Millimask Agfa plates.
3. See LAMBERTZ et al (1971), GEORGE et al (1970), SMITH (1968) for similar bleaching processes.

vi) Bleach for 2 minutes. Agfa reversal bleach:

5 gm potassium dichromate

5 ml concentrated sulphuric acid in 1 litre of distilled water

vii) Wash in running water for 5 minutes

viii) Clear for 90 seconds.

50 gm sodium sulphate (anhydrous)

1 gm sodium hydroxide in 1 litre of distilled water

ix) Wash in running water for 5 minutes.

x) Desensitize for 3 minutes.

2230 ml industrial methylated spirits

200 ml distilled water

32 ml glycerol

240 mg potassium bromide

200 mg phenosafrinine

xi) Wash in industrial methylated spirits for 2 minutes

xii) Wash in Drysonal[1] for 2 minutes

xiii) Dry in a nitrogen atmosphere

Steps (i), (ii) - (x) were carried out under continuous agitation. The temperature of the solutions was kept at 20°C throughout the bleaching process.

1. TETENAL-PHOTOWERK, Hamburg-Berlin.

Although the effect of the phenosafrinine dye (indicator) in desensitization is considered to be that of a filter[1] (the emulsion takes a red-bluish colour) there was no noticeable change in the diffraction efficiency measurements when the dye was eliminated. The holograms bleached in this way were as stable as those immersed in the dye solution. The purpose of the stress relief step, the baths in methylated spirits and Drysonal and the drying in nitrogen, is to prevent as much as possible, movements of the emulsion due to tanning and non-uniform drying, PENNINGTON et al (1970).

Diffraction efficiency measurements were obtained in a manner generally accepted for comparison, that is, diffraction efficiency measurements of a thick hologram sinusoidal grating, LATTA (1968), KOGELNIK (1967)[2]. According to KOGELNIK a hologram grating is regarded as thick if the couple wave theory parameter Q, defined below, is much greater than unity. We have

$$Q = \frac{2\pi \lambda d}{n (\Delta x)^2} \qquad (115)$$

where d, n, Δx represent the average values after bleaching of: emulsion thickness, refractive index and grating period (Eq. 22) respectively.

To comply with this, during exposure the plates were held by gravity in a kinematic holder. The plate normal made an angle of 7^{o}

1. According to GEORGE et al (1970) the dye works only at low densities ($D < 1$). As will be seen later, the original silver density was high, $D > 4$. See also NORMAN (1972). For bleached holograms containing non silver metal compound see NISHIDA (1974).

2. See ROBERTSON et al Ed. (1970).

with respect to the plane of incidence, and its projection in that plane bisected the 40° angle between the two plane wavefronts. The polarization of these was perpendicular to the plane of incidence and the ratio 1:1.

An angle of 40° between the beams and used light of $\lambda = 4965\text{Å}$ may be regarded as intermediate values for holographic illumination contouring arrangements. It is worth remembering at this point, that emulsion relief effects[1] are to be avoided in order to obtain optimum characteristics from a hologram dielectric grating, therefore, an average spatial frequency grating of 1400 lines/mm (for an angle of 40°) seems to be a good choice. Then for Millimask Agfa plates ($d = 7\ \mu$, $n = 1.5$,) $Q = 13$.

Fig.(43) defines the relevant beams during reconstruction and in which RI represents the master wavefront in holographic illumination contouring.

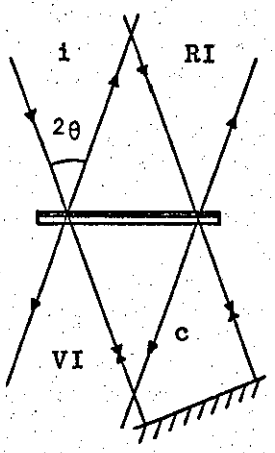

Fig.(43)

1. SMITH, p537 (1968), LAMBERTZ et al p1344 (1971), UPATNIEKS (1969).

The diffraction efficiencies[1] are plotted for $\lambda = 4965\text{Å}$ and $\lambda = 4880\text{Å}$, Fig. (44). It was noted that the maximum value for (RI/i)100 generally occurred for an exposure nearly twice the exposure needed for $(RI/c)100_{max}$. The exposure for maximum efficiency corresponds to density values greater than 4.[2]

The maximum value for (VI/i)100 occurs when the fraction of undiffracted light is minimum, result that agrees with McMAHON (1969-1970). The results for (RI/i)100 applied to holographic illumination contouring would of course be improved if the beam i would be incident on the back of the plate.

Fig. (45) shows clearly the effects of drying on diffraction efficiency. A drop on diffraction efficiency values is apparent when both the washing of plates in methylated spirits and the drying in nitrogen, is eliminated.

Lately a second bleaching technique has been found to provide better results in holographic illumination contouring than the previously discussed bleach: greater diffraction efficiency and lower wavefront distortion.

The bleaching procedure consists of the modification of the procedure first proposed by THIRY (1972), improved by GRAUBE (1974) and discussed by VAN RENESSE (1975).

1. After bleaching the plates were repositioned exactly in its original place as for holographic illumination contouring.

2. For AGFA 8E75 and $\lambda = 6328\text{Å}$, the maximum efficiency corresponds to exposure values about 4500 ergs/cm^2.

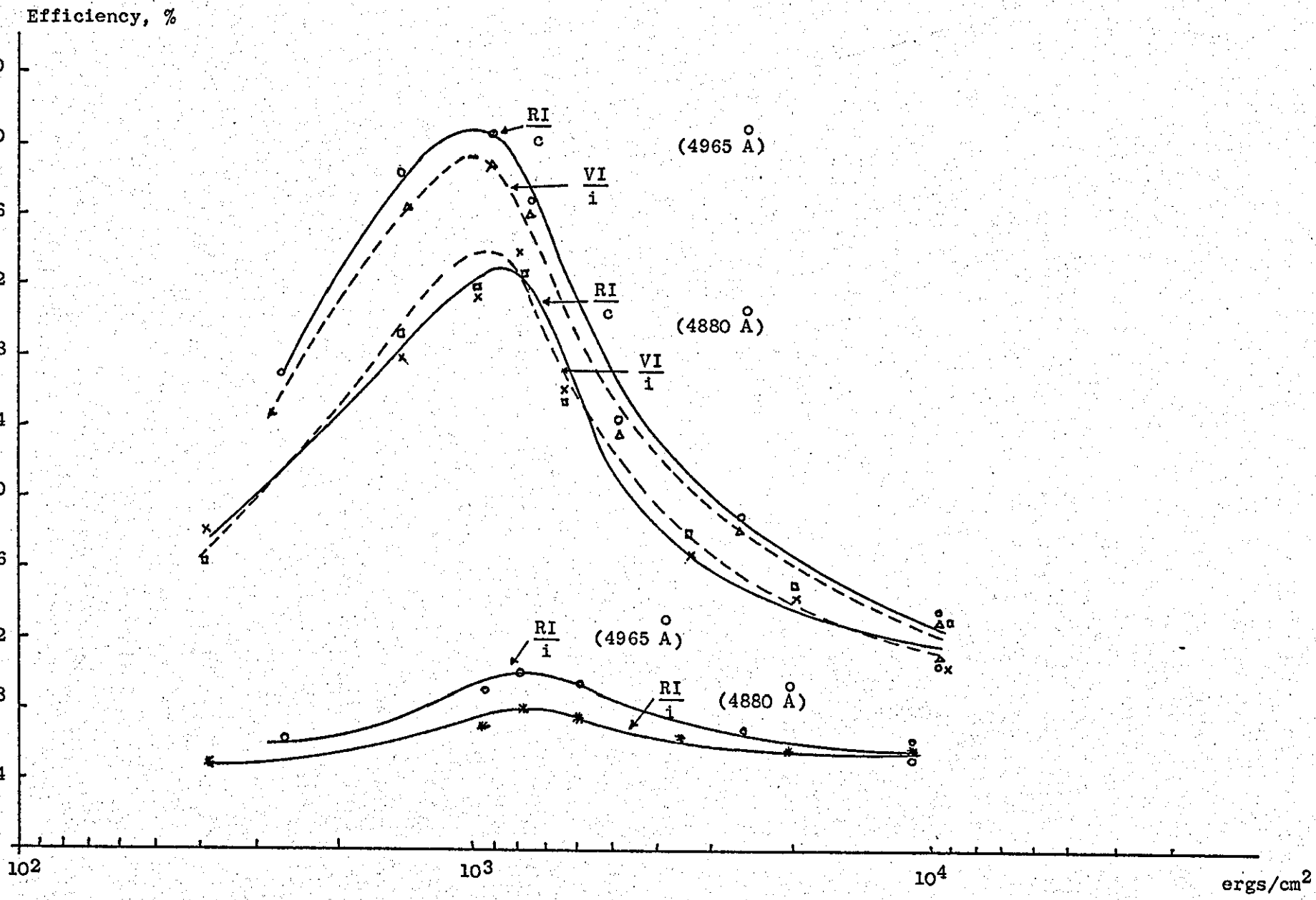

Fig.(44) Diffraction efficiencies of bleached holograms for 4965Å and 4880Å.

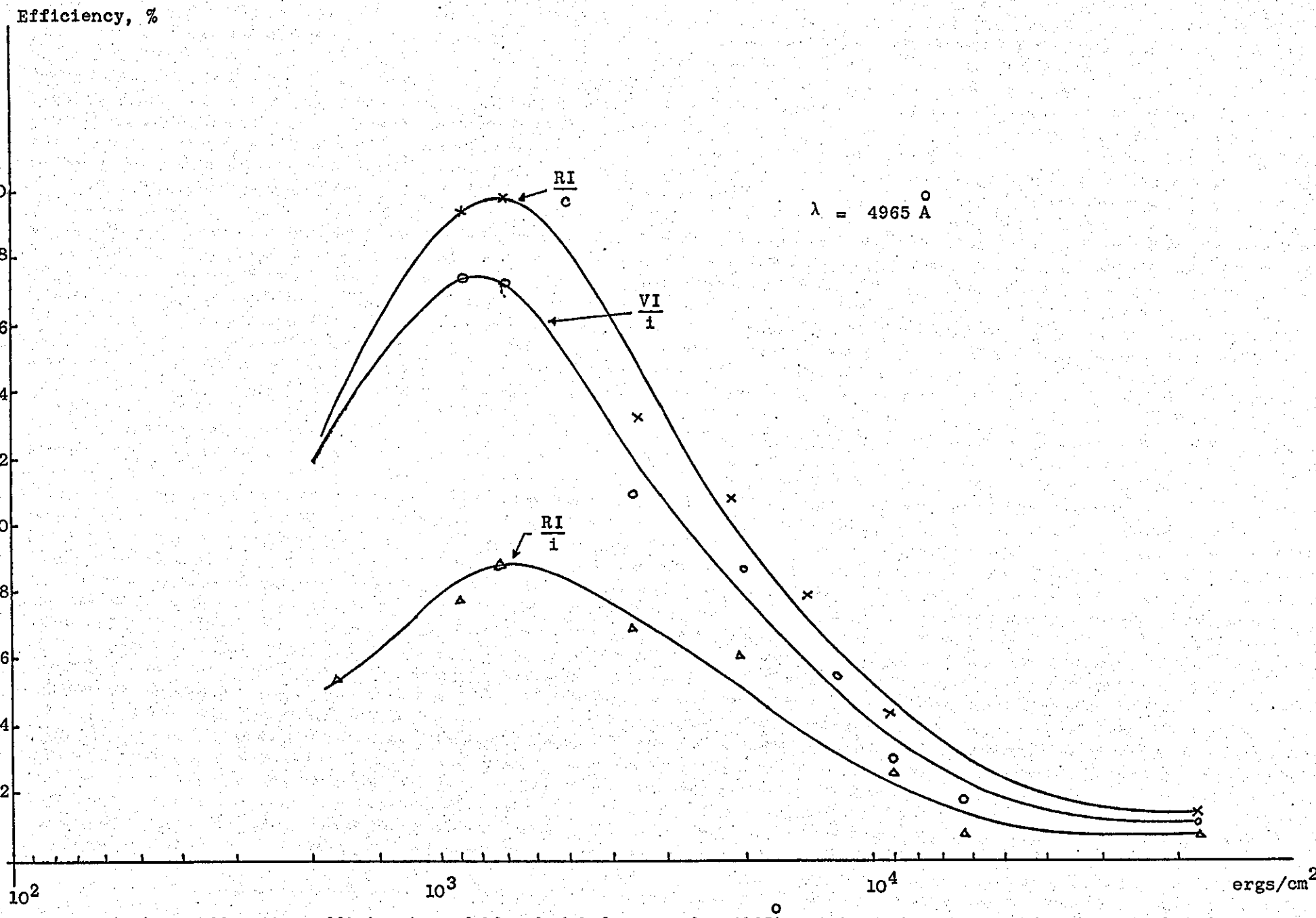

Fig.(45) Diffraction efficiencies of bleached holograms for 4965Å obtained when the washing in methylated spirits and drying in nitrogen were eliminated.

The processing of the holographic plates was carried out as described below:

1. Stress relief as for Agfa bleach.
2. Exposure of about 1000 ergs/cm^2 for Millimask Agfa plates. Density 2-3.
3. Develop for 5 minutes in Agfa Gevaert G3P.
4. Stop. 1% solution of acetic acid, 1-2 minutes.
5. Fix for 5 minutes in Agfa-Gevaert G334.
6. Wash in running water for 10 minutes.
7. Wash in Drysonal for 2 minutes.
8. Immediately, while still wet, the plate is placed in a tank in the same attitude as for step 1. Add 5 ml of bromine in the tank. The plate will clear in 15 seconds. (CAUTION: this step must be carried out in a fume cover, and the necessary body protection must be worn).
9. Leave the plate in the fume cover for $\frac{1}{2}$-1 hour.

It is advisable to provide a slow air current to evenly distribute the action of the bromine vapour over the whole plate, specially when the plate is completely dry before step 8. The tank must be partially covered to avoid a rapid escape of the vapour. Steps 1, 3-7 were carried out under continuous agitation, and the temperature of the solutions was kept at 20°C.

To assess the performance of these two bleaching procedures in ESPI the following real time experiment was carried out.

Fig. (46)(a) and (b) illustrate the arrangement of the optical components used with the ESPI system and the test object respectively.

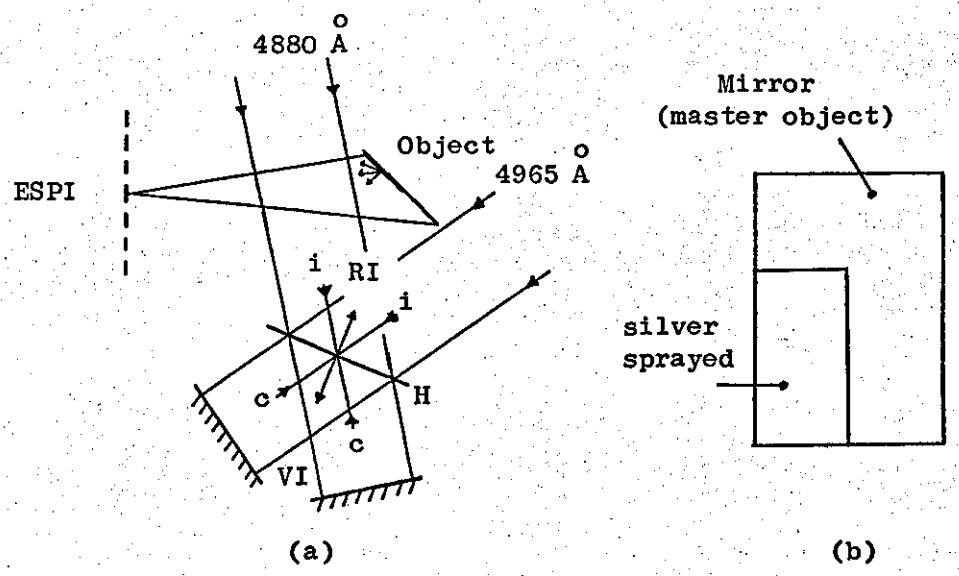

Fig.(46)

Three pairs of Millimask Agfa plates were utilised. One plate of each pair was stress relieved, and all the plates were twice exposed, half of the exposure for $\lambda = 4965\text{Å}$ and the other half for $\lambda = 4880\text{Å}$.

The first pair consisted of amplitude holograms, the second and third pairs were bleached by the bromine (Br) and Agfa techniques respectively. The total exposures were 300, 750 and 3000 ergs/cm^2 for the first, second and third pair of plates respectively, and the laser output was adjusted to give equal exposure times for both exposures and to compensate for the wavelength response of the plates.

The purpose of the silver sprayed part of the object was to check the exact relocation of the plates, and the mirror part acted as a master object for holographic illumination contouring. Both parts were used in real time to assess the wavefront distortion introduced by the processing of the plates[1].

1. See HARIHARAN (1975) for the phase shift in phase holograms.

Fig.(47) shows the residual fringes having the scattered part of the object in the background, and the oval shape corresponds to the reference beam. The fringes are still observed outside this region because the specular part of the object acts as a reference.

All stress relieved plates gave better results with respect to the residual fringes. The non-stress relieved plates are shown on Fig.(47) with the symbol '. Figures marked (a), (a'), (c), (c'), (e), (e') and (b), (b'), (d), (d'), (f), (f') correspond to $\lambda = 4880\text{Å}$ and $\lambda = 4965\text{Å}$ respectively. Pairs (a) and (b) correspond to amplitude holograms and pairs (c), (d) and (e), (f) correspond to the plates bleached by the bromine and Agfa process respectively. It can be observed that the stress relieved plates have less residual fringes than the other plates, and the same is said for the plates bleached by the bromine process with respect to the ones bleached by the Agfa process, the former giving better results. The minimum residual fringe, two hours after the processing of the plates, was $\frac{1}{4}$ of a fringe for $\lambda = 4880\text{Å}$ and $\frac{1}{2}$ of a fringe for $\lambda = 4965\text{Å}$. The difference in the number of residual fringes with wavelength (more fringes for 4965Å) can be seen on Fig.(47). This aspect is not well understood at the moment.

The results obtained with the specular part of the object are presented below. The fringes produced by the interference of the master-mirror object wavefront and the reconstructed wavefront (virtual image) are non-localised and can be projected on a screen. The fringes are also found in the direction of the $\lambda/4$ mirrors due to the interference of the reconstructed and reference wavefronts in those directions, such that the fringes are projected back into the ESPI system via the master mirror object and are detected by the television camera.

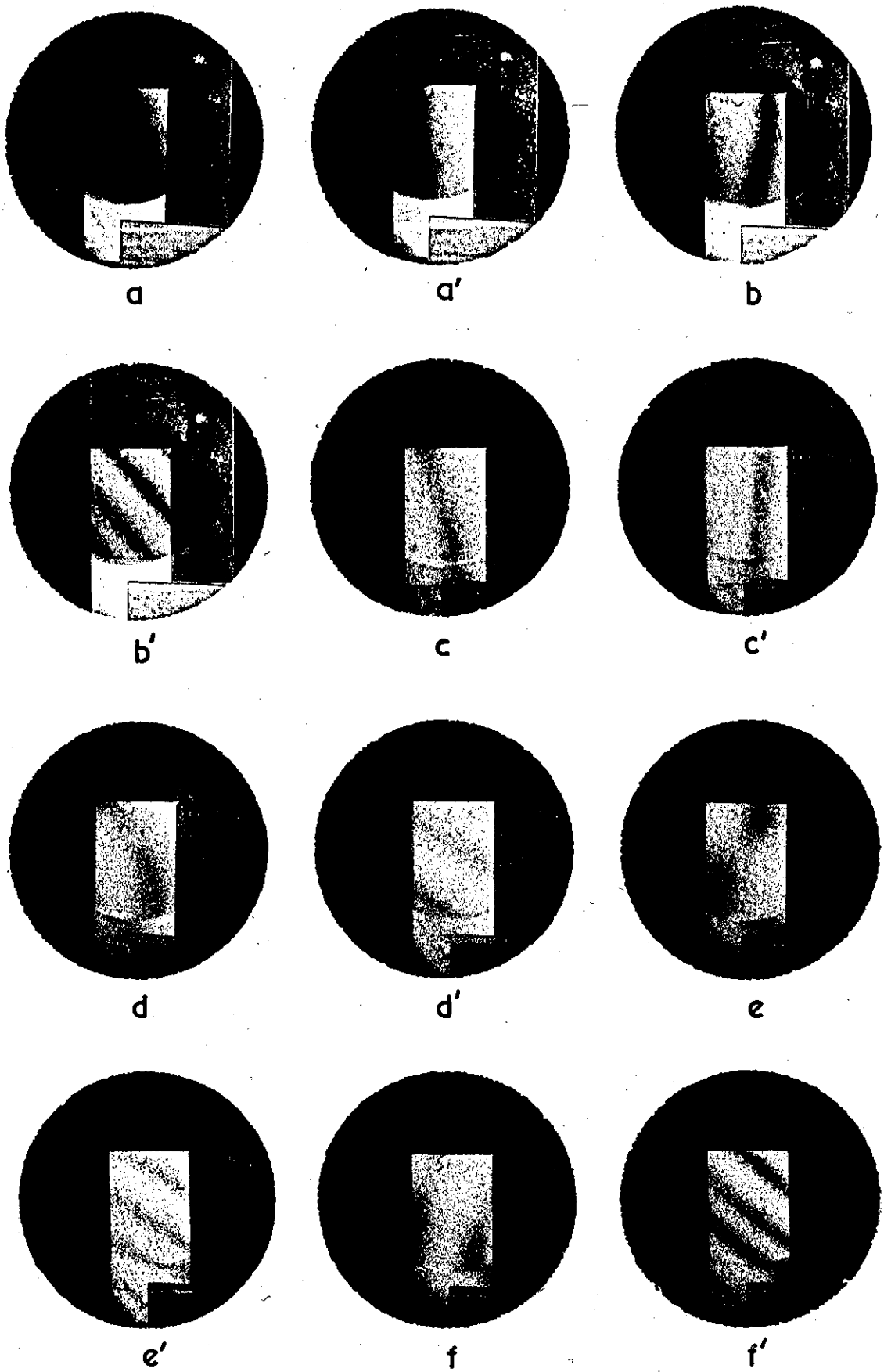

Fig. 47 Spurious fringes due to emulsion movement.

UNIVERSITY OF TECHNOLOGY
LOUGHBOROUGH,
MECHANICAL ENGINEERING.

Fig.(48) shows the photographs taken from the television screen of the two bleached pairs of plates. The photographs marked (c), (c'), (d), (d') and (e), (e'), (f), (f') show the residual fringes corresponding to the plates bleached by the bromine and Agfa process respectively. The amplitude holograms did not give enough light intensity for the fringes to be observed on television.

Table II shows the diffraction efficiencies for the bleach holograms of Figs. (47) and (48). The efficiencies for the amplitude holograms were less than 0.5%.

TABLE II

	$\lambda = 4880\text{Å}^{o}$				$\lambda = 4965\text{Å}^{o}$			
Bleach		$\frac{VI}{i}100$	$\frac{RI}{c}100$	$\frac{RI}{i}100$		$\frac{VI}{i}100$	$\frac{RI}{c}100$	$\frac{RI}{i}100$
Br	c	14.3	18.2	3	c'	21.2	24	3.86
	d	14.8	19.5	3.4	d'	22.1	24.8	3.91
AGFA	e	5.4	7.1	3.1	e'	6.3	6.7	3.3
	f	5.7	6.8	3	f'	9.0	9.4	4.18

It can be seen from the table that the (RI/i)100 efficiencies are slightly higher for the plates bleached by the bromine process, and that this bleach gives much better results than the Agfa bleach when the (RI/c)100 efficiencies are considered.

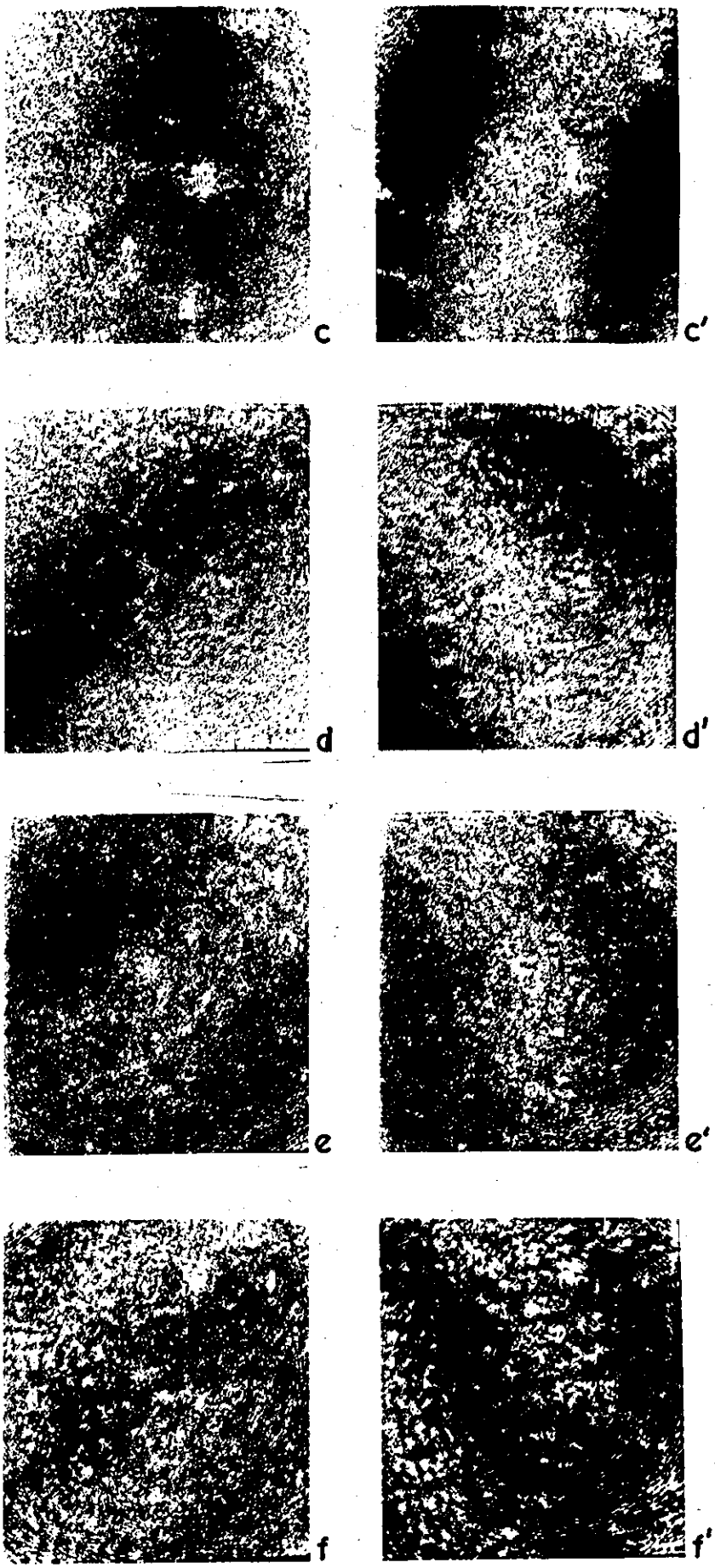

Fig. 48 Photographs taken from a television screen showing spurious fringes due to emulsion movement.

UNIVERSITY OF TECHNOLOGY
LOUGHBOROUGH,
MECHANICAL ENGINEERING.

SCOPE AND APPLICATIONS OF ESPI CONTOURING METHODS

The principle of contouring surfaces of any curvature by ESPI has been established. The use of ESPI has significant advantages over holographic methods. It offers contour difference information between surfaces of similar shape instead of contour information with respect to a flat reference plane. It does not require reconstruction of a wavefront, except in the holographic illumination contouring method, where only one hologram is required for the inspection of components in a production line. The contour fringes are localised on the surface, and the system offers in-line illumination and viewing directions. Furthermore the superposition of the signal and reference wavefronts is in-line and not off-axis as in holography, simplifying the optical arrangement. The optical signal is processed electronically thus offering a real-time operation. The application of ESPI to smooth surfaces can be regarded as reduced sensitivity interferometry.

The ESPI system offers a real time analysis of the propagation of total refractive index changes, and the contouring of transparent objects. In particular cases the object, a light bulb for example, can be rotated to give information about different directions, in a rapid way.

There are limitations to the information that can be deduced from a single contour fringe pattern. The zero order fringe cannot be identified (though it is not necessarily present). It should be noted that, if present, it may be dark or bright or of intermediate intensity, depending on the relative lengths of the reference and signal paths, as indicated by Eq.(109). Knowledge of the zero order fringe

position and other fringe numbers is necessary in the case of holographic illumination contouring to enable one to determine the absolute shape difference between the two surfaces which are effectively compared. Without knowledge of the fringe order number, only relative measurements are possible. The fringe analysis for irregularly curved surfaces (as done by holographic illumination contouring) must take account of the changing sensitivity over the surface. The rapid inspection of such components will require computer processing of the data.

It is expected that dye lasers will permit the application of the methods described (I, II and III) to contour intervals extending over a wide range. For example a range from 180 μm to 3½ μm should be available from one common dye. Moreover the sensitivity will be continuously variable over this range.

Aspects of contouring to be further investigated include: the de-correlation of speckle patterns as a function of surface roughness and wavelength difference, fringe interpretation and computer-aided analysis, extension of the range of applications through the use of dye lasers, the development of the holographic illumination method to contour sizeable components and the modification of the ESPI rig to provide a variable magnification, by interchanging of lenses, without varying the distance of the object from the system, thus producing a more compact system. The size of the system will increase as the aperture is increased.

SYMBOLS

CLA Centre line average

Constant range - see p 59.

Contour interval, contour fringe, constant range - see p 61.

Figure interference - see p52.

High difference, contour interval, depth change per fringe - see p51.

Interference lines - see p61.

r,s - see p54.

Smooth wavefront - see p54.

$\Delta\phi_s$ - see p54.

Δ - see p66.

δ - see p66.

α - see p76.

APPENDIX A

PHOTOGRAPHIC PLATE CHARACTERISTICS

Let us concentrate our study on the parameters which describe the behaviour of a silver-halide emulsion from empirical charts.

The photographic plate characteristics are based on the Hurter-Driffield (H&D) curve and on the transmittance-exposure curve, Fig.(49)(a) and (b), respectively.

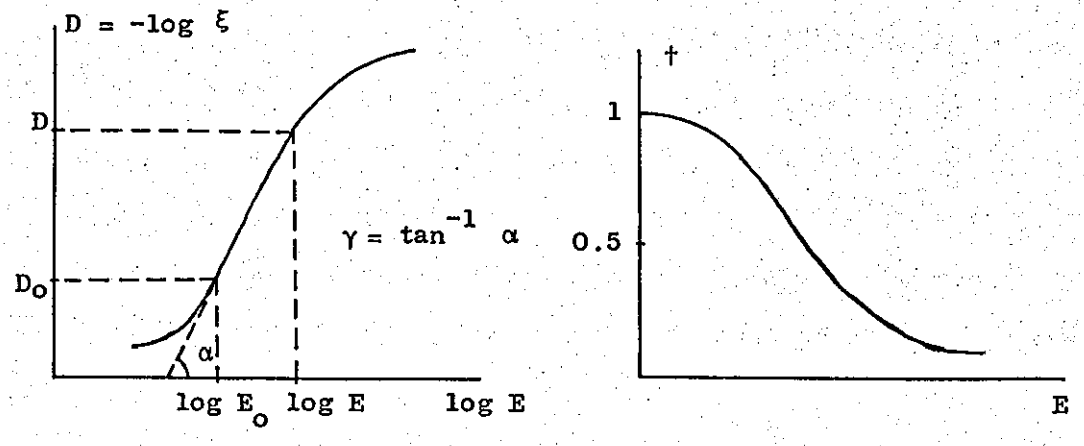

Fig.(49)

Intensity

Let us define, for simplicity, the intensity[1] of an electromagnetic plane wave, at a point P in a homogeneous and isotropic medium (free space), as the time average of the magnitude of the Poynting vector. This corresponds to the time average of the energy density per unit time per unit area normal to the flow, watts/m^2.

1. KLEIN, p122 (1970) call it "irradiance" "flux density" "radiant incidence",
BUTTERS, p149 (1971), "Irradiance", ROBERTS (1972).

The Maxwell's equations, in the rationalized MKS system[1], for an electromagnetic perturbation in the medium described above takes the form

$$\text{curl } \underset{\sim}{E} = -\mu \dot{\underset{\sim}{H}} \qquad (116) \qquad \text{div } \underset{\sim}{E} = 0 \qquad (118)$$

$$\text{curl } \underset{\sim}{H} = \varepsilon \dot{\underset{\sim}{E}} \qquad (117) \qquad \text{div } \underset{\sim}{H} = 0 \qquad (119)$$

where

μ - permeability

μ_o - permeability in vacuo $\simeq 4\pi(10^{-7})$ Weber/amp-m

μ' - relative permeability

$$\mu = \mu_o \mu' , \quad \underset{\sim}{B} = \mu \underset{\sim}{H} \qquad (120)$$

and

ε - permittivity

ε_o - permittivity in vacuo $8.9\ (10^{-12})$ coul^2/nt-m^2

ε' - relative permittivity

$$\varepsilon = \varepsilon_o \varepsilon' , \quad \underset{\sim}{D} = \varepsilon \underset{\sim}{E} \qquad (121)$$

Next we follow BORN, et al § 1.2 (1970)[2] in the International System of units as it is our case. Thus, it is found that

$$\nabla^2 \underset{\sim}{E} - \mu\varepsilon \ddot{\underset{\sim}{E}} = 0 \qquad (122)$$

comparing Eqs.(122) and (1) and using Eqs.(120) and (121) we have

$$v_p = \frac{1}{\sqrt{\varepsilon\mu}} \qquad (123)$$

and

$$v_p = \frac{1}{\sqrt{\varepsilon_o \mu_o}} \cdot \frac{1}{\sqrt{\varepsilon' \mu'}} = \frac{c}{\sqrt{\varepsilon' \mu'}}$$

Then the refractive index is defined as

$$n = \frac{c}{v_p} = \sqrt{\varepsilon' \mu'} \qquad (124)$$

1. CONDON, pp4-3 (1958), International System.

2. Gaussian system of units.

Also it can be shown that the Poynting vector takes the form[1]

$$\underset{\sim}{S} = \underset{\sim}{E} \times \underset{\sim}{H} = E\,H\,\hat{s} \qquad (125)$$

where $\hat{s}$ is the unit vector in the direction of propagation[2].

Using the relation $\sqrt{\mu}H = \sqrt{\epsilon}\,E$ and Eq.(123) the magnitude of $\underset{\sim}{S}$ becomes

$$S = \frac{\epsilon}{\sqrt{\epsilon\,\mu}}\,E^2 = v_p\,\epsilon\,E^2 = 2\,v_p\,u_E \qquad (126)$$

where u_E is the energy per unit volume stored in the electromagnetic (plane) wave.

Therefore the expression for intensity is written as

$$I_p = \langle S \rangle = v_p\,\epsilon\,\langle E^2 \rangle \qquad (127)$$

where, as it is being considered, E represents a harmonic solution of the scalar wave equation, Eq.(122)[3].

It is customary in holographic interferometry to represent intensity in a convenient form such that it is equal to the square of the amplitude of the electric vector, thus

$$I = 2\,\langle E^2 \rangle \qquad \left(\frac{\text{Watts}}{m^2}\right) \qquad (128)$$

1. BORN et al, pp7,24 (1970) in the Gaussian system of units.
2. See p15.
3. See Eqs.(1) and (5)

Exposure

Exposure is defined by[1]

$$E = I_p t \propto I\ t \qquad (\text{ergs/cm}^2) \qquad (129)$$

where t represents exposure time.

Although an exposure metre measures I_p, it will be considered for simplicity in the mathematical operations

$$E = I\ t \qquad (130)$$

as the equation which represents the exposure[2].

Other parameters

After the holographic plate has been exposed and developed the intensity transmittance $\xi(x,y)$ of the plate is defined by

$$\xi = \frac{I_t}{I_i} \qquad (130)$$

and the complex amplitude transmittance $\dagger$ by

$$\dagger = \frac{U_t}{U_i} \qquad (132)$$

where the subscripts i and t indicate "incident" and "transmitted" respectively.

1. Note the different meaning of E in Eqs.(128) and (129). Also we will refer to I as the intensity of light incident on the holographic plate during exposure.

2. BUTTERS § 9.5 (1971).

Using Eq.(10) the complex amplitude transmittance may be written as[1]

$$\dagger = \sqrt{\xi} \qquad (133)$$

and Eq.(131) becomes

$$\xi = \dagger\dagger^{*} \qquad (135)$$

The photographic density D is defined as

$$D = \log \left(\frac{1}{\xi} \right) = - \log \xi = - 2 \log \dagger \qquad (136)$$

From Fig.(49)(a) we obtain

$$D = D_o + \gamma \log \frac{E}{E_o} \qquad (137)$$

where D_o correspond to the bias exposure E_o and γ is the slope.

1. Eq.(133) is true when a liquid gate is used to overcome, in great extent, the phase shifts introduced by variations in the thickness of the base and film emulsion (relief). Otherwise the expression for $\dagger$ is written as

$$\dagger(x,y) = \sqrt{\xi\ (x,y)}\ \exp \left[j\ \phi(x,y) \right] \qquad (134)$$

where $\phi(x,y)$ represent the phase change introduced by the plate. As is mentioned in Chapter III, ultra flat holographic plates were used and care was taken to minimise undesirable distortion of the emulsion due to the reversal bleaching process.
In our context, the consideration of Eq.(134) is not critical and Eq.(133) is used instead, KASPAR et al, p970 (1968).
When holograms are used in advertising, unwanted scatter light (flare) produced by the relief of the emulsion, is greatly reduced by gluing together the hologram and a flat glass plate by means of a matching index liquid thus forming a liquid gate.

From the last two expressions we have

$$\dagger = \dagger_o \left(\frac{E}{E_o} \right)^{-\frac{\gamma}{2}}$$

$$= \dagger_o \left(1 + \frac{\Delta E}{E_o}\right)^{-\frac{\gamma}{2}} = \dagger_o \left(1 + \frac{\Delta_I}{I_o}\right)^{-\frac{\gamma}{2}} \qquad (138)$$

where $E_o = I_o t$ and $\Delta E = \left| E - E_o \right|$, see Fig.(49)(b).

Being $\Delta E/E_o$ a small number, Eq.(138) may be approximated by the first two terms of its binomial expansion, then

$$\dagger = \dagger_o \left(1 - \frac{\gamma}{2} \frac{\Delta_I}{I_o}\right) \qquad (139)$$

APPENDIX B

TECHNICAL INFORMATION

The electronic unit used to process the optical signal in ESPI is illustrated in Figs.(50) and (51)[1]. Fig.(50)(a) shows: the television camera; the camera control unit; the synchronous pulse generator and the general locking system which also controls the video disc store unit shown in Fig.(50)(b). Fig.(51) depicts a flow diagram of the signal processor of the ESPI system; it includes a sync. pulse remover that does not appear in later versions, the subtractor circuit, and full wave rectifier section (with a sync. and blanking adder circuit), and finally a filtering circuit. The line-phase control, adjusts the relative positions of the outgoing sync. pulses to the sync. pulses applied to the general locking circuit.

The following abbreviations and symbols are used in Figs.(50) and (51).

B/rem	-	B or/and remote
CAM	-	camera
Ext ref	-	external reference
FWR	-	full wave rectifier
MB	-	mixed blanking
MS	-	mixed sync.
S&B adder	-	sync. and blanking adder
VTR	-	video tape recorder or disc store
Xtal	-	crystal oscillator
⌀	-	adjustable
⌀	-	pre-set

1. See p95.

An argon laser SPECTRA PHYSICS model 171 was used with an intra-cavity etalon to provide a few metres of coherence length. For light intensity readings a power meter Coherent Radiation Laboratories model 212 was used. (It measures watts/0.5 cm^2, so this fraction must be multiplied by 2 if watts/cm^2 are required.

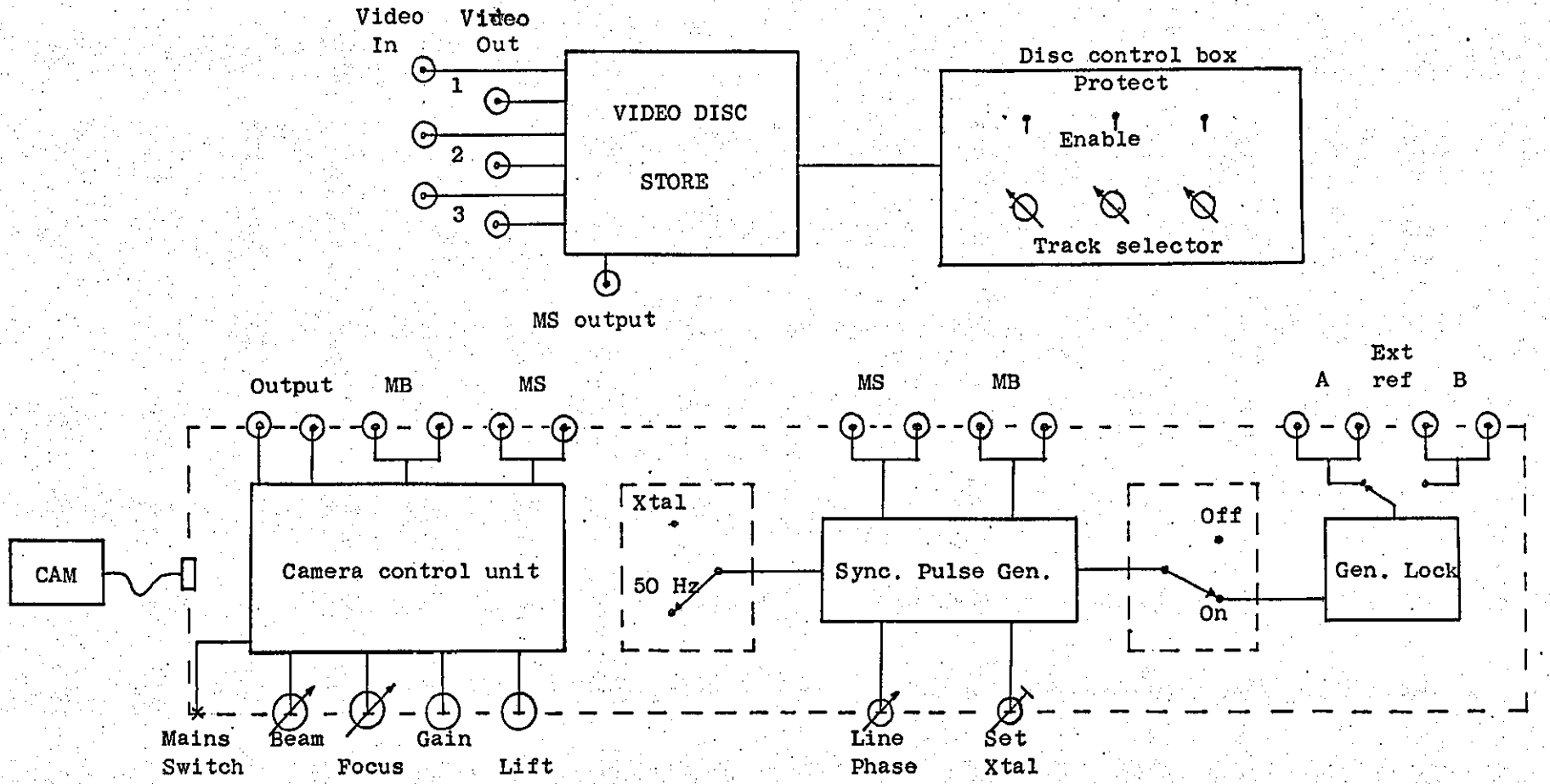

Fig.(50) ESPI Electronic Unit

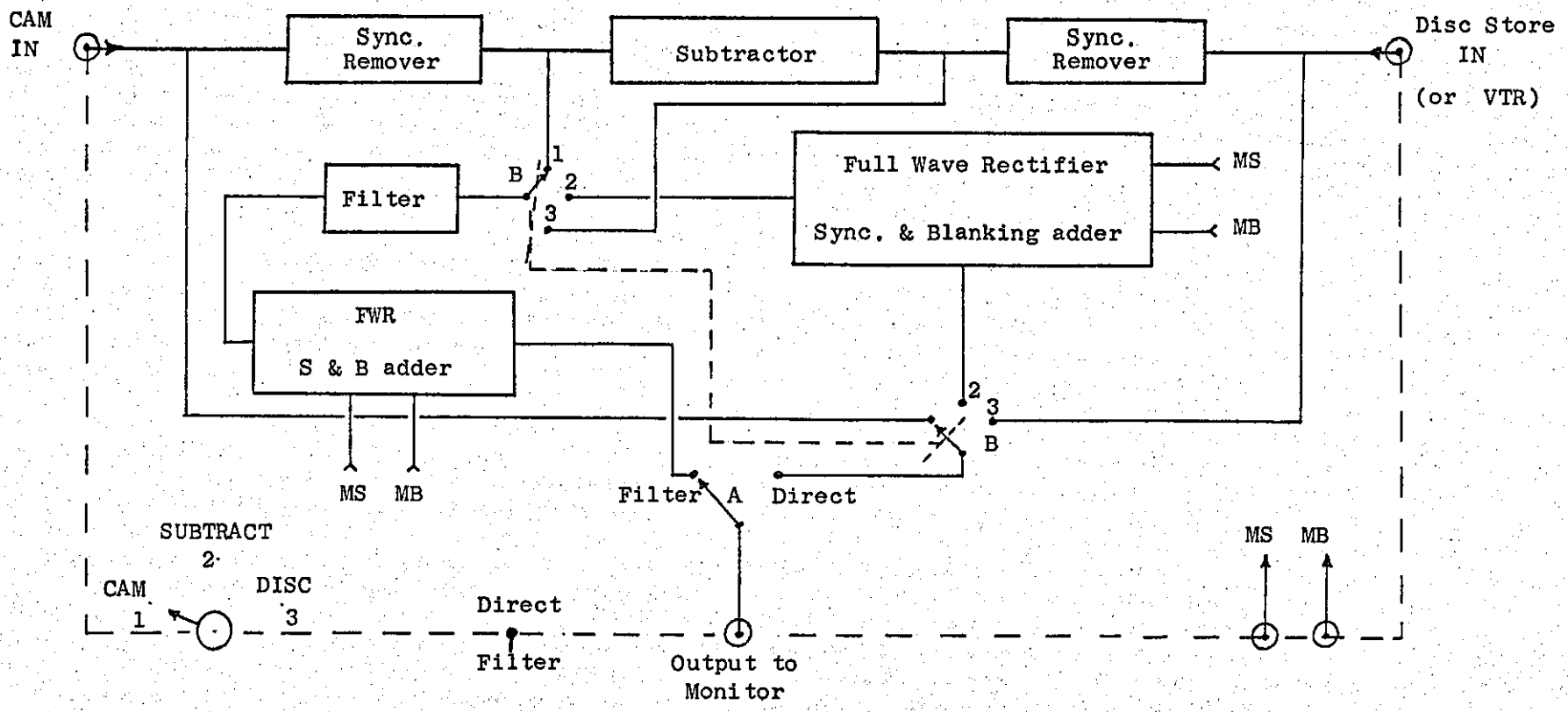

Fig.(51) Flow diagram of the ESPI signal processor

APPENDIX C

INTRODUCTION TO DIFFRACTION AND FOURIER ANALYSIS

Although the phenomenon of diffraction occurs as the optical wavefront propagates in space the diffraction by an obstacle, a diffraction grating[1] for example, is more apparent.

Holography forms by the interference of wavefronts a pattern of interference lines unique to the formative optical system[2]. This spatial distribution of intensity, when recorded, creates a diffraction grating which contains the optical information: phase and amplitude. The retrieval of information is obtained by diffraction of the illuminating wavefront by the grating.

It happens that the distribution of light at a point in space (for instance at a distance z from a grating) can be represented by the mathematical transformation of the distribution of light at a different point, (at the grating).

This appendix is intended as an introduction to Diffraction Theory and Fourier Analysis. These subjects are treated in detail by BORN et al (1970) and GOODMAN (1968).

1. "Hologram grating" after KOGELNIK (1967).
2. BUTTERS § 2.8 (1971).

Sinusoidal diffraction grating

Consider the interference of two plane wavefronts as illustrated in Fig.(52)(a). Let us assume for simplicity that the z axis bisects the angle between the two directions of propagation, $\theta = \theta_1 = \theta_2$ in Fig.(4), and that a photographic film is placed on the xy plane to record the interference lines thus forming a sinusoidal amplitude grating[1].

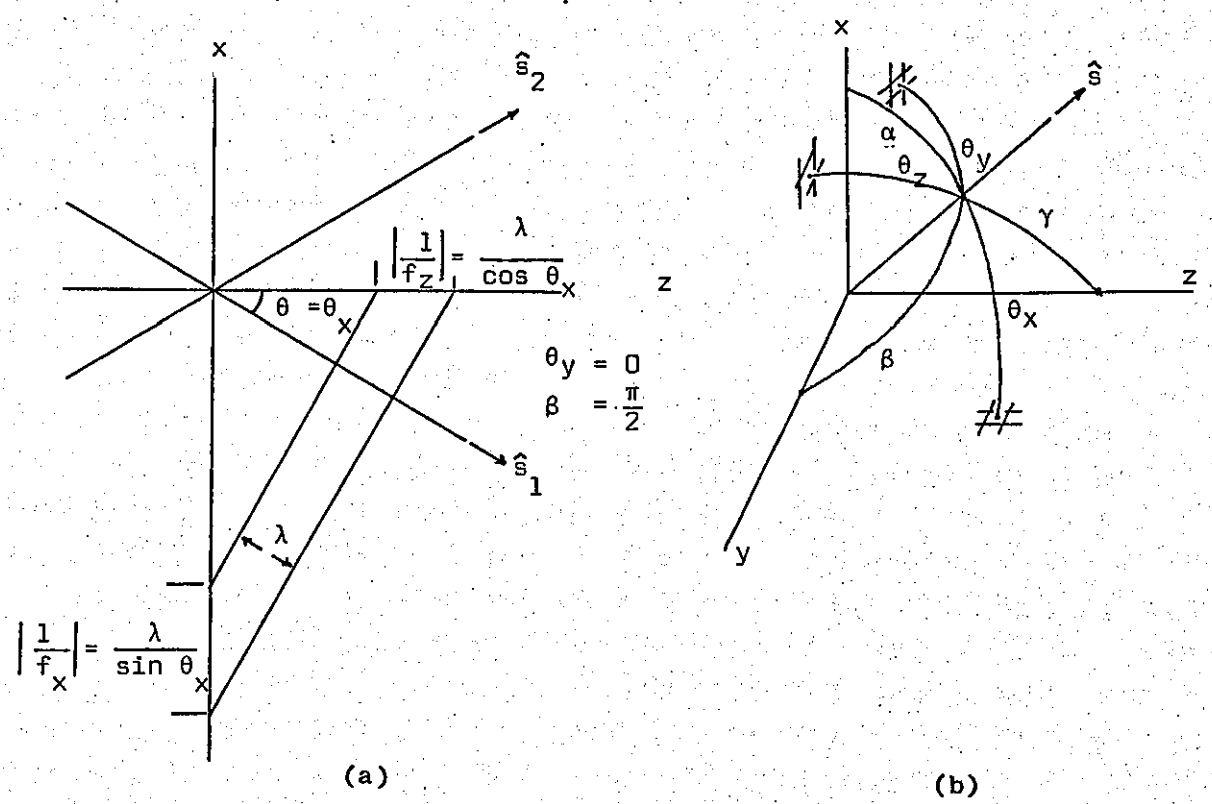

Fig.(52)

As is shown by Fig.(52)(b), θ_x, θ_y, θ_z are the angles that the unit vector $\hat{s}$ makes with the planes perpendicular to the axis x,y,z

1. See Appendix A for photographic film characteristics. For sinusoidal phase grating see KOGELNIK (1967).

respectively, and cos α, cos β, cos γ are the direction cosines of $\underset{\sim}{r}$, see Fig.(3).

Thus:

$$U = A \exp\left[-j \frac{2\pi}{\lambda} (\hat{s}.\underset{\sim}{r})\right] = A \exp\left[-j\, 2\pi(f_x x + f_y y + f_z z)\right] \tag{140}$$

$$\underset{\sim}{r}.\hat{s} = x \cos \alpha + y \cos \beta + z \cos \gamma$$

and

$$f_x = \frac{\cos \alpha}{\lambda} = \frac{\sin \theta_x}{\lambda}$$

$$f_y = \frac{\cos \beta}{\lambda} = \frac{\sin \theta_y}{\lambda} \tag{141}$$

$$f_z = \frac{\cos \gamma}{\lambda} = \frac{\sin \theta_z}{\lambda}$$

The amplitude transmittance of the sinusoidal amplitude grating is given by[1] Eq.(142) and depicted in Fig.(53).

Thus:

$$t = \frac{1}{2} + \frac{m}{2} \cos 2\pi f_o x \tag{142}$$

where $f_o = \frac{2 \sin \theta}{\lambda}$, see Eq.(22).

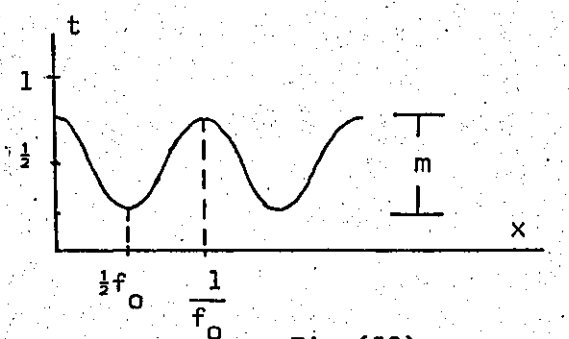

Fig.(53)

1. Eq.(142) comes from the expression $\cos^2\theta = \frac{1}{2}(1 + m \cos 2\theta)$ where m is a weighting factor, $0 < m < 1$, which reduces the diffraction efficiency of the hologram grating. See KOGELNIK, Eq.(2) (1967), and COLLIER et al Eq.(8.31) (1971) where the negative sign indicates a negative slope in the amplitude transmittance-exposure curve. Also see GOODMAN, Figs.4-6, (1968).

Suppose the grating screen is illuminated by a plane wavefront U_i for which $\theta_i = \theta_x$ ($\equiv \theta_i$ in Fig.(4)) as illustrated by Fig.(54). Then for z = 0,

$$U_i = A \exp\left[- j\, 2\pi f_i x \right] \tag{143}$$

where $f_i = - \dfrac{\sin \theta_x}{\lambda}$

The complex amplitude of the field just after screen is then[1]

$$U_t (x, y, 0) = U_i t$$

$$= \frac{A}{2} \exp\left[j\, 2\pi\, f_i x\right] + \frac{mA}{4} \exp\left[j\, 2\pi\, f_i x\right] \exp\left[j\, 2\pi\, f_o x\right] + \frac{mA}{4} \exp\left[j\, 2\pi\, f_i x\right]$$

$$\exp\left[- j\, 2\pi\, f_o x\right]$$

$$= \frac{A}{2} \exp\left[j\, 2\pi\, f_i x\right] + \frac{mA}{4} \exp\left[j\, 2\pi (f_i + f_o) x\right] + \frac{mA}{4} \exp\left[j\, 2\pi (f_i - f_o) x\right]$$

$$= \frac{A}{2} \exp\left[j\, 2\pi \left(\frac{\sin\theta_x}{\lambda} \right) x\right] + \frac{mA}{4} \exp\left[j\, 2\pi \left(\frac{3 \sin\theta_x}{\lambda} \right) x\right] + \frac{mA}{4} \exp\left[j\, 2\pi - \frac{\sin\theta_x}{\lambda}) x\right]$$

$$= U_o + U_- + U_+ \tag{144}$$

where U_o, U_- and U_+ represent plane wavefronts, Fig.(54).

According to Eq.(141) we have

for U_o: $f_x = \dfrac{\sin \theta_x}{\lambda}$; $f_z = \dfrac{\sin \theta_z}{\lambda}$; $\theta_z = \alpha_o$ $(= - \frac{\pi}{2} + \theta_x)$

for U_-: $f_x = \dfrac{3 \sin\theta_x}{\lambda}$; $f_z = \dfrac{\sin \theta_z}{\lambda}$; $\theta_z = \alpha_- = \mathrm{Cos}^{-1} (3 \sin\theta_x)$

for U_+: $f_x = - \dfrac{\sin \theta_x}{\lambda}$; $f_z = \dfrac{\sin \theta_z}{\lambda}$; $\theta_z = \alpha_+ = \left(\dfrac{\pi}{2} - \theta_x \right)$

(145)

and $f_y = 0$ everywhere[2].

1. Note that in Eq.(144) the negative sign of f_i has been considered.
2. NOTE: $|\alpha_o| > |\alpha_-|$, $\alpha_o = \cos^{-1} (\sin \theta_x)$, $\alpha_- = \cos^{-1} (3 \sin \theta_x)$.

/Continued

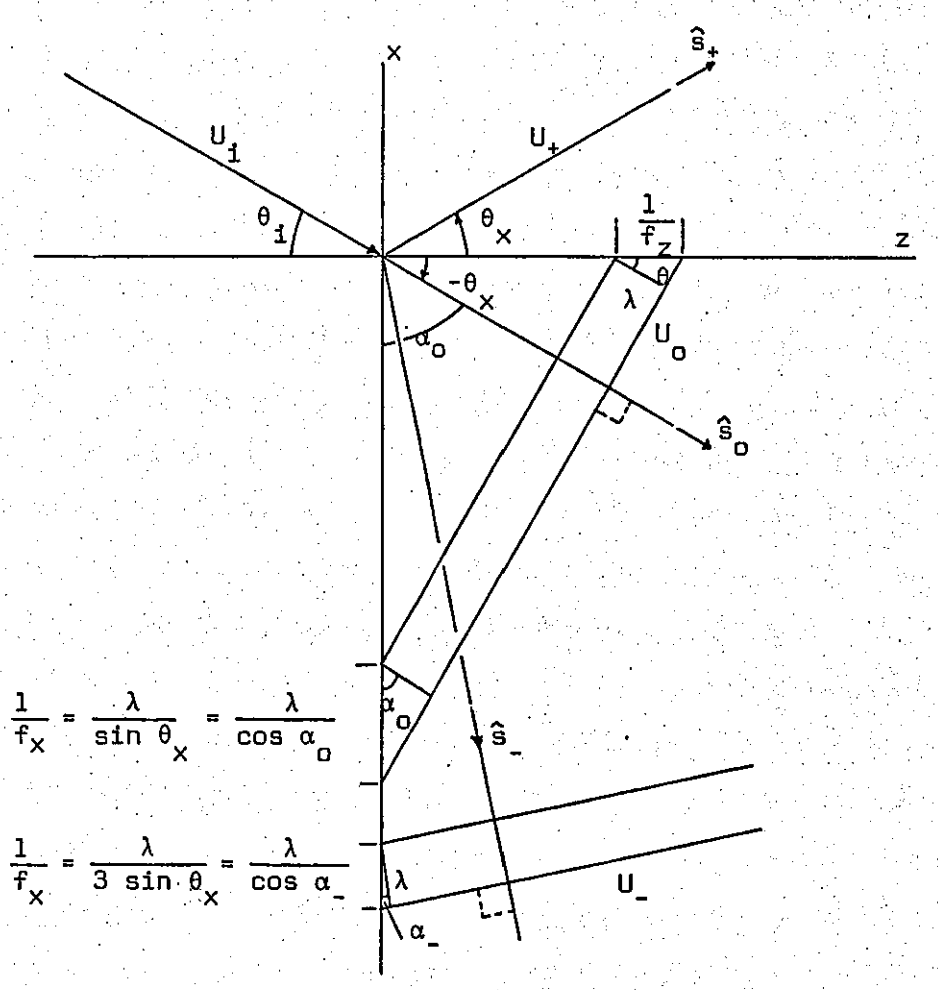

Fig.(54)

2(continued)

If, for example, $\theta_1 = \theta_2 = \theta_i \simeq 19^\circ$ then $|\alpha_o| \simeq 71^\circ$, $\alpha_- = 0$.

If $\theta_i \neq \theta_1 \neq \theta_2$ $(\neq \theta)$ in Figs.(4) and (54) then $\hat{s}_-$ is parallel to the x axis for $\sin\theta_i + \sin\theta_1 + \sin\theta_2 = 1$.

If $\theta_i \neq \theta_1 = \theta_2$ the condition for $\alpha_- = 0$ becomes

$$\theta_i = \sin^{-1}(1 - 2\sin\theta)$$

NOTE: For $\theta_i = 0$ and $\theta_1 = \theta_2$ Eq.(144) becomes

$$U_t = \frac{A}{2} + \frac{mA}{4}\exp\left[j\,2\pi\left(\frac{2\sin\theta_x}{\lambda}\right)\right] + \frac{mA}{4}\exp\left[j\,2\pi\left(-\frac{2\sin\theta_x}{\lambda}\right)\right] \qquad (146)$$

$$= U_o + U_- + U_+$$

See COLLIER et al, p102 (1971).

/Continued.

The complex amplitude at a distance z from the grating screen is the product of the field amplitude at $z = 0$, Eq.(144) and a phase factor which takes into account the propagation of each plane wave in space[1]. The complex amplitude of a plane wavefront at $z = 0$ is[2*], using Eq.(140)

$$U(x,y,o) = A \exp\left[-j\, 2\pi\, (f_x\, x + f_y\, y)\right], \quad z = 0 \tag{147}$$

whereas Eq.(140) represents the field amplitude at a distance z, then

$$U(x,y,z) = A \exp\{-j\, 2\pi\, (f_x\, x + f_y\, y + f_z\, z)\}$$

$$= A \exp\{-j\, 2\pi \left[f_x\, x + f_y\, y + \frac{1}{\lambda}\, (1 - (\lambda f_x)^2 + (\lambda f_y)^2)^{\frac{1}{2}}\, z\right]\}$$

$$= A \exp\left[-j\, 2\pi\, (f_x\, x + f_y\, y)\right] \exp\left[-j\, \frac{2\pi}{\lambda}\, (1 - (\lambda f_x)^2 + (\lambda f_y)^2)^{\frac{1}{2}}\, z\right]$$

$$= U(x,y,o) \exp\left[-j\, \frac{2\pi}{\lambda}\, (1 - (\lambda f_x)^2 + (\lambda f_y)^2)^{\frac{1}{2}}\, z\right] \tag{148}$$

2(continued)

Furthermore the condition for $\alpha_+ = 0$ and $\alpha_- = 0$ in Fig.(55) is that

$$\frac{2 \sin \theta_x}{\lambda} = \frac{1}{\lambda} = f_o$$

$$\Delta x = \lambda$$

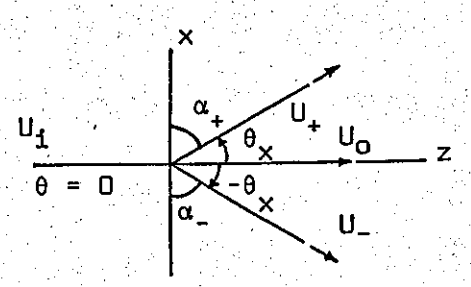

Fig.(55)

1. See GOODMAN § 3.7 having in mind one, two or three plane wavefronts as it is in the case of Eq.(144).

2* Eq.(147) becomes Eq.(143) for $\beta = \frac{\pi}{2}$; $f_y = 0$.

Applying Eq.(148) to each of the terms in Eq.(144) the expression for $U_t(x,y,z)$ is obtained[1].

Diffraction from an aperture

Consider, as an illustration, a single slit on an x_1y_1 plane at $z = 0$ of width w along the x_1 axis and not bounded along the y_1 axis[2], Fig.(56). Let the aperture be illuminated by a unit amplitude plane wavefront, $U_i = 1$, and divided in n regions of width Δx.

The field amplitude at $z = 0$ consists of an infinite number of point sources[3] each of which contributes to the field at P, on the x_oy_o plane, by an amount

$$U(x_o, z) = \frac{A}{r} \exp\left[-j\,(k.r - \phi)\right] \qquad (149)$$

1. This obeys the superposition principle in linear invariant systems. See GOODMAN for the evanescent waves concept according to Eq.(148).
2. All equations are reduced to one variable, x.
3. Huygens wavelets.

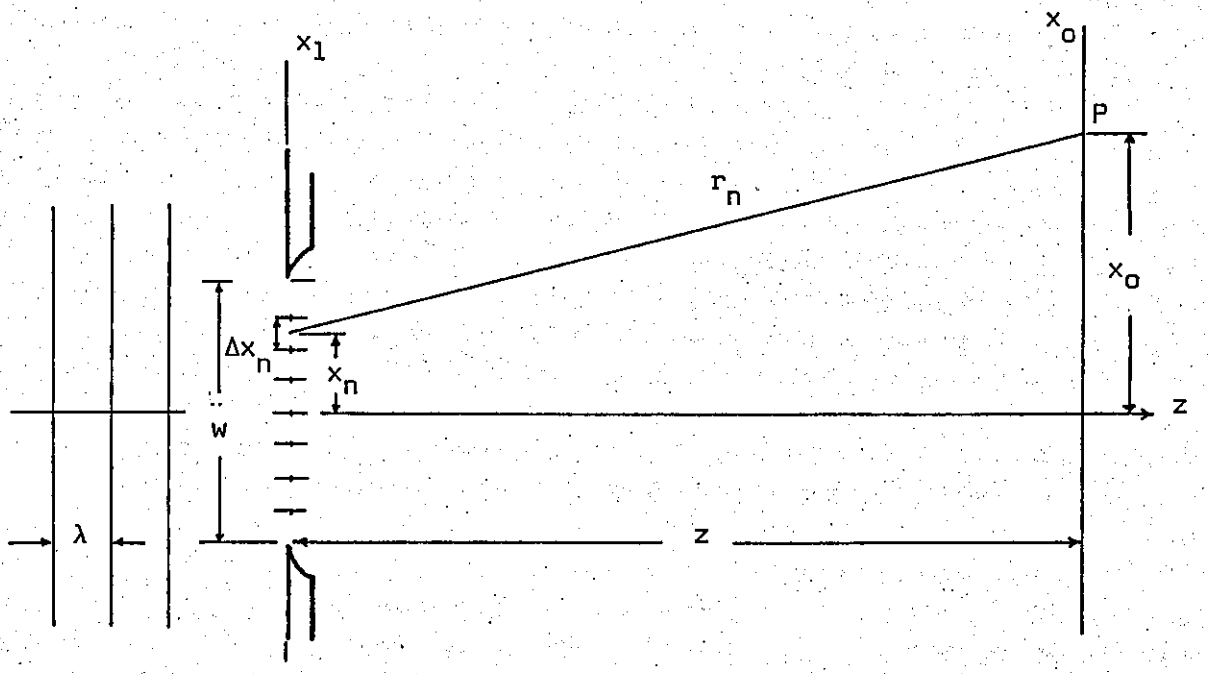

Fig.(56)

For the moment let us assume that the number of point sources on the aperture is M so that $\frac{\Delta x}{w} M$ represents density of points. If $\Delta x \leq \lambda$ no interference occurs due to point sources in Δx and all the wavefronts coming from that region are in phase. Let us call the contribution of sources within Δx_n on the field at P, $U_{\Delta x_n}(P)$ thus

$$U_{\Delta x_n}(P) = \frac{\Delta x_n M}{w} \frac{A_n}{r_n} \exp\left[-j\left(\frac{2\pi}{\lambda} r_n + \phi_n\right)\right]$$

$$= \frac{\Delta x_n M}{w} \frac{A_n}{r_n} \exp\left[+j\,\phi_n\right] \exp\left[-j\,\frac{2\pi}{\lambda} r_n\right] \qquad (150)$$

$$= g(x_n) \exp\left[-j\,\frac{2\pi}{\lambda} r_n\right] \Delta x_n$$

where Eq.(7) has been used such that

$$g(x_n) = \frac{M A_n}{w} \left(\frac{1}{r_n}\right) e^{j\phi} \qquad (151)$$

The complex amplitude at P due to the n regions is given by

$$U_{n\,\Delta x}(P) = \sum_{n} g(x_n) \exp\left[-j\,K\,r_n\right]\ \Delta x_n \qquad (152)$$

If we let $n \to \infty$ then $\Delta x_n \longrightarrow dx_1$, $\sum_{n}^{\infty} \longrightarrow \int_{-\frac{W}{2}}^{\frac{W}{2}}$ and, of course, the number of point sources M becomes infinite. The field amplitude at P is then expressed by

$$U_p(x_o,z) = C \int_{-\frac{W}{2}}^{\frac{W}{2}} g(x_1) \exp\left[-j\,K\,r\right]\ dx_1 \qquad (153)$$

where C is a complex constant which allows $g(x_1)$ to be considered as a function of x_1 under an initial approximation. Let us assume the distance z from the plane of the aperture to the parallel plane containing P to be greater than the width W[1], such that, $\frac{1}{r_n}$ in Eq.(151) becomes the factor $\frac{1}{z}$ included in C.[2] Therefore $g(x_1)$ can be considered as the complex amplitude distribution in the aperture being zero outside it. Eq.(153) can then be written as

$$U_p(x_o, z) = C \int_{-\infty}^{\infty} g(x_1) \exp\left[-j\,K\,r\right]\ dx_1 \qquad (154)$$

a convenient expression in the discussion that follows.

1. For an aperture of finite xy dimensions z must be greater than the maximum linear dimension of the aperture.

2. r_n on the exponent in Eq.(152) becomes r and not z because of its product with the large number K, see GOODMAN, p58 (1968).

If z is large enough for the expression

$$r = \left[(x_o - x_1)^2 + z^2 \right]^{\frac{1}{2}} = z \left[1 + \left(\frac{x_o - x_1}{z} \right)^2 \right]^{\frac{1}{2}} \qquad (155)$$

to be approximated by the first two terms of its binomial expansion, we then obtain[1]

$$r = z \left[1 + \frac{1}{2} \left(\frac{x_o - x_1}{2} \right)^2 \right] = z \left[1 + \frac{x_o^2}{2z^2} - \frac{x_o x_1}{z^2} + \frac{x_1^2}{2z^2} \right] \qquad (156)$$

From Eqs.(154) and (156) it follows that[2]

$$U_p(x_o,z) = C \exp \left[-j \frac{K x_o^2}{z} \right] \int_{-\infty}^{\infty} g(x_1) \exp \left[-j \frac{K x_1^2}{2z} \right] \exp \left[j K \frac{x_o x_1}{z} \right] d_{x_1} \qquad (157)$$

which represents the Fresnel diffraction of a (normally incident) monochromatic plane wave by an aperture[3].

If the Fraunhofer approximation

$$z >> \frac{K x_1^2}{2} \qquad (158)$$

is applied then the term $\exp \left(-j K \frac{x_1^2}{2z}\right)$ is unity over the aperture.

For $x_{1max} = \pm \frac{w}{2}$ we have[4]

$$z >> \frac{w^2}{\lambda} \qquad (159)$$

1. Known as the Fresnel approximation. See discussion on GOODMAN, p59.
2. The factor exp(-jkz) is included in C.
3. As described at the beginning of this section.
4. $z >> \frac{\pi}{4} \frac{w^2}{\lambda} \simeq \frac{w^2}{\lambda}$

and Eq.(157) becomes

$$U_p(x_o,z) = C \exp\left[-j K \frac{x_o^2}{z}\right] \int_{-\infty}^{\infty} g(x_1) \exp\left[j K \frac{x_o x_1}{z}\right] dx_1 \qquad (160)$$

This equation represents the Fraunhofer diffraction of a (normally incident) monochromatic plane wave by an aperture. Eqs.(157) and (160) can be rewritten in the following way:

Fresnel diffraction,

$$U_p(x_o,z) = C \exp\left[-j K \frac{x_o^2}{z}\right] \mathcal{F}\{g(x_1) \exp\left[-j K \frac{x_1^2}{2z}\right]\}_{f_{x_1} = -\frac{x_o}{\lambda z}} \qquad (161)$$

Fraunhofer diffraction,

$$U_p(x_o,z) = C \exp\left[-j K \frac{x_o^2}{z}\right] \mathcal{F}\{g(x_1)\}_{f_{x_1} = -\frac{x_o}{\lambda z}} \qquad (162)$$

where $\mathcal{F}\{\ \}$ denotes the Fourier transform and f_x is the spatial frequency in the frequency domain[1].

Therefore since $g(x_1)$ represents the complex amplitude distribution of light in the plane x_1y_1 (spatial distribution), the Fourier transformation represents, in the Fraunhofer region, the distribution of the diffracted light (frequency distribution)[2].

1. See GOODMAN, Ch.2 (1968)., BRACEWELL (1965), STROKE, Ch.VII (1966), for a treatment of Fourier transform with the same nomenclature used in this work.
2. Spatial distribution (mm/lines). Frequency distribution (lines/mm).

Fourier analysis

A periodic function $f(x)$ can be represented by the Fourier series in terms of cosine and sine functions as

$$f(x) = \frac{A_o}{2} + \sum_{n=1}^{\infty} \left(A_n \cos \frac{n\pi x}{\ell} + B_n \sin \frac{n\pi x}{\ell} \right)$$

$$A_n = \frac{1}{\ell} \int_{-\ell}^{\ell} f(x) \cos \frac{n\pi x}{\ell} \, dx \qquad (163)$$

$$B_n = \frac{1}{\ell} \int_{-\ell}^{\ell} f(x) \sin \frac{n\pi x}{\ell} \, dx$$

or represented in exponential form

$$f(x) = \sum_{n=-\infty}^{\infty} C_n \exp \left[j \frac{n\pi x}{\ell} \right]$$

$$C_n = \frac{1}{2\ell} \int_{-\ell}^{\ell} f(x) \exp \left[-j \frac{n\pi x}{\ell} \right] dx \qquad (164)$$

where a complicated function $f(x)$ is decomposed in an infinite number of simpler exponential functions.

Consider a periodic function $f_\ell(x)$, Fig.(57) solid line, of period 2ℓ.

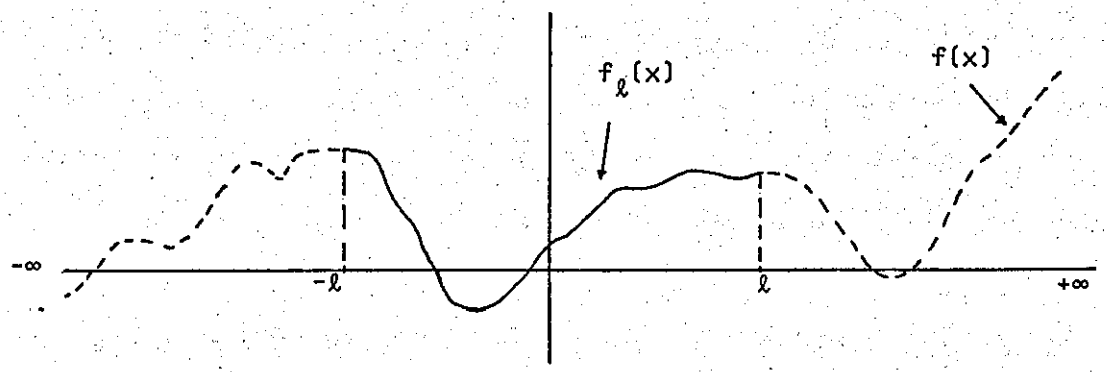

Fig.(57)

According to Eq.(164) we have

$$f_{\ell}(x) = \sum_{n=-\infty}^{\infty} C_n \exp\left[j \frac{n\pi x}{\ell} \right]$$

$$= \sum_{-\infty}^{\infty} \frac{1}{2\ell} \{ \int_{-\ell}^{\ell} f_{\ell}(x) \exp\left[-j\, 2\pi \left(\frac{n}{2\ell}\right)x \right] dx \} \exp\left[j\, 2\pi \left(\frac{n}{2\ell}\right)x \right] \tag{165}$$

$$= \sum_{-\infty}^{\infty} \Delta f \ \{G_{\ell}(f_n)\} \ \exp\left[j\, 2\pi \left(\frac{n}{2\ell}\right)x \right], \quad f_n = \frac{n}{2\ell}$$

where

$$G_{\ell}(f_n) = \int_{-\ell}^{\ell} f_{\ell}(x) \exp\left[-j\, 2\pi \left(\frac{n}{2\ell}\right)x \right] dx \tag{166}$$

and

$$\Delta f = f_{n+1} - f_n = \frac{1}{2\ell} \tag{167}$$

We can now consider the function $f(x)$, solid and dotted lines in Fig.(57) as a periodic function of infinite period. Thus as $\ell \longrightarrow \infty$, $\Delta f \longrightarrow df$, $\sum_{-\infty}^{\infty} \longrightarrow \int_{-\infty}^{\infty}$, and Eq.(164) becomes

$$f(x) = \int_{-\infty}^{\infty} G(f) \exp\left[j\, 2\pi\, f\, x \right] df = \mathcal{F}^{-1}\{ G(f) \} \tag{168}$$

$$G(f) = \int_{-\infty}^{\infty} f(x) \exp\left[-j\, 2\pi\ f\, x \right] dx = \mathcal{F}\{ f(x) \} \tag{169}$$

where $G(f)$ is the Fourier transform of $f(x)$ and $\mathcal{F}^{-1}\{G(f)\}$ denotes the inverse Fourier transform.

Eq.(168) can be interpreted as the decomposition of a function $f(x)$ in a set of exponential functions where $G(f)$ is a weighting factor. Furthermore, this equation can also be understood[1] as a set

1. GOODMAN § 3.7 (1968), also on p69 see the Fourier treatise of the diffraction by a sinusoidal amplitude grating.

of plane waves, at z = 0, travelling in different directions with amplitudes G(f) df, see Eq.(143).

We can tackle the above Fourier analysis in the opposite direction using the shift and convolution theorems. Consider the function $f_o(x)$ defined on the interval $x_1 \leq x \leq x_1 + x_o$ as it is illustrated in Fig.(58) (solid line).

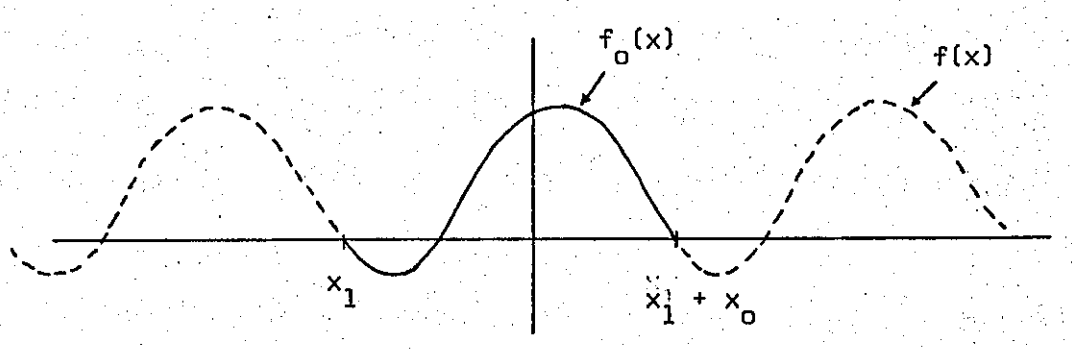

Fig.(58)

Consider also the function f(x), Fig.(58) (solid and dotted lines), which can be expressed as an infinite linear combination of $f_o(x)$ functions.

Hence[1]

$$f(x) = \sum_{n=-\infty}^{\infty} f_o(x - n x_o)$$

$$= \sum_{-\infty}^{\infty} f_o(x) * \delta(x - n x_o)$$

$$= f_o(x) * \sum_{-\infty}^{\infty} \delta(x - n x_o) \qquad (170)$$

represent a linear combination of weighted and displaced functions, where the symbol * denotes a convolution operation[1].

1. GOODMAN, Eq.(2-19) (1968).

The function f(x) can also be expressed by Eq.(168)

$$f(x) = \int_{-\infty}^{\infty} G(f) \exp\left[j\, 2\pi f\, x \right] dx \qquad (171)$$

Applying the convolution theorem to Eq.(170) we have[1]

$$G(f) = G_o(f) \frac{1}{x_o} \sum_{n=-\infty}^{\infty} \delta(f - \frac{n}{x_o}) \qquad (172)$$

From the last two equations it follows that

$$f(x) = \int_{-\infty}^{\infty} \frac{1}{x_o} G_o(f) \sum_{n=-\infty}^{\infty} \delta(f - \frac{n}{x_o}) \exp\left[j\, 2\pi\, f\, x \right] df \qquad (173)$$

Interchanging the summation and integration we obtain

$$f(x) = \sum_{n=-\infty}^{\infty} \frac{1}{x_o} \int_{-\infty}^{\infty} G_o(f)\ \delta(f - \frac{n}{x_o}) \exp\left[j\, 2\pi\, f\, x \right] df \qquad (174)$$

where the product in the integrand is defined only when $f = \frac{n}{x_o}$. Then taking the constant factors outside the integral and using a definition of the δ function[2] we can write

$$\begin{aligned} f(x) &= \sum_{n=-\infty}^{\infty} \frac{1}{x_o} G_o\ (\frac{n}{x_o}) \exp\left[j\, 2\pi \frac{n}{x_o} x \right] \\ &= \sum_{n=-\infty}^{\infty} C_n \exp\left[j\, 2\pi \frac{n}{x_o} x \right] \end{aligned} \qquad (175)$$

$$x_o = 2\ell$$

and

$$C_n = \frac{1}{x_o} G_o\ (\frac{n}{x_o}) = \frac{1}{x_o} \int_{x_1}^{x_1 + x_o} g(x) \exp\left[-j\, 2\pi \frac{n}{x_o} x \right] dx$$

$$x_o = 2\ell$$

$$= \frac{1}{2\ell} \int_{-\ell}^{\ell} f(x) \exp\left[-j\pi \frac{n}{\ell} x \right] dx \qquad (176)$$

which are equations (164).

1. $\mathcal{F}\{ \sum_{n=-\infty}^{\infty} \delta(x - n\, x_o) \} = \frac{1}{x_o} \sum_{n=-\infty}^{\infty} \delta(f - \frac{n}{x_o})$

2. $\int_{-\infty}^{\infty} \delta(x)\, dx = 1, \qquad \delta(x) = 0 \quad x \neq 0.$

REFERENCES

Abramson, N. The holo-diagram V: A device for practical interpreting of hologram interference fringes. Appl.Opt. 11(5), 1143-1147, 1972 - Sandwich holography: An analogue method for the evaluation of holographic fringes. The Engineering Uses of Coherent Optics. Cambridge Univ. Press, (to be published) 1975.

Adams, F.D. and Maddux, E. Synthesis of holography and speckle photography to measure 3-D displacements. Appl. Opt. 13(2), 219, 1974.

Agfa-Gevaert, Technical information leaflet. The new micronmask plate, 1969.

Aleksandrov, E.B. and Bonch-Bruevich, A.M. Investigation of surface strains by the hologram technique. Soviet Phys.- Tech. Phys. 12(2), 258-265, 1967.

Allen, J.B. and Meadows, D.M. Removal of unwanted patterns from moire contour maps by grid translation techniques. Appl.Opt. 10(1), 210-213, 1971.

Altman, J.H. Pure relief images on Type 649F plates. Appl.Opt. 5(10), 1689-1690, 1966.

Archbold, E. The history of a holographic non-destructive test procedure. The Engineering Uses of Coherent Optics. Cambridge Univ. Press, (to be published), 1975.

Archbold, E., Burch, J.M. and Ennos, A.E. The application of holography to the comparison of cylinder bores. J.Sci.Instrum. 44, 489-494, 1967 - Recording of in-plane surface displacement by double-exposure speckle photography. Optica Acta, 17(12), 883-898, 1970.

Archbold, E. and Ennos, A.E. Observation of surface vibration modes by stroboscopic hologram interferometry. Nature, 217(5132), 942-943, 1968 - Displacement measurement from double-exposure laser photographs. Optica Acta, 19(4), 253-271, 1972 - Applications of holography and speckle photography to the measurement of displacement and strain. J.Strain Anal. 9(1), 10-16, 1974.

Bellani, V.F. and Sona, A. Measurements of 3-D displacements by scanning a double-exposure hologram. Appl.Opt. 13(6), 1337-1341, 1974.

Benoit, P. and Mathieu, E. Real time contour line visualization of an object. Opt.Commun. 12(2), 175-180, 1974.

Berggren, R. Analysis of interferograms. Optica Spectra, 22-25, Dec. 1970.

Biedermann, K. and Johansson, S. Development effect and the MTF of high-resolution photographic materials for holography. J.Opt.Soc.Amer. 64(6), 862-870, 1974.

Birch, K.G. Oblique incidence interferometry applied to non-optical surfaces. J.Phys.E: Sci.Instrum. 6, 1045-1048, 1973.

Boone, P.M. Measurement of displacement, strain and stress by holography. The Engineering Uses of Coherent Optics. Cambridge Univ. Press, (to be published) 1975.

Boone, P. and Verbiest, R. Application of hologram interferometry to plate deformation and translation measurements. Optica Acta. 16(5), 555-567, 1969.

Born, M. and Wolf, E. Principles of Optics. 4th ed. Pergamon Press, 1970.

Bracewell, R.N. The Fourier Integral and Its Applications. McGraw-Hill, 1962.

Bruning, J.H., Herriott, D.R., Gallagher, J.E., Rosenfeld, D.P., White, A.D. and Brangaccio, D.J.
Digital wavefront measuring interferometer for testing optical surfaces and lenses.
Appl.Opt. 13(11), 2693-2703, 1974.

Burch, J.M. Laser speckle metrology. SPIE, Seminar Proc. pp.149-155. Thompson, B.J. and Develis, J.B., Eds. Vol.15, 1971 - Generation of speckle patterns in coherent and partially coherent illumination. paper 1, Conf.Speckle Phenomena and their Applications. Loughborough University of Technology, 1974 - Holographic measurement of displacement and strain - an introduction. J.Strain.Anal. 9(1), 1-3, 1974 - Outlines of optical metrology. The Engineering Uses of Coherent Optics. Cambridge Univ. Press (to be published) 1975.

Burch, J.M. and Ennos, A.E. A holographically-corrected low power microscope. Proc.Int.Symp.Holography, Besancon, paper 10-2, 1970.

Burckhardt, C.B. and Doherty, E.T. A bleach process for high-efficiency low-noise holograms. Appl.Opt. 8(12), 2479-2482, 1969.

Butters, J.N. Holography and its technology. Peter Peregrinus Ltd. 1971 - Electronic speckle pattern interferometry: a general review background to subsequent papers. The Engineering Uses of Coherent Optics. Cambridge Univ. Press (to be published) 1975.

Butters, J.N., Denby, D. and Leendertz, J.A. A method for reducing movement in holographic emulsions. J.Phys.E: Sci.Instrum. 2(2), 116-117, 1969.

Butters, J.N. and Leendertz, J.A. Holographic and video techniques applied to engineering measurement. Meas.Contr. 4(12), 349-354, 1971 - A double exposure technique for speckle pattern interferometry. J.Phys.E: Sci.Instrum. 4, 277-279, 1971 - Speckle pattern and holographic techniques in engineering metrology. Opt. and Laser Technol. 3(1), 26-30, 1971 - Application of video techniques and speckle pattern interferometry to engineering measurement. SPIE, Seminar Proc. pp.361-374. Thompson, B.J. and Develis, J.B. Eds., Vol.15, 1971 - Component inspection using speckle pattern. Proc.Electro-Optics Int.Conf. 1974. Kiver Communications Ltd., 1974.

Cathey, W.T.Jr. Three-dimensional wavefront reconstruction using a phase hologram. J.Opt.Soc.Amer. 55, 457, 1965.

Champagne, E.B. Quantitative data reduction with the use of fringe control techniques in conjunction with holographic interferometry. Proc.Symp.Eng.Appl.Holography, pp.133-144, SPIE, Redondo Beach, California, 1972.

Chang, M. and George N. Holographic dielectric grating: theory and practice. Appl.Opt. 9(3), 713-719, 1970.

Chiang, F.P. A new three-dimensional strain analysis technique by scattered-light speckle interferometry. The Engineering Uses of Coherent Optics. Cambridge Univ.Press, (to be published), 1975.

Chiang, F.P. and Jaisingh, G. A new optical system for moiré methods. Exp.Mech. 459-462, Nov. 1974.

Clarke, D. Nomenclature of polarized light: linear polarization. Appl.Opt. 13(1), 3-5, 1974 - Nomenclature of polarized light: Elliptical polarization. Appl.Opt. 13(2), 222-224, 1974.

Collier, R.J., Burckhardt, C.B. and Lin, L.H. Optical Holography. Academic Press, 1971.

Condon, E.U. and Odishaw, H. Handbook of Physics. McGraw-Hill, 1958.

Dandliker, B., Eliasson, B., Ineichen, B. and Mottier, F.M. Quantitative determination of bending and torsion through holographic interferometry. The Engineering Uses of Coherent Optics. Cambridge Univ.Press (to be published) 1975.

Denby, D. and Leendertz, J.A. Plane-surface strain examination by speckle-pattern interferometry using electronic processing. J.Strain Anal., 9(1), 17-25, 1974.

Denby, D., Quintanilla, G.E. and Butters, J.N. Contouring by electronic speckle pattern interferometry. The Engineering Uses of Coherent Optics, Cambridge Univ. Press, (to be published) 1975.

Dessus, B. and Leblanc, M. The "fringe method" and its application to the measurement of deformations, vibrations, contour lines and differences of objects. Opto-electronics, 5, 369-391, 1973.

Ennos, A.E. Holography and its applications. Contemp.Phys. 8(2), 153-170, 1967 - Measurement of in-plane surface strain by hologram interferometry, J.Phys.E: Sci.Instrum. 1(2), 731-734, 1968 - Strain measurement. Section 8.5, Holographic non-destructive testing, Erf. R.K.,Ed. Academic Press, 1974 - Optical fingerprinting with the laser for engineering measurement. The Engineering Uses of Coherent Optics. Cambridge Univ. Press, (to be published) 1975.

Erf, R.K. Holographic non-destructive testing. Academic Press, Erf, R.K. Ed. 1974.

Fitzgerald, J., Hörster, H. and Junginger, J.G.
Temperature evaluation of incandescent lamps by means of holographic interferometry. Proc.Int.Symp.Holography, Besancon, paper 7-5, 1970.

Francon, M. Holography. Academic Press, 1974.

Friesem, A.A., Kozma, A. and Adams, G.F. Recording parameters of spatially modulated coherent wavefronts. Appl.Opt. 6(5), 851-856, 1967.

Friezem, A.A., Levy, U. and Zilberberg, Y. Real-time holographic contour mapping with dye lasers. The Engineering Uses of Coherent Optics, Cambridge Univ. Press, (to be published) 1975.

Fryer, P.A. Vibration analysis by holography. Rep.Prog.Phys. 33, 489-531, 1970.

Gabor, D. A new microscopic principle. Nature 161, 771, 1948.

Gara, A.D., Majkowski, R.F. and Stapleton, T.T. Holographic system for automatic surface mapping. Appl.Opt. 12(9), 2172-2179, 1973.

Gates, J.W.C. Holography with scatter plates. J.Phys.E: Sci.Instrum. 1(2), 989-994, 1968.

Goodman, J.W. Introduction to Fourier Optics. McGraw-Hill, 1968.

Graube, A. Advances in bleaching methods for photographically recorded holograms. Appl.Opt. 13(12), 2942-2946, 1974.

Haines, K. and Hildebrand, B.P. Contour generation by wavefront reconstruction. Phys.Lett. 19(1), 10-11, 1965 - Surface-deformation measurement using the wavefront reconstruction technique. Appl.Opt. 5(4), 595-602, 1966.

Halliday, D. and Resnick, R. Fundamentals of Physics. John Wiley and Sons, 1970.

Hämäläinen, R.M.K., Karppinen, H. and Salminen, O. Measurement of parameters of bleached holograms. Phys. Fenn. 9, 77-83, 1974.

Hariharan, P. and Hegedus, Z.S. Relative phase shift of images reconstructed by phase and amplitude holograms. Appl.Opt. 14(2), 273-274, 1975.

Hildebrand, B.P. and Haines, K.A. Interferometric measurements using the wavefront reconstruction technique. Appl.Opt. 5(1), 172-173, 1966.

Hovanesian, J.Der. Moiré contouring using new scanned ruling method. The Engineering Uses of Coherent Optics. Cambridge Univ. Press, (to be published) 1975.

Hovanesian, J.D., Brcic, V. and Powell, R.L. A new experimental stress-optic method: stress-holo-interferometry. Exp.Mech. 8(8), 362-368, 1968.

Hovanesian, J.Der. and Hung, Y.Y. Moiré contour-sum contour-difference, and vibration analysis of arbitrary objects. Appl.Opt. 10(12), 2734-2738, 1971.

Hughes, R.G. The determination of vibration patterns using a pulsed laser with holographic and electronic speckle pattern interferometry techniques. The Engineering Uses of Coherent Optics. Cambridge Univ. Press, (to be published) 1975.

Jaerisch, W. and Makosch, G. Optical contour mapping of surfaces. Appl.Opt. 12(7), 1552-1557, 1973.

Jahnke, E., Emde, F. and Losch, F. Tables of Higher Functions. 6th ed. McGraw-Hill, 1960.

Jenkins, F.A. and White, H.E. Fundamentals of Optics. 3rd ed. McGraw-Hill, 1957.

Kaspar, F.G. and Lamberts, R.L. Effects of some photographic characteristics on the light flux in a holographic image. J.Opt.Soc.Amer. 58(7), 970-976, 1968.

King, P.W. Holographic interferometry technique utilizing two plates and relative fringe orders for measuring micro-displacement. Appl.Opt. 13(2), 231-233, 1974.

Klein, M.V. Optics. John Wiley and Sons, 1970.

Kogelnik, H. Reconstructing response and efficiency of hologram gratings. Proc.Symp.Modern Opt. pp.605-617, Fox, J. Ed. Polytechnic Press, Brooklyn, N.Y. 1967 - Bragg diffraction in hologram gratings with multiple internal reflections. J.Opt.Soc.Amer. 57, 431-433, 1967.

Lamberts, R.L. and Kurtz, C.N. Reversal bleaching for low flare light in holograms. Appl.Opt. 10(6), 1342-1347, 1971.

Latta, J.N. The bleaching of holographic diffraction gratings for maximum efficiency. Appl.Opt. 7(2), 2409-2416, 1968.

Lee, T.C. Holographic recording on thermoplastic films. Appl.Opt. 13(4), 888-895, 1974.

Leendertz, J.A. Interferometric displacement measurement on scattering surfaces utilizing speckle effect. J.Phys.E: Sci.Instrum. 3, 214-218, 1970.

Leger, D., Mathieu, E. and Perrin, J.C. Optical surface roughness determination using speckle correlation technique. Appl.Opt. 14(4), 872-877, 1975.

Leith, E.N. and Upatnieks, J. Reconstructed wavefronts and communication theory. J.Opt.Soc.Amer. 52(10), 1123-1130, 1962.

Lin, L.H. Hologram formation in hardened dichromated gelatin films. Appl.Opt. 8(5), 963-966, 1969.

Lin, L.H. and Beauchamp, H.L. Write-read-erase in situ optical memory using thermoplastic holograms. Appl.Opt. 9(9), 2088-2092, 1970.

Longhurst, R.S. Geometrical and Physical Optics. 2nd ed., Longmans, 1967.

Luxmoore, A. Measurement of in-plane displacements and strains by moiré and speckle methods. The Engineering Uses of Coherent Optics. Cambridge Univ. Press, (to be published), 1975.

Macovski, A., Ramsey, S.D. and Schaefer, L.F. Time-lapse interferometry and contouring using television systems. Appl.Opt. 10(12), 2722-2726, 1971.

Matsumoto, T., Iwata, K. and Nagata, R. Distortionless recording in double-exposure holographic interferometry. Appl.Opt. 12(7), 1660-1662, 1973.

McMahon, D.H. and Franklin, A.R. Efficient, high-quality, R-10 bleached holographic diffraction gratings. Appl.Opt. 8(9), 1927-1929, 1969.

McMahon, D.H. and Maloney, W.T. Measurements of the stability of bleached photographic phase holograms. Appl.Opt. 9(6), 1363-1368, 1970.

McKechnie, T.S. Reduction of speckle by a moving aperture. Conf. speckle phenomena and their applications, Loughborough University of Technology, 1974.

Nishida, N. Bleached phase hologram containing nonsilver metal compound. Appl.Opt. 13(12), 2769-2770, 1974.

Ost, J. and Storck, E. Techniques for generation and adjustment of reference and reconstructing waves in precision holography. Opt.Technol., 251-254, 1969.

Pennington, K.S. and Harper, J.S. Techniques for producing low-noise, improved efficiency holograms. Appl.Opt. 9(7), 1643-1650, 1970 - New Phototechnology suitable for recording phase holograms and similar information in hardened gelatin. Appl.Phys.Lett. 18(3), 80-84, 1971.

Phillips, N.J. and Coaton, J.R. Holography as a diagnostic technique in the study of lamps and lighting. Ltg.Res.Technol. 5(3), 156-159, 1973.

Post, D. Holography and interferometry in photoelasticity. Exp.Mech. 12(3), 113-123, 1972.

Powell, R.L. and Stetson, K.A. Interferometric vibration analysis by wavefront reconstruction. Opt.Soc.Amer. 55(12), 1593-1598, 1965.

Renesse van, R.L. Advances in bleaching methods for photographically recorded holograms: comments. Appl.Opt. 14(8), 1763-1764, 1975.

Roberts, D.A. Lab. notes on photometric units (for those who can't avoid them). Optical Spectra, 37-40, Feb. 1972.

Robertson, E.R. and Harvey, J.M. (Eds). The Engineering Uses of Holography. Cambridge Univ. Press, 1970.

Rowe, S.H. and Welford, W.T. Surface topography of non-optical surfaces by projected interference fringes. Nature, 216, 786-787, 1967.

Rudder, C.L. Polarization filtering in holography. Appl.Phys.Lett. 10(10), 270-272, 1967.

Russo, V. and Sottini, S. Bleached holograms. Appl.Opt. 7(1), 202, 1968.

Shankoff, T.A. Phase holograms in dichromated gelatin. Appl.Opt. 7(10), 2101-2105, 1968.

Shurcliff, W. Polarized light: production and use. Harvard, U.P. Cambridge, Mass. 1962.

Smith, H.M. Photographic relief images. J.Opt.Soc.Amer. 58(4), 533-539, 1968.

Sollid, J.E. Holographic interferometry applied to measurements of small static displacements of diffusely reflecting surfaces. Appl.Opt. 8(8), 1587-1595, 1969.

Stetson, K.A. and Powell, R.L. Interferometric hologram evaluation and real-time vibration analysis of diffuse objects. J.Opt.Soc.Amer. 55, 1694-1695, 1965 - Fringe interpretation of hologram interferometry of rigid-body motions and homogeneous deformations. J.Opt.Soc.Amer. 64(1), 1-10, 1974.

Stroke, G.W. An Introduction to Coherent Optics and Holography. Academic Press, 1966.

Sweeney, D.W. and Vest, C.M. Measurement of three-dimensional refractive-index fields by holographic interferometry. Proc.Symp.Eng.Appl.Holography, pp.237-250, SPIE, Redondo Beach, California, 1972.

Takasaki, H. Moiré topography. Appl.Opt. 9(6), 1467-1472, 1970 - Moiré topography. Appl.Opt. 12(4), 845-850, 1973.

Theocaris, P.S. Moiré fringes in strain analysis. Pergamon Press Ltd., 1969.

Thiry, H. New technique of bleaching photographic emulsions and its applications to holography. Appl.Opt. 11(7), 1652-1653, 1972.

Thomas, G.B.Jr. Calculus and Analytic Geometry. 4th ed., Addison-Wesley, 1972.

Tolansky, S. An Introduction to Interferometry. Longman, 2nd ed., 1973.

Tsuruta, T. and Shiotake, N. Holographic generation of contour map of diffusely reflecting surface by using immersion method. Japan J.Appl.Phys. 6, 661-662, 1967.

Upatnieks, J. and Leonard, C. Diffraction efficiency of bleached, photographically recorded interference patterns. Appl.Opt. 8(1), 85-89, 1969 - Efficiency and image contrast of dielectric holograms. J.Opt.Soc.Amer. 60(3), 297-305, 1970.

Urbach, J.C. and Reinhard, W.M. Properties and limitations of hologram recording materials. Appl.Opt. 8(11), 2269-2281, 1969.

Vander, L.A. Holographic data storage and retrieval. The Engineering Uses of Coherent Optics. Cambridge Univ. Press, (to be published) 1975.

Varner, J.R. Desensitized hologram interferometry. Appl.Opt. 9(9), 2098-2100, 1970 - Holographic contouring: alternatives and applications. SPIE Seminar Proc. pp.239-248, Thompson, B.J. and Develis, J.B., Eds., Vol.15, 1971 - Holographic contouring techniques applicable to mechanical testing. Materials Research and Standards, 31-52, Sept. 1971 - Holographic and moiré surface contouring. Ch.5, 1974(a). The use of contour maps for measuring surface displacement. Section 8.4, 1974(b). Erf, R.K. Ed., Holographic non-destructive testing. Academic Press, 1974.

Vest, C.M. Comment on: Holographic interferometry applied to measurements of small static displacements of diffusely reflecting surfaces. Appl.Opt. 12(3), 612-613, 1973.

Vienot, J.Ch., Bulabois, J. and Pasteur, J. Applications of Holography. Eds. Besancon, 1970.

Wall, M.R. The form of holographic vibration fringes. The Engineering Uses of Holography. Robertson, E.R. and Harvey, J.M. Eds. Cambridge Univ. Press, 355-380, 1968.

Waters, J.P. Object motion compensation in CW holography. Section 8.2, Holographic non-destructive testing. Erf, R.K., Ed. Academic Press, 1974.

Way, F.C. Surface evaluation of airfoils via contouring. Proc.Symp.Eng.Appl.Holography, pp.57-64, SPIE, Redondo Beach, California, 1972.

Wuerker, R.F. Particle and flow field measurements by laser holography. The Engineering Uses of Coherent Optics. Cambridge Univ. Press, (to be published) 1975.

Wykes, C. De-correlation of speckle pattern with wavelength. Loughborough University of Technology. (unpublished) 1975.

Zelenka, J.S. and Varner, J.R. A new method for generating depth contours holographically. Appl.Opt. 7(10), 2107-2110, 1968 - Multiple-index holographic contouring. Appl.Opt. 8(7), 1431-1434, 1969.

AUTHOR'S DECLARATION

This is to certify that neither the thesis nor the original work contained therein has been submitted to this or any other institution for a higher degree.